ALKBH7 mediates necrosis via rewiring of glyoxal metabolism

Chaitanya A. Kulkarni[1], Sergiy M. Nadtochiy[1], Leslie Kennedy[2], Jimmy Zhang[1], Sophea Chhim[3], Hanan Alwaseem[4], Elizabeth Murphy[2], Dragony Fu[3], Paul S. Brookes[1*]

[1]Department of Anesthesiology & Perioperative Medicine, University of Rochester Medical Center, Rochester NY. [2]NHLBI Intramural Research Program, National Institutes of Health, Bethesda MD. Departments of [3]Biology, and [4]Chemistry, University of Rochester, Rochester NY.

*Correspondence to: Paul S. Brookes, PhD.
Box 604 Anesthesiology,
University of Rochester Medical Center,
601 Elmwood Avenue,
Rochester, NY 14642, USA.
paul_brookes@urmc.rochester.edu

Key Words: Mitochondria, ALKBH7, α-KG dioxygenase, Glyoxalase, Metabolism, Ischemia

Word Count: ~4100 main doc' not including methods, refs, fig legends

ABSTRACT

Alkb homolog 7 (ALKBH7) is a mitochondrial α-ketoglutarate dioxygenase required for DNA alkylation induced necrosis, but its function and substrates remain unclear. Herein we show ALKBH7 regulates dialdehyde metabolism, which impacts the cardiac response to ischemia-reperfusion (IR) injury. Using a multi-omics approach, we find no evidence ALKBH7 functions as a prolyl-hydroxylase, but we do find *Alkbh7*$^{-/-}$ mice have elevated glyoxalase I (GLO-1), a dialdehyde detoxifying enzyme. Metabolic pathways related to the glycolytic by-product methylglyoxal (MGO) are rewired in *Alkbh7*$^{-/-}$ mice, along with elevated levels of MGO protein adducts. Despite greater glycative stress, hearts from *Alkbh7*$^{-/-}$ mice are protected against IR injury, in a manner blocked by GLO-1 inhibition. Integrating these observations, we propose ALKBH7 regulates glyoxal metabolism, and that protection against necrosis and cardiac IR injury bought on by ALKBH7 deficiency originates from the signaling response to elevated MGO stress.

INTRODUCTION

The α-ketoglutarate (α-KG) dioxygenases are a diverse enzyme superfamily, whose primary biochemical function is the addition of hydroxyl (–OH) to protein or nucleic acid substrates.[1] The family includes the TET 5-methylcytosine hydroxylases, the EGLN prolyl-hydroxylases that regulate hypoxia inducible factor (HIF), and the JmjC domain-containing histone demethylases. All α-KG dioxygenases use α-KG and O_2 as biochemical substrates and generate succinate as product. The AlkB homologs (ALKBHs) are a distinct family of nine α-KG dioxygenases that are homologs of *E. coli* AlkB.[2] The bacterial AlkB enzyme catalyzes demethylation of DNA damaged by alkylating agents, via hydroxylation of the methylated DNA followed by spontaneous decomposition to release formaldehyde and recover the DNA base.[3,4] Many eukaryotic ALKBHs have been shown to act on DNA or RNA substrates, including mammalian ALKBHs 1-3, 5, 8 and FTO.[5-8] The subject of this investigation is ALKBH7, a poorly characterized mitochondrial α-KG dioxygenase which has no known substrates.

In contrast to a role in DNA repair or RNA modification, structural studies have revealed ALKBH7 lacks a critical nucleotide recognition lid required for binding DNA or RNA.[9] Moreover, a study of mitochondria from several tissues of *Alkbh7*$^{-/-}$ mice showed no differences in mtDNA modifications (6-methyladenine, 5-methylcytosine, etc.) vs. wild-type (WT) at young ages, although *Alkbh7*$^{-/-}$ mtDNA did accumulate more modifications in old-age.[10] Together these observations suggest ALKBH7 may not play significant roles in either the repair of known AlkB substrates, or in oxidizing as-yet unknown nucleic acid substrates. Similarly, efforts to identify potential protein substrates of ALKBH7 have not yielded insight to its function, with both a yeast-2-hybrid screen and several large mitochondrial protein:protein interaction databases not reporting any ALKBH7-binding proteins.[11-14]

While the nucleic acid or protein substrate(s) of ALKBH7 remain(s) unclear, previous studies using RNAi or genetic ablation in human cells have found that ALKBH7 is required for programmed necrosis induced by DNA alkylating agents.[15] Moreover, *Alkbh7*$^{-/-}$ mice exhibit protection against alkylation-induced cell death in certain tissues.[16] Notably this phenotype is only observed in males, even though *Alkbh7* is not a sex-linked gene. Furthermore, the *Alkbh7*$^{-/-}$ mouse exhibits obesity due to defective fatty acid β-oxidation,[17] and an *Alkbh7* mis-sense mutation (R191Q) has been linked to prostate cancer.[18] However, it is unknown how these phenotypes are linked to the biochemical function of ALKBH7 as an α-KG dioxygenase.

The heart is a mitochondria-rich tissue, and cardiomyocyte necrosis plays a key role in cardiac pathology such as that occurring in ischemia-reperfusion (IR) injury.[19] As such, the requirement for

ALKBH7 in other models of necrosis[15] makes the protein a potential target for the modulation of cell death in response to IR injury. Herein, focusing on heart tissue we employed a multi-omics approach to elucidate ALKBH7 biology, finding that hearts from *Alkbh7*$^{-/-}$ mice are protected against IR injury. We also find that a core component of this protected phenotype is the rewiring of glucose and glyoxal metabolism in response to elevated glycative stress. These findings imply potential therapeutic utility for ALKBH7 inhibitors to prevent necrosis in IR and other conditions.

RESULTS

The complete original data used to generate all figures in the main document and supplement are contained in a spreadsheet available at DOI: 10.6084/m9.figshare.12200273 (DOI reserved, unembargoed upon publication).

Proteomic analysis to identify ALKBH7 substrates suggests it is not a prolyl-hydroxylase.

Several members of the α-KG dioxygenase superfamily possess prolyl-hydroxylase activity, and ALKBH7 is known to auto-hydroxylate on Leucine 110, suggesting it has hydroxylase activity.[9] To investigate the hypothesis that ALKBH7 may be a prolyl-hydroxylase, a tandem-mass-tag (TMT) proteomic approach was employed to identify potential targets, assuming such targets would contain less hydroxyproline (P-OH) in *Alkbh7*$^{-/-}$ vs. WT samples. Using heart tissue from *Alkbh7*$^{-/-}$ and WT mice (**Fig. 1 - Suppl. 1**), a total of 451 P-OH containing peptides were identified, and their abundances normalized to those of their 238 parent proteins. Differential analysis, applying thresholds of ±1.5-fold change and $p<0.05$ for significance, revealed only a handful of peptides with altered P-OH (volcano plot **Fig. 1A**, top 5 up/down hits in **Fig. 1B**). Only one peptide showed significantly less P-OH: the β-oxidation enzyme hydroxyacyl-CoA dehydrogenase (*Hadh* gene).

It is reported that *Alkbh7*$^{-/-}$ mice are obese and harbor a baseline defect in β-oxidation of long-chain fatty acids such as oleate, which can be overcome when stimulated by fasting.[17] To determine β-oxidation levels in the heart, a mostly fat-burning organ, Seahorse XF analysis of isolated cardiomyocytes from *Alkbh7*$^{-/-}$ and WT mice was undertaken, revealing a small but significant decrease in oleate oxidation at baseline, with this effect disappearing upon stimulation of maximal respiration (**Fig. 1 - Suppl. 2**). Although HADH is primarily involved in the β-oxidation of short chain fatty acids, we hypothesized based on P-OH proteomic data and the obese phenotype that prolyl-hydroxylation of HADH may regulate its activity. However, western blotting showed no alteration in HADH protein levels

between WT and *Alkbh7*$^{-/-}$ (**Fig. 1B**), and activity assays of both short-chain HADH (*Hadh* gene) and long-chain HADH (*Hadha* gene) revealed no differences between genotypes (**Fig. 1D**). As such, we consider it unlikely that prolyl-hydroxylation by ALKBH7 is an underlying cause of defective β-oxidation in the *Alkbh7*$^{-/-}$ mouse.

To identify potential ALKBH7 binding partners, a FLAG-tag pull-down interactome experiment was performed, under either baseline or DNA alkylation stress conditions (see **Fig. 2 - Suppl. 1**). As the Table in **Supplementary File 1** shows, several mitochondrial heat shock proteins were identified as ALKBH7 interactors, despite no such proteins being differentially hydroxylated (**Fig. 1A**). This finding is in agreement with a recent antibody-based immunoprecipitation study which suggested a role for ALKBH7 in proteostasis,[20] although the functional significance of this for necrosis is unclear (see **Fig. 5 - Suppl. 2** and related text). An additional protein hit was the NDUFS7 subunit of respiratory complex I, which the BioPlex interactome database also reports as an ALKBH7 interacting protein.[21] However, enzyme assays in heart and liver mitochondria from WT and *Alkbh7*$^{-/-}$ mice revealed no differences in the activities of complex I and several other key mitochondrial enzymes (**Fig. 2 - Suppl. 2**), suggesting no role for ALKBH7 in regulating complex I function. Overall, consistent with a general paucity of ALKBH7 binding proteins,[11-14] we consider it unlikely that the necrosis function of ALKBH7 is due to prolyl-hydroxylation or the binding and modulation of mitochondrial heat shock proteins or respiratory complexes.

Proteomic abundance analysis in Alkbh7*$^{-/-}$ *indicates re-wiring of glyoxal metabolism.

In parallel with analysis of P-OH, the TMT proteomic experiment also yielded relative abundance values for 3,737 proteins in *Alkbh7*$^{-/-}$ and WT hearts, with a volcano plot (**Fig. 2A**) revealing several differences which may underlie the metabolic phenotype of the knockout animals.[A] The lipid droplet protein perilipin-5, which signals via Sirt1/PPAR-α to drive mitochondrial biogenesis and fat oxidation,[22] was 25% lower in *Alkbh7*$^{-/-}$ vs. WT. In addition, fructose-1,6-bisphosphatase 2 (FBP2/PFK2) was 31% lower in *Alkbh7*$^{-/-}$ vs. WT, a finding typically associated with acceleration of glycolysis.[23] It was also recently found that a mutation in ALKBH7 is selected for in the evolution of bats toward a nectivorous (sugar-rich) diet, [24] suggesting that the enzyme is inherently linked to glucose metabolism.

[A] Although ALKBH7 itself appears in the proteomic data set, this is not an indication of improper deletion. The original knockout targeted exons 2-5 containing the active site, whereas the peptides found here were in exon 1. While we cannot exclude the possibility of dominant negative effects due to an inactive truncation product, limited experiments with heterozygous animals (not shown) did not reproduce any phenotypes observed in homozygous knockouts.

In addition, a highly significant (p=0.00006) 1.6-fold elevation was seen in lactoylglutathione lyase (glyoxalase I, GLO-1) in *Alkbh7*$^{-/-}$ vs. WT. This observation was confirmed by enzymatic activity assay (**Fig. 2B**) and by western blot (**Fig. 2D/E**), with a similar activity difference also observed in *Alkbh7*$^{-/-}$ vs. WT liver tissue (**Fig. 2 - Suppl. 2**). GLO-1 is part of the dialdehyde detoxification pathway that handles toxic metabolites such as the glycolytic by-product methylglyoxal (MGO), recycling it to D-lactate, thus avoiding the generation of advanced glycation end products (**Fig. 2F**).[25] No change was seen in the activity of the companion enzyme GLO-2 in *Alkbh7*$^{-/-}$ (**Fig. 2C**). The only other protein significantly upregulated in *Alkbh7*$^{-/-}$ was heme binding protein 1 (Hebp1), and notably a recent study found both GLO-1 and Hebp1 were upregulated in Alzheimer's disease,[26] suggesting these proteins may share a common upstream regulator. Overall, despite extensive proteome coverage, a surprisingly small number of proteins (4) were up- or down-regulated in *Alkbh7*$^{-/-}$ heart.

Although ALKBH7 is generally thought to be mitochondrial, several of the differences observed between WT and *Alkbh7*$^{-/-}$ heart were cytosolic proteins, including GLO-1. In this regard, western blotting (**Fig. 1 - Suppl. 1**) showed immunoreactivity for ALKBH7 in the cytosolic compartment (uncontaminated by the mitochondrial marker ANT-1) as well as in mitochondria, suggesting ALKBH7 may not be exclusively mitochondrial. The relative importance of sub-populations of ALKBH7 in driving necrosis or other phenotypes is currently unclear, and it is possible that differences in expression of cytosolic proteins may originate from the cytosolic population of the ALKBH7 enzyme.

Metabolomics analysis in Alkbh7*$^{-/-}$ *confirms rewired glyoxal metabolism.

To further probe metabolism in *Alkbh7*$^{-/-}$ hearts, a steady-state metabolomics analysis was undertaken (**Fig. 3A**), which revealed perturbations in several key metabolites related to MGO stress. The antioxidants carnosine and glutathione (GSH) were both significantly lower in *Alkbh7*$^{-/-}$, consistent with their being utilized in the detoxification of MGO.[27] As noted above (**Fig. 2F**), GLO-2 recycles GSH consumed by GLO-1, so an elevation in GLO-1 activity without a concomitant upregulation of GLO-2 would be predicted to result in GSH depletion. Furthermore, numerous metabolites in the lower half of glycolysis were elevated in *Alkbh7*$^{-/-}$, suggesting acceleration of this pathway (**Fig. 3B**). To test this hypothesis directly, ^{13}C-glucose tracing was employed to measure glycolytic flux in perfused mouse hearts,[28] and the results in **Fig. 3C** show that glycolytic flux was indeed faster in *Alkbh7*$^{-/-}$. While this might be anticipated to result in elevated MGO levels, unfortunately due to the labile nature of MGO attempts to measure free MGO levels in WT and *Alkbh7*$^{-/-}$ samples were unsuccessful. However,

157 further evidence for elevated MGO stress in *Alkbh7*$^{-/-}$ was seen in the form of elevated MGO protein
158 adduct levels in both cytosol and mitochondria (**Fig. 3D-F**). Overall, these data suggest the *Alkbh7*$^{-/-}$
159 heart experiences elevated glycative stress. Notably, neither α-ketoglutarate nor succinate (the
160 respective substrate and product of α-KG dioxygenases) were significantly altered between WT and
161 *Alkbh7*$^{-/-}$, indicating the enzyme does not contribute to the overall bulk turnover of these metabolites,
162 relative to Krebs' cycle activity. This is in agreement with the finding that neither α-KGDH nor SDH
163 activities were different between *Alkbh7*$^{-/-}$ and WT (**Fig. 2 - Suppl. 2**).
164
165 ***Loss of ALKBH7 protects the heart from ischemia-reperfusion (IR) injury.***
166 In addition to metabolic effects, a key phenotype resulting from *Alkbh7* ablation is protection
167 against necrosis.[15] In seeking links between glyoxal metabolism and necrosis, it is notable that both
168 glycative stress and necrosis are implicated in the pathology of cardiac IR injury.[29-31] In addition, a
169 mitochondrially-targeted MGO scavenging molecule was recently shown to protect the heart against IR
170 injury.[32] To test the hypothesis that loss of ALKBH7 may protect against IR, perfused hearts from WT
171 and *Alkbh7*$^{-/-}$ mice were subjected to IR injury (25 min. global ischemia, 60 min. reperfusion). As shown
172 in **Fig. 4A/B**, male *Alkbh7*$^{-/-}$ hearts exhibited significantly improved post-ischemic functional recovery
173 and significantly lower infarct size (an indicator of necrosis) compared to WT.
174 Consistent with sexual dimorphism in the necrosis effects of ALKBH7,[16] no protection against IR
175 injury was observed in hearts from female *Alkbh7*$^{-/-}$ mice (**Fig. 4 - Suppl. 1 A/B**). Interestingly, it was
176 found that female *Alkbh7*$^{-/-}$ mice still exhibited an elevation in GLO-1 at both the protein and activity
177 level (**Fig. 4 - Suppl. 1 C/D/E**). However, the elevated GLO-1 activity in female *Alkbh7*$^{-/-}$ only
178 approached the levels seen in WT males, owing to a lower baseline GLO-1 activity in females.
179 Underlying this lower GLO-1 activity, we also found that that female *Alkbh7*$^{-/-}$ mice did not exhibit an
180 elevation in MGO adduct formation relative to WT (**Fig. 4 - Suppl. 1 F/G/H**). This suggests that glycative
181 stress is blunted in females, such that female *Alkbh7*$^{-/-}$ mice may not reach a threshold of GLO-1
182 activity required for protection. Later results highlight the requirement of GLO-1 for protection of male
183 *Alkbh7*$^{-/-}$ mice.
184 Several paradigms of cardioprotection are known to decline with age, [33-36] and consistent with
185 this we also found that protection against IR injury was lost in aged male *Alkbh7*$^{-/-}$ mice (**Fig. 4 - Suppl.**
186 **2**). Notably, GLO-1 activity has been shown to decline with age. [25] Together, these results suggest that

ALKBH7 may play a role in necrosis by regulating MGO metabolism, and its ablation triggers a signaling response that endows protection against IR in the heart.

Acute pharmacologic ALKBH inhibition elicits cardioprotection.

The activity of α-KG dioxygenases can be inhibited by D- or L- isomers of the non-canonical metabolite 2-hydroxyglutarate (2-HG),[37] with L-2-HG inhibiting ALKBHs more potently than D-2-HG.[38,39] In addition, acute administration of the generic α-KG dioxygenase inhibitor dimethyloxalylglycine was shown to confer protection against hypoxic injury in a cardiomyocyte model of IR.[40] Since genetic ablation of ALKBH7 was cardioprotective, we thus hypothesized its pharmacologic inhibition may serve a similar purpose. As **Fig. 5 - Suppl. 1** shows, administration of L-2-HG as its dimethyl ester (a common delivery strategy for dicarboxylates) was cardioprotective in WT hearts, eliciting enhanced functional recovery and lower infarct size (albeit the latter non-significant). While L-2-HG is known to have multiple targets, these data suggest the development of more specific ALKBH7 inhibitors may be a promising therapeutic strategy for IR injury.

Cardioprotection in Alkbh7$^{-/-}$ is not due to the mitochondrial unfolded protein response.

We recently showed that activation of the mitochondrial unfolded protein response (UPR^{mt}) is sufficient to induce cardioprotection against IR injury.[41] The genes encoding *LonP1* and *ClpP*, two mitochondrial proteases involved in UPR^{mt} signaling,[42] are also located on mouse chromosome 17 adjacent to the *Alkbh7* gene. In addition, a recent proteomic study proposed a role for ALKBH7 in mitochondrial proteostasis,[20] and our pull-down experiment identified several mitochondrial heat-shock proteins as potential ALKBH7 interactors (**Supplementary File 1**). Furthermore, the related protein ALKBH1 has been shown to partially localize to mitochondria, and its knock-down induces a UPR^{mt}.[43] As such, we hypothesized constitutive UPR^{mt} activation might underlie the cardioprotective effects of ALKBH7 ablation. However, western blotting (**Fig. 5 – Suppl. 2**) showed only small increases in LonP1 and ClpP protein in *Alkbh7$^{-/-}$* (the former non-significant), and a significant decrease in HSP60 (*Hspd1*) protein. We also did not find any UPR^{mt} target proteins upregulated in our proteomics analysis (**Fig. 2**). Overall these observations suggest that modulation of the UPR^{mt} is not a key mechanism by which ALKBH7 regulates necrosis.

Cardioprotection in Alkbh7$^{-/-}$ is not via the mitochondrial permeability transition pore.

A core component of the necrotic cell death machinery is the mitochondrial permeability transition (PT) pore, which is regulated by the cis/trans prolyl-isomerase cyclophilin D (CypD, *ppif*).[44] Parallels between CypD and ALKBH7 function have previously been speculated.[9] In addition, although somewhat counter-intuitive, it has been shown that MGO can inhibit the PT pore,[45] and our data suggest *Alkbh7*$^{-/-}$ mice experience greater MGO stress (**Figs. 2,3**). Thus, we hypothesized ALKBH7 may regulate the PT pore. However, an osmotic swelling PT pore assay in isolated cardiac mitochondria from WT and *Alkbh7*$^{-/-}$ mice revealed only a slight blunting of pore opening in *Alkbh7*$^{-/-}$ (**Fig. 5A/B**). In addition, pore opening in both genotypes was inhibited by CypD inhibitor cyclosporin A, suggesting no differences in the underlying ability of CypD to regulate the pore. An isolated mitochondrial Ca^{2+} handling assay (**Fig. 5C-E**) showed a slight elevation in the amount of Ca^{2+} required to trigger the pore in *Alkbh7*$^{-/-}$, and no difference in Ca^{2+} uptake kinetics. Furthermore, blue-native gel analysis of ATP synthase multimers, which are postulated to contribute to the composition of the PT pore,[46] showed no differences between *Alkbh7*$^{-/-}$ and WT (**Fig. 5 - Suppl. 3**). Together these findings suggest the mitochondrial PT pore is not a central mechanism by which ALKBH7 regulates necrosis.

Cardioprotection in Alkbh7*$^{-/-}$ *requires glycolysis.

Several paradigms of cardioprotection against IR injury have been linked to elevated glycolysis.[28] Since *Alkbh7*$^{-/-}$ mice exhibit elevated glycolysis, we decided to test the requirement for elevated glycolysis in the protected phenotype, by perfusing knockout hearts in the absence of glucose (i.e., fat as the only metabolic substrate). While no difference in baseline function was observed (thus indicating no overall defect in adapting to burning fat only), **Fig. 6 - Suppl. 1** shows that removal of glucose abrogated cardioprotection in *Alkbh7*$^{-/-}$. Contrary to observations with a rich substrate mix (**Fig. 4**), infarct size was significantly greater in glucose-free-perfused *Alkbh7*$^{-/-}$ hearts vs. WT. These data indicate that, as with several other modes of cardioprotection (e.g., ischemic preconditioning), glucose metabolism is a necessary component of the protection stemming from ALKBH7 loss.

Cardioprotection in Alkbh7*$^{-/-}$ *requires GLO-1.

Since we also showed that GLO-1 was elevated in response to ALKBH7 loss, we hypothesized this may also be an underlying component of the protected phenotype seen in the knockouts. To probe the requirement for elevated GLO-1 in cardioprotection, the GLO-1 inhibitor *S*-p-Bromobenzylglutathione cyclopentyl diester (SBB-GSH-CpE) was administered to hearts prior to

ischemia. As **Fig. 6** shows, 1 μM SBB-GSH-CpE had no effect on WT hearts (c.f. **Fig. 4**), but completely abrogated cardioprotection in *Alkbh7*$^{-/-}$ hearts. Separate experiments to assay GLO-1 enzyme activity in SBB-GSH-CpE treated hearts indicated this protocol resulted in 34 ± 8% GLO-1 inhibition (mean ± SD).

A significant depression of cardiac function was observed immediately upon SBB-GSH-CpE administration to *Alkbh7*$^{-/-}$ hearts, with no effect in WT (**Fig. 6A**). Due to its higher baseline level of MGO stress (**Fig. 3D-F**), the *Alkbh7*$^{-/-}$ heart is likely more dependent on GLO-1 activity and may therefore be hypersensitized to its inhibition. This finding suggests an important role for anti-glycation enzymes such as GLO-1 in cardiac functional homeostasis. In this regard, the mitochondrial protein DJ-1 has been shown to function as a glyoxal detoxifying enzyme,[47] and was also recently shown to confer cardioprotection.[48,49] However, no differences in the levels of DJ-1 were observed in *Alkbh7*$^{-/-}$ hearts (**Fig. 6C**), suggesting that the signaling pathways engaged by ALKBH7 loss are somewhat specific to GLO-1 and may not engage other dialdehyde detoxification pathways.

DISCUSSION

Summarizing the current findings, a comprehensive analysis of the *Alkbh7*$^{-/-}$ mouse heart suggests ALKBH7 is not a functional prolyl-hydroxylase that regulates mitochondrial activity, and that its role in necrosis involves rewiring of MGO metabolism. While our prolyl-hydroxylation proteomic findings were made at baseline, it may be argued that ALKBH7 could adopt a prolyl-hydroxylase function only under stress conditions. However, like all other α-KG dioxygenases, ALKBH7 uses oxygen as a substrate, so would be unlikely to engage additional hydroxylation substrates under oxygen-limited conditions such as ischemia.

We propose a scheme linking ALKBH7 loss to cardioprotection and glycative stress, as outlined in **Fig. 6D**. Specifically, ALKBH7 loss triggers a mild defect in fat oxidation and an elevated rate of glycolysis, possibly via perilipin 5 and fructose-1,6-bisphosphatase 2 (proteomic data). The resulting glycative stress triggers rewiring of glyoxal metabolism, in particular GLO-1 induction, which then endows the added benefit of protection against IR injury. In addition, elevation of glycolysis *per se* may contribute to the cardioprotected phenotype (**Fig. 6 - Suppl. 1**).[28] The relative position of GLO-1 as a downstream consequence of altered metabolism or as a driver of it, is currently unclear. In this regard, a recent systems genetic analysis identified *Glo1* as an important gene in the regulation of lipid metabolism,[50] suggesting GLO-1 and metabolic fuel switching may be parallel responses to ALKBH7 loss. The exact mechanism by which ALKBH7, thought to be a mitochondrial protein, can communicate

to GLO-1, a cytosolic protein, is unclear, although our finding that a portion of ALKBH7 protein is located in the cytosol raises the possibility that it is the cytosolic component of ALKBH7 which mediates these effects.

A surprising finding herein was that GLO-1 was upregulated in *Alkbh7*$^{-/-}$ mice without concomitant upregulation of its companion enzyme GLO-2. The GLO-1/GLO-2 system (**Fig. 2F**) typically recycles GSH, and as predicted *Alkbh7*$^{-/-}$ mice exhibited depleted GSH levels. While such a finding might cast focus on oxidative stress as a phenotypic driver in *Alkbh7*$^{-/-}$, recent discoveries have implicated the GLO-1/GLO-2 system in epigenetic signaling. Specifically, the product of GLO-1, S-lactoylglutathione (SLG), has been shown to mediate the lactylation of lysine residues,[51] including in histones,[52] which may represent a link between metabolism and gene regulation. As such, it is possible that SLG levels may be elevated in *Alkbh7*$^{-/-}$, which could drive epigenetic changes that underlie the phenotypes of the knockout. Unfortunately, attempts to quantify lysine-lactylation by western blotting were hampered by a cross-reactivity of the antibody with MGO adducts (pre-print at https://osf.io/sba8j).

The origins of the sexual dimorphism in necrosis and IR injury in *Alkbh7*$^{-/-}$ mice remain unclear. In this regard, a recent study identified S-nitrosoglutathione reductase (GSNO-R) as a potential modulator of IR injury in male vs. female mice[53]. Notably GSNO-R can function as a formaldehyde dehydrogenase, and formaldehyde is a product of the DNA demethylation reaction carried out by many ALKBHs. As such, it is possible the role of ALKBH7 in necrosis may involve generation of formaldehyde, such that ALKBH7 deletion in males is protective by lowering the levels of this metabolite, whereas females have elevated GSNO-R levels so are already conditioned to lower formaldehyde levels.

The results herein may also provide insight to the complex biology of the diabetic heart. The incidence and progression of cardiac pathology such as heart failure is significantly worse in diabetes, and this is thought to be partly due to elevated glycative stress.[54,55] However, somewhat paradoxically the diabetic heart is relatively protected against acute IR injury.[56-58] As such, it is interesting to speculate whether the mechanisms of ischemic tolerance seen in the male *Alkbh7*$^{-/-}$ heart, stemming from GLO-1 upregulation, may also apply to the diabetic heart. An additional ramification of the current results may be in the area of cancer biology, where there has been interest in the potential use of GLO-1 inhibitors to target metabolic vulnerabilities of cancer cells. [51,59] The apparent cardiotoxic effects of SBB-GSH-CpE (**Fig. 6**) suggest that caution may be required in the use of such drugs to ensure they do not elicit cardiac toxicity.

Although the precise biologic function and substrates of the ALKBH7 enzyme remain unknown, it is tempting to speculate that the native function of the enzyme may be in the detoxification of MGO or reactive intermediates prior to the formation of glycative adducts, such that ALKBH7 deletion drives the responses seen herein, to limit formation of MGO and its downstream intermediates. Recently it was found that an R182Q substitution in ALKBH7 was positively selected for during the evolution of nectivorous bats (whose diet is mostly sugar),[24] thus furthering the notion that ALKBH7 is inherently linked to glucose metabolism, a major source of MGO. Overall, our findings highlight the importance of MGO homeostasis in the heart and suggest novel therapeutic targets for protection of tissues against IR injury. Further work is required to elucidate the signaling mechanisms that link the biochemical function of ALKBH7 to MGO metabolism.

ACKNOWLEDGEMENTS

Work in the laboratory of PSB is funded by a grant from the US National Institutes of Health (R01-HL071158). CAK is funded by a post-doctoral fellowship from the American Heart Association (#19POST34380212). LK and EM are funded by the NHLBI-NIH Intramural Research Program (ZO1-HL002066). DF was funded by a Rochester Aging Research Center Pilot Grant. We acknowledge S. Patel and M. Gucek in the NHLBI Proteomics Core Facility for collaborating on the proteomics in murine hearts. We thank Rudi Fasan (Rochester) for help with synthesis of dimethyl-L-2HG.

CONFLICT OF INTEREST

The authors declare they have no conflicts of interest, financial or otherwise, to disclose regarding this work.

METHODS

Animals & materials

Alkbh7$^{-/-}$ mice on a C57BL/6J background[16,17] were bred conventionally (WT x KO), PCR genotyped at weaning, and maintained according to the "NIH Guide" (8th edition, 2011) on an IACUC approved protocol, with food and water available ad libitum. The colony has been back crossed into fresh C57BL/6J stocks for at least 20 generations. Since murine *Alkbh7*$^{-/-}$ phenotypes are only seen in males, primarily male mice were used (except where indicated), with littermate wild-type controls, at ages of 8-12 weeks (young) or 1.5 years (old). All procedures were performed following administration

of heparin (250 units) and tribromoethanol anesthesia (200mg/kg ip). All chemicals and other reagents were from Sigma-Aldrich (St. Louis MO) or VWR (Radnor PA), unless otherwise noted. For the synthesis of dimethyl-L-2-hydroxyglutarate, a drop of concentrated HCl was added to a solution of 0.5 g (S)-(+)-5-oxo-2-tetrahydrofurancarboxylic acid (Sigma-Aldrich #301469) in 3.84 ml dry MeOH. The reaction mixture was heated to reflux and stirred vigorously overnight, then quenched with saturated NaHCO3, filtered and concentrated in vacuo. Crude material was purified via flash chromatography on silica (50% EtOAc in n-hexane) to obtain the desired product as a clear oil, as reported. [60]

Isolated perfused hearts

Following heparin/anesthesia, the aorta was cannulated in-situ and the heart transferred to the perfusion apparatus, then retrograde perfused at 37°C with gassed (95% O_2/5% CO_2) Krebs-Henseleit buffer (KHB), as described.[28] Left ventricular pressure was digitally recorded at 1 kHz via a transducer-linked water-filled balloon. Following 15 min. equilibration, ischemia-reperfusion (IR) injury comprised 25 min global non-flow ischemia plus 60 min. reperfusion. Hearts were then sliced and stained with triphenyltetrazoliumchloride for 20 min., fixed in 4% formalin for 24h., and slices digitally imaged for infarct size calculation by planimetry. KHB contained 5 mM glucose, 1.2 mM lactate, 0.5 mM pyruvate and 100 µM palmitate (conjugated 6:1 with fat-free bovine serum albumin) as metabolic substrates, unless indicated. The following experiments were conducted: **(i)** IR alone: WT and *Alkbh7*$^{-/-}$ hearts subjected to IR in 3 cohorts: young males, young females, old males. **(ii)** GLO-1 inhibitor IR: Young male WT and *Alkbh7*$^{-/-}$ hearts were subjected to IR, with 1 µM SBB-GSH-CpE delivered for 10 min. prior to ischemia. A small number of SBB-GSH-CpE treated WT hearts were snap-frozen without ischemia, for measurement of GLO-1 activity. **(iii)** Glucose-free IR: Young male WT and *Alkbh7*$^{-/-}$ hearts were perfused with KHB containing palmitate-BSA alone (no glucose, lactate, pyruvate) and subjected to IR injury. **(iv)** Proteomics & steady-state metabolomics: Young male WT and *Alkbh7*$^{-/-}$ hearts were perfused for 15 min. then snap-frozen and stored at $^{-}$80°C until analysis. **(v)** Metabolic flux: Young male WT and *Alkbh7*$^{-/-}$ hearts were perfused with KHB. Following equilibration, glucose in KHB was replaced with 5 mM [U-^{13}C] glucose, and perfusion continued for 5 min., followed by snap-freezing and storage at $^{-}$80°C until analysis. **(vi)** Dimethyl L-2-hydroxyglutarate plus IR: Young male WT hearts were subjected to IR, with 10 µM DM-L-2-HG delivered for 20 min. prior to ischemia.

Isolated mitochondrial experiments

Mouse heart mitochondria were isolated by differential centrifugation in sucrose based media essentially as described.[61,62] Following anesthesia, hearts were extirpated into ice-cold media comprising 300 mM sucrose, 20 mM Tris-HCl, 2 mM EGTA, pH 7.35 at 4°C. Tissue was chopped and washed twice to remove blood then homogenized in 4 ml media (IKA Tissumizer, 22,000 rpm). Homogenates were centrifuged at 800 x g, 5 min. Supernatants were centrifuged at 10,800 x g, 5 min., and pellets washed by a further 2 centrifugation steps with final resuspension in 30 µl. For Ca^{2+} handling experiments (see below) the final spin utilized EGTA-free media. Protein was determined by the Lowry method.[63] Mitochondrial permeability transition (PT) pore opening, induced by 100 µM $CaCl_2$, was measured via spectrophotometric light scatter at 520 nm using a Beckman DU800 spectrophotometer, as described.[64] Mitochondria were incubated at 0.5 mg/ml in buffer comprising 120 mM KCl, 3 mM KH_2PO_4, 50 mM Tris, 5 mM succinate and 5 µM rotenone, pH 7.35 at 37˚C. Following $CaCl_2$ addition (100µM), swelling was monitored for 20 min. In some incubations, cyclosporin A (5 µM) was added prior to $CaCl_2$.

Mitochondrial Ca^{2+} handling was assayed using the fluorescent extra-mitochondrial dye Ca^{2+}-green-5N. Mitochondria were incubated at 0.25 mg/ml in buffer comprising 50 mM KCl, 150 mM sucrose, 2 mM KH_2PO_4, 20 mM Tris, 5 mM succinate, 5 µM rotenone and 500 nM Ca^{2+}-green-5N, pH 7.35 at 37˚C. Pulses of 10 µM $CaCl_2$ were added every 2 min., and fluorescence measured using an Agilent Cary Varian Eclipse spectrofluorimeter (λ_{EX} 506 nm, λ_{EM} 530 nm), as described.[65]

Liver mitochondria were isolated by differential centrifugation essentially as previously described.[62] Livers were removed from anesthetized male WT and *Alkbh7*$^{-/-}$ mice and chopped into small pieces with double scissors in ice-cold liver mitochondria isolation medium (LMIM, 250 mM sucrose, 10 mM Tris hydrochloride, 1 mM EGTA, pH 7.4 at 4°C) and homogenized using a glass Dounce homogenizer. The homogenate was centrifuged at 1,000 x *g* for 3 min .and the supernatant decanted to a fresh tube, avoiding fat. This was followed by three rounds of centrifugation at 10,000 x *g*, 10 min., discarding the supernatant each time. The pellet was resuspended in 1 ml LMIM and protein quantified by the Lowry method.[63]

Protein extraction and preparation for proteomics

Proteomic analysis was performed essentially as described.[66] Male WT and *Alkbh7*$^{-/-}$ hearts for proteomic analysis were perfused in Langendorff mode as described above for 5 min., snap-frozen in liquid N_2 with Wollenberger tongs, then ground to powder and stored in two portions at -80 °C. One

404 half of each heart was shipped on dry ice from Rochester NY to NHLBI (Bethesda MD) for proteomic
405 analysis. Frozen heart samples were homogenized in 280 mM sucrose, 10 mM HEPES, 1 mM EGTA, and
406 1% (w/v) laurylmaltoside supplemented with 1X protease inhibitors (Millipore Sigma #4693159001)
407 and 1X phosphatase inhibitors (Millipore Sigma # 4906837001) in a Precellys 24® with Cryolys (Bertin
408 technologies). Protein was determined using a Bradford assay (Sigma #B6916), and 100 µg protein was
409 brought to 100 µl final volume with 100 mM triethylammonium bicarbonate (TEAB). Protein was
410 reduced with 10 mM dithiothreitol at 55°C for 60 min. rocking at 650 rpm, then alkylated with 18 mM
411 iodoacetamide for 60 min. protected from light. Protein was precipitated overnight with 6 volumes
412 acetone at -20 °C, then resuspended 100 mM triethylammonium bicarbonate (TEAB) and sonicated
413 briefly in a chilled water bath sonicator. Protein was digested with 50 µg Trypsin (Promega #V5111)
414 overnight at 37 °C with shaking at 650 rpm. Tryptic peptides were tagged with Tandem Mass Tag (TMT)
415 labeling reagents (Thermo Fisher #90110 and #A37724) according to the manufacturer's instructions.
416 Labeled peptides were then lyophilized, resuspended in 50 mM ammonium bicarbonate, and layered
417 over resin (G-Biosciences #GBS10-800) to remove residual detergent, according to manufacturer
418 instructions. Eluted labeled tryptic peptides were lyophilized, resuspended in 0.1% (v/v) formic acid
419 (FA), and desalted using Hydrophilic-Lipophilic-Balanced (HLB) columns (Waters #186000383)
420 according to manufacturer instructions. Eluted peptides were lyophilized and resuspended for off-line
421 fractionation.
422
423 *HPLC fractionation & LC-MS analysis*
424 Dried and labeled tryptic peptides were reconstituted with basic reverse-phase liquid
425 chromatographic (bRPLC) buffer A (10 mM TEAB, pH 8.0) and separated using a C18 column (Xbridge
426 130 Å, 3.5 µm, 4.6 mm x 150mm, Waters) on a 1200 series HPLC (Agilent). The linear gradient
427 comprised 5 – 40% solvent B (10 mM TEAB, acetonitrile, pH 8.0) over 96 minutes, with fractions
428 collected every minute. The 96 fractions were later combined manually to 17 fractions and lyophilized.
429 Protein identification by LC-MS/MS employed an Orbitrap Fusion Lumos Tribid mass
430 spectrometer (Thermo Scientific) interfaced with an Ultimate 3000 Nano-HPLC apparatus (Thermo
431 Scientific). Peptides were fractionated by EASY-Spray PepMAP RPLC C18 column (2 µm, 100 Å, 75 µm x
432 50 cm) using a 120 min. linear gradient of 5 - 35% acetonitrile in 0.1% FA at 300 nl/min flow rate. The
433 instrument was operated in data-dependent acquisition mode (DDA) using fourier transform (FT) mass
434 analyzer for one survey MS scan. This was done on selected precursor ions followed by top 3 second

data-dependent higher-energy collision (HCD)-MS/MS scans for precursor peptides with 2-7 charged ions above a threshold ion count of 10,000 with normalized collision energy of 37%. Survey scans of peptide precursors from 300 to 2000 m/z were performed at 120k resolution and MS/MS scans were acquired at 50,000 resolution with a m/z range 100-2000.

Protein identification and analysis

All MS and MS/MS raw spectra of TMT experiments were processed and searched using Sequest HT and Mascot algorithms within Proteome Discoverer 2.2 software (PD2.2, Thermo Scientific). Precursor mass tolerance was set at 12 ppm, fragment ion mass tolerance to 0.05 Da, trypsin enzyme with 2 mis cleavages. Carbamidomethylation of cysteine was set as a fixed modification; and TMT 6-plex (lysine), TMT 6-plex (N-term), deamidation of glutamine and asparagine, oxidation of proline and methionine were set as variable modifications. The mouse sequence database from Swiss-prot was used for database search. Identified peptides were filtered for maximum 1% false discovery rate (FDR) using the Percolator algorithm in PD 2.2 along with additional peptide confidence set to high. The final lists of protein identification and quantitation were filtered by PD 2.2 with at least 2 unique peptides per protein identified with medium confidence.

The method overall detected 49,427 peptides representing 5,642 proteins. Filtering for proteins with more than 2 peptides identified in either search engine (Mascot or Sequest) yielded 3,737 proteins with an average 29.13% sequence coverage (95% confidence interval 28.49–29.76%). Filtering the total peptide set for P-OH containing peptides yielded 625 peptides, with 451 of these having a corresponding abundance value for the parent protein, originating from a total of 238 individual proteins. The abundance of each P-OH containing peptide was normalized to abundance of its parent protein, to determine relative hydroxylation levels between WT and *Alkbh7*$^{-/-}$ paired samples.

Immunoprecipitation to identify ALKBH7 binding partners

The coding region for human ALKBH7 was and cloned into pcDNA3.1 (Invitrogen) for expression as C-terminal 3xFLAG tag fusion protein. Transient transfection and cellular extract production were performed as previously described.[67] Negative control cells were transfected with vector only. Briefly, 2.5 × 106 HEK 293T cells were transiently transfected by calcium phosphate DNA precipitation with 20 µg of plasmid DNA, followed by preparation of the lysate by hypotonic freeze-thaw lysis at 48 h. post-transfection. Whole-cell extract was rotated with 10 µl of FLAG M2 antibody resin (Sigma) for 2 h. at 4

°C in lysis buffer (150 mM NaCl, 20 mM HEPES, 2 mM MgCl2, 0.2 mM EGTA, 10 % (v/v) glycerol, 1 mM dithiothreitol, 0.1 mM phenylmethylsulfonyl fluoride, 0.1 % (v/v) NP-40, pH 7.9). Resin was washed extensively using the same buffer, and bound proteins eluted with two sequential volumes of wash buffer containing 100 μg/ml of 3×FLAG peptide (Sigma). Frozen stocks of the HEK293 cell line were obtained at least annually from ATCC (Manassas VA). Cell line identity was not independently authenticated by us, but cells were confirmed to be free of mycoplasma contamination.

Protein identification was performed by the MIT Center for Cancer Research Biopolymers Laboratory (https://ki.mit.edu/sbc/biopolymers). Gel slices of protein bands were excised, reduced, alkylated, and digested in solution with trypsin, followed by purification and desalting of peptides on analytical C18 column tips. Peptide samples were analyzed by chromatography on an Agilent model 1100 Nanoflow high-pressure liquid chromatography (HPLC) system coupled by electrospray ionization to a Thermo LTQ ion-trap mass spectrometer. Protein identification through tandem mass spectrum correlation was performed using SEQUEST. Spectra had to match full tryptic peptides of at least 7 amino acids, have a normalized difference in cross-correlation scores (ΔCn) of at least 0.1, and have minimum cross-correlation scores (Xcorr) of 1.8 for singly charged, 2.5 for doubly charged, and 3.5 for triply charged spectra with at least 50 % ion coverage. Proteins from the vector-only control condition were eliminated from the mass spectrometric analysis.

Metabolomics

Male WT and *Alkbh7*$^{-/-}$ hearts for metabolomics analysis were perfused in Langendorff mode as described above for 5 min., snap-frozen in liquid N_2 with Wollenberger tongs, then ground to powder and stored in two portions at -80°C. Heart powder was serially extracted in 80% aqueous methanol, extracts evaporated to dryness under N_2 and resuspended in 50% aqueous methanol. Liquid chromatography-tandem mass spectrometry (LC-MS/MS) analysis was performed by resolving metabolites on a Synergi Fusion RP C18 column (Phenomenex, Torrance CA) with an acetonitrile elution ramp. Metabolites were identified by retention times and by single reaction monitoring (SRM) on a Thermo Quantum TSQ triple-quadrupole mass spectrometer (Thermo Scientific, Waltham MA) as previously described.[28,68]

Metabolite identification used a custom SRM library for which fragmentation patterns including confirming ions at different collision energies were empirically determined from a library of purchased chemical standards. Data were analyzed using XCalibur Qual Browser (Thermo Scientific), with relative

metabolite content being normalized to the sum of all metabolites in each sample run. 8 pairs of samples were prepared and analyzed in April 2017 in a core facility setting, yielding data for 61 metabolites. A further 9 pairs of samples were prepared and analyzed in April 2019 in the senior author's laboratory, yielding additional data for 71 metabolites. Overall the analysis included 90 metabolites in total with 43 common between both data sets. As such the number of biological replicates varied between 8 and 17 depending on the metabolite in question. To process the metabolomic data set, outliers were flagged where the group-wise (WT or *Alkbh7*$^{-/-}$) data for a given metabolite exhibited a greater than 25% standard error, and individual values outside the 95% confidence intervals were removed. Missing values were imputed as weighted medians,[69] only in situations where more than 75% of original values were still present. Of a potential 2286 total data points, 21 outliers and 32 missing values were imputed, representing 2.3% of the total data set.

For the measurement of glycolytic flux, following 20 min. of stable normoxic perfusion, ^{12}C glucose in KH buffer was replaced with [U-^{13}C] glucose, and hearts perfused for a further 5 min. Hearts were then freeze-clamped and processed similar to steady-state metabolomics, with a custom SRM library used to detect isotopologues of common metabolites. Fractional saturation of selected metabolites with ^{13}C label was determined, with correction for natural ^{13}C abundance, as described previously.[28,68]

Western blotting

Hearts from male WT and *Alkbh7*$^{-/-}$ mice were fractionated by differential centrifugation as previously described.[70] Protein content was determined by the Folin-Phenol (Lowry) assay. [63] Non-mitochondrial samples were diluted two-fold in SDS-PAGE sample loading buffer and incubated at 100°C for 5 min. Mitochondrial samples were diluted two-fold in sample loading buffer containing 5 times the standard concentration of SDS and incubated at 25°C for 30 min. Samples were separated by SDS-PAGE (12.5 % or 15 % gels) and transferred to 0.2 µm nitrocellulose membranes and probed with antibodies as recommended by manufacturer's protocols. Antibodies used include anti-ALKBH7 (#A2331, Abclonal, Woburn MA), anti-HSPD1 (#AP2859b Abgent, San Diego CA), anti-LONP1 (#AP19551c Abgent), anti-CLPP (#PA5-79051 Thermo-Fisher, Waltham MA), anti-methylglyoxal (#ab243074 Abcam, Cambridge MA), anti-GLO1 (#ab137098 Abcam), anti-HADHSC (#sc-376525 Santa Cruz Biotech', Dallas TX), Anti DJ-1 (#2134, Cell Signaling Technology, Danvers MA), and anti ANT1 (#ab110322, Abcam). Detection employed horseradish peroxidase-linked secondary antibodies with

chemiluminescent detection (KwikQuant, Kindle Bioscience, Greenwich CT). Sample loading was normalized to Ponceau S staining of membranes immediately after transfer. For most blots frozen samples were used following appropriate fractionation, but for MGO adduct blots we found the signal decayed over time with sample storage at minus 80°C, so freshly harvested samples were used.

Blue-native electrophoresis

Mitochondrial respiratory supercomplexes were extracted and analyzed essentially as described by Beutner *et al*.[71] Briefly, mitochondria (0.5mg/ml) were incubated for 5 min. in respiration buffer comprising 120 mM KCl, 10 mM HEPES, 1 mM EGTA, 5 mM KH_2PO_4, 5 mM $MgCl_2$, pH 7.3 at 37˚C. After centrifugation (14000 x *g*, 10 min.) pellets were suspended in 25 µl of buffer comprising 50 mM NaCl, 40 mM imidazole, 2 mM aminocaproic acid, 1 mM EDTA, 5.7% (w/v) digitonin, pH 7 at 4˚C, and incubated on ice for 20 min. Samples were then centrifuged (14000 x *g*, 10 min.), supernatants mixed 1:1 with loading buffer (50 mM aminocaproic acid, 5% (w/v) Coomassie Blue-G), followed by resolution on 5-8% gradient blue-native gels. For the complex V in-gel assay, the gel was incubated for 2 h. in buffer comprising 35 mM Tris, 270 mM glycine, pH 8.3 at 25˚C. White precipitate complex V activity bands were visualized by adding 135 mM $MgSO_4$, 6.5 mM $Pb(NO_3)_2$, and 7.8 mM ATP to the buffer. The reaction was stopped by adding 50 % methanol and gel imaged.

Cardiomyocyte isolation and Seahorse respirometry

Ca^{2+} tolerant primary adult cardiomyocytes were isolated from male WT and *Alkbh7*$^{-/-}$ mouse hearts by collagenase digestion as previously described.[61,68] yielding ~800,000 rod-shaped cells with >80% viability by Trypan blue assay. The final cell pellet was divided into two portions, each of which was suspended in 1 ml cardiomyocyte incubation buffer (glucose-free DMEM supplemented with 4 mM L-glutamine, 10 mM HEPES, 100 µM sodium pyruvate, 5 mM D-glucose, 500 µM L-carnitine hydrochloride, and 100 µM oleate conjugated 6:1 to fat-free bovine serum albumin (BSA,)pH 7.4 at 37 °C). From this suspension, cells were seeded at 2000/well on laminin-coated Seahorse XF96 V3-PS plates (Agilent, Santa Clara CA) and incubated for 1 h. in a 37 oC humidified incubator. Cardiomyocyte incubation buffer was replaced with unbuffered DMEM (pH 7.4) containing 4 mM L-glutamine, 100 µM sodium pyruvate, 10 mM 2-deoxy-D-glucose, 500 µM L-carnitine hydrochloride and 100 µM oleate conjugated to BSA. The plate was incubated for 30 min at 37 °C, and then oxygen consumption rate (OCR) was measured with a Seahorse XF96 extracellular flux analyzer (Agilent) at baseline and

following sequential injections of 1 μM FCCP + 1 μg/mL oligomycin, 5 μM etomoxir and 1 μM antimycin A + 5 μM rotenone.

Enzyme assays

Enzyme activities were determined in isolated mitochondria and cytosol from hearts and livers of WT and *Alkbh7*$^{-/-}$ mice, as indicated. Mitochondria were freeze/thawed 3x. Complex I was measured spectrophotometrically at 340 nm as the rotenone-sensitive, coenzyme Q_1-linked oxidation of NADH, as previously reported.[72] Cardiac or liver mitochondria were incubated in potassium phosphate buffer (pH 7.2) at 37 ^{o}C containing 2.5 mg/ml BSA, 1 mM KCN, 75 μM NADH. NADH oxidation was followed at 340 nm (ε = 6180 $M^{-1}cm^{-1}$) for 5 min. after addition of 100 μM co-enzyme Q_1. At the end of each run 10 μM rotenone was added and the rotenone-insensitive rate subtracted.

Complex II was measured spectrophotometrically at 60 nm as the rate of succinate-driven, thenoyltrifluoroacetone (TTFA)-sensitive, co-enzyme Q_2-linked reduction of dichlorophenolindophenol (DCPIP) as previously reported.[73] Cardiac and liver mitochondria were incubated in potassium phosphate buffer (pH 7.4) at 37 ^{o}C containing 120 μM DCPIP, 1 mM KCN, 10 μM rotenone, and 50 μM co-enzyme Q_2. The rate of DCPIP reduction was followed at 600 nM (ε = 21 $mM^{-1}cm^{-1}$) for 5 min. after addition of 5 μM succinate. At the end of each run 1 mM TTFA was added and the TTFA-insensitive rate subtracted.

α-Ketoglutarate dehydrogenase was measured spectrophotometrically at 340 nm as the α-ketoglutarate-dependent, 2-Keto-3-methyl-valerate (KMV) sensitive reduction of NAD^+, as described.[74] Cardiac and liver mitochondria were incubated in assay buffer comprising 35 mM KH_2PO_4, 5 mM $MgCl_2$, 0.5 mM EDTA, 0.05 % v/v Triton X-100, 500 μM NAD^+, 200 μM thiamine pyrophosphate, 40 μM reduced Coenzyme-A, 2 mM KCN, 25 μM rotenone, pH 7.25 at 37 ^{o}C. The reaction was initiated by addition of 2 mM α-ketoglutarate and the rate of NAD^+ reduction measured at 340 nm (ε = 6220 $M^{-1}cm^{-1}$) for 5 min. At the end of each run 25 mM KMV was added and the KMV-insensitive rate subtracted.

Citrate synthase was measured spectrophotometrically at 412 nm as the oxaloacetate and Acetyl CoA-linked production of 2-nitro-5-thiobenzoate (TNB) from 5,5'-dithiobis-(2-nitrobenzoic acid, DTNB).[75] Cardiac and liver mitochondria were incubated in assay buffer (100mM Tris, 0.1 % v/v Tritox X-100, 100 μM acetyl CoA, 200 μM DTNB, pH 8.0 at 37 ^{o}C), the reaction initiated by addition of 200 μM

589 oxaloacetate, and the initial linear (pre-plateau) rate of TNB formation measured at 412 nm (ε = 13.6
590 $mM^{-1}cm^{-1}$).

591 The activity of short chain and long chain specific isoforms 3-HydroxyacylCoA dehydrogenase
592 (HADH) was measured spectrophotometrically at 340 nm as the corresponding 3-oxoacyl CoA-linked
593 oxidation of NADH, following literature procedure.[76,77] Cardiac and liver mitochondria were incubated
594 in potassium phosphate buffer (pH 6.3) at 37 °C containing 100 µM NADH, 100 µM dithiothreitol and
595 0.1 % w/v Triton X-100. The reaction was initiated by addition of 50 µM 3-ketopalmitoyl CoA (for long
596 chain HADH) or 50 µM acetoacetyl CoA (for short chain HADH) and the initial liner rate of NADH
597 oxidation followed at 340 nm (ε = 6.22 $mM^{-1}cm^{-1}$).

598 Glyoxalase I (GLO-1) activity was measured spectrophotometrically at 240 nm as the rate of
599 formation of *S*-D-lactoylglutathione (SLG) from the hemithioacetal adduct pre-formed *in situ* by
600 incubation of methylglyoxal and glutathione, as reported.[78] 2 mM glutathione and 2 mM methylglyoxal
601 were incubated in 50 mM sodium phosphate buffer (pH 6.6) at 37 °C for 10 min. Cardiac or liver
602 cytosolic extracts were then added, and the initial linear rate of SLG formation followed at 240 nm (ε =
603 2.86 $mM^{-1}cm^{-1}$) for 5 min.

604 Glyoxalase II (GLO-2) activity was measured spectrophotometrically at 240 nm as the rate of
605 hydrolysis of SLG, as reported.[78] 30 µM SLG was incubated in 50 mM Tris HCl buffer (pH 7.4) at 37 ^{o}C.
606 Cardiac or liver cytosolic extracts were added to the cuvette and the initial linear rate of SLG hydrolysis
607 followed at 240 nm (ε = 3.10 $mM^{-1}cm^{-1}$) for 5 min.

608

609 *Statistics*

610 For all experiments, a single N (biological replicate) was considered to be the material arising
611 from a single animal. N ranged from 3 to 17 depending on experiment, and is indicated in each figure
612 or legend. Statistical significance was assessed by ANOVA with post-hoc Student's t-test. Where
613 appropriate (comparisons between littermate paired samples), paired t-tests were used. Samples from
614 WT and *Alkbh7*$^{-/-}$ were run in random order, and whenever possible experiments were performed in a
615 blinded manner with the experimenter agnostic to the identity of the samples.

616

FIGURE LEGENDS

Figure 1. Proteomic analysis of prolyl-hydroxylation in WT vs. *Alkbh7*$^{-/-}$. Hearts from young male WT or *Alkbh7*$^{-/-}$ mice were analyzed by tandem mass tag LC-MS/MS as per the methods. Abundance of each P-OH peptide was normalized to the abundance of its parent protein. **(A):** Volcano plot showing relative levels of 451 P-OH containing peptides. X-axis shows Log_{10} of fold change (*Alkbh7*$^{-/-}$ / WT) and Y-axis shows Log_{10} of significance (paired t-test, N=5). Proteins crossing thresholds (gray lines) in upper left or right quadrants are labeled. **(B):** Table showing the top 5 P-OH containing peptides exhibiting increased or decreased relative abundance in *Alkbh7*$^{-/-}$ vs. WT. Table shows raw abundance of each P-OH peptide, abundance of the parent protein, and normalized abundance of the P-OH peptide. Annotated sequences highlight the hydroxylated proline residues in red. **(C):** Western blot showing abundance of HADH-SC (*Hadh*) in WT or *Alkbh7*$^{-/-}$ heart mitochondria with quantitation below, normalized to protein loading determined by Ponceau S stained membrane. **(D):** Spectrophotometric activity assays of short-chain and long-chain HADH in WT or *Alkbh7*$^{-/-}$ heart mitochondria. Bar graphs in panels C/D show means ± SE, N=3-5, with p-values (paired t-test) shown above error bars. In bar graphs, N for each group is shown in parentheses.

Figure 1 - Supplement 1. Western blot showing absence of ALKBH7 protein in *Alkbh7*$^{-/-}$ mouse heart. Hearts were fractionated into mitochondrial and cytosolic fractions by western blot. **(A):** Blot showing ALKBH7 in WT mitochondria is lost in *Alkbh7*$^{-/-}$ mitochondria. Protein loading is shown in the Ponceau S stained membrane below. Each lane represents a single animal. **(B):** Blot showing mild ALKBH7 immunoreactivity in cytosolic fraction as well as mitochondria in WT, which is lost from both fractions in the knockout. Protein loading is shown in the Ponceau S stained membrane below. Also shown is a blot for adenine nucleotide translocase 1 (ANT1), indicating no contamination of the cytosolic fraction with mitochondria. N=1 mouse per genotype. Blots are representative of at least 3 independent experiments.

Figure 1 - Supplement 2. Seahorse XF measurement of long chain fatty acid oxidation in WT vs. *Alkbh7*$^{-/-}$ cardiomyocytes. Cardiomyocytes were isolated and XF measurements made as described in the methods. Graphs show oxygen consumption rate in media containing BSA-conjugated oleate as metabolic substrate. Data are shown for baseline, maximal respiration (stimulated by uncoupler FCCP in the presence of oligomycin), and in the presence of the CPT-1 inhibitor etomoxir. Note different Y-axis scales between graphs. Data are means ± SEM, N=7-9, p-values (unpaired t-test) shown above error bars. N for each experiment shown in parentheses.

Figure 2. Proteomic analysis of protein abundance in WT vs. *Alkbh7*$^{-/-}$. Hearts from young male WT or *Alkbh7*$^{-/-}$ mice were analyzed by tandem mass tag LC-MS/MS as per the methods. **(A):** Volcano plot showing relative levels of 3,737 proteins. X-axis shows Log_{10} of fold change (*Alkbh7*$^{-/-}$ / WT) and Y-axis shows Log_{10} of significance (paired t-test, N=5). Proteins crossing thresholds (gray lines) in upper left or right quadrants are labeled. **(B):** Activity of GLO-1 in WT or *Alkbh7*$^{-/-}$ heart cytosol. **(C):** Activity of GLO-2 in WT or *Alkbh7*$^{-/-}$ heart cytosol. **(D):** Western blot showing abundance of GLO-1 in WT or *Alkbh7*$^{-/-}$ heart cytosol, with Ponceau stained membrane below. **(E)**: Quantitation of GLO-1 blot, normalized to protein loading. Bar graphs in panels B/C/E show means ± SE, N=4-5, with p-values (paired t-test) shown above error bars. **(F):** Schematic showing the methylglyoxal detoxification system and its relationship to glycolysis. Abbreviations: AGEs: Advanced glycation end products, GSH: glutathione. MGO: methylglyoxal. In bar graphs, N for each group is shown in parentheses.

Figure 2 - Supplement 1. Representative gel from FLAG-tagged ALKBH7 pull-down experiment. Lane 1 shows control (empty vector) cells. Remaining 4 lanes are ALKBH7-FLAG cells treated with MMS for indicated times. Proteins were cut from lane 3 (1 hr. post-MMS) for identification (see Table S1).

Figure 2 - Supplement 2. Enzyme activities in WT and *Alkbh7*$^{-/-}$ tissues. Activities of (top to bottom) citrate synthase, respiratory complex I, respiratory complex II, and α-ketoglutarate dehydrogenase, were measured spectrophotometrically as per the methods, in **(A)** Heart mitochondria, **(B)** Liver mitochondria. Panel **(C)** shows GLO-1 and GLO-2 activity in liver cytosol, complementing the heart data in Figure 2B/C. All data are means ± SEM, N=4-5, p values (paired t-tests) are shown above the error bars. N for each experiment shown in parentheses.

Figure 3. Metabolomics analysis in WT vs. *Alkbh7*$^{-/-}$. Hearts from young male WT or *Alkbh7*$^{-/-}$ mice were analyzed by LC-MS/MS based metabolomics as per the methods. **(A):** Volcano plot showing relative levels of 90 metabolites in the steady state. X-axis shows Log_{10} of fold change (*Alkbh7*$^{-/-}$ / WT) and Y-axis shows Log_{10} of significance (paired t-test, N=8-17 depending on metabolite). Metabolites crossing thresholds (gray lines) in upper left or right quadrants are labeled. A pathway impact analysis is shown in Fig. S4. **(B):** Schematic showing glycolysis and its relationship to methylglyoxal (MGO). Metabolites quantified in ^{13}C-flux measurements (panel C) are highlighted blue. **(C):** ^{13}C-glucose flux measurements of glycolytic activity in *Alkbh7*$^{-/-}$ vs. WT hearts. Y-axis shows fractional saturation (F-SAT) of each metabolite within 5 min. from exogenously delivered [U-^{13}C] glucose. Note: UDP-Glc-Nac is shown on separate axes for clarity. **(D/E):** Western blot showing abundance of MGO-adducts in *Alkbh7*$^{-/-}$ and WT heart cytosol (D) or mitochondria (E). Ponceau stained membranes are shown below. **(F):** Quantitation of MGO adduct content from blots, normalized to protein loading. Bar graphs in panels C/F show means ± SE, N=4-5, with p-values (paired t-test) shown above error bars. In bar graphs, N for each group is shown in parentheses.

Figure 3 - Supplement 1. Representation of metabolic pathways based on detected metabolites. Pathway analysis was performed using open source MetaboAnalyst 3.0 software (www.metaboanalyst.ca), using all detected metabolites from the steady state analysis (Figure 3A). Greater warm coloring of a metabolic pathway indicates greater coverage, permitting conclusions to be drawn about that pathway.

Figure 4. Response to ex-vivo cardiac ischemia-reperfusion (IR) injury in WT vs. *Alkbh7*$^{-/-}$. Hearts from young male WT and *Alkbh7*$^{-/-}$ mice were Langendorff perfused and subjected to 25 min. ischemia plus 60 min. reperfusion. **(A):** Cardiac function assessed by left ventricular balloon pressure transducer. Graph shows the product of heart rate multiplied by left ventricular developed pressure, as a percentage of the initial (pre-ischemic) value. **(B):** Post IR staining with TTC for quantitation of myocardial infarct size. Representative TTC-stained heart slices are shown, with pseudo-colored mask images used for quantitation by planimetry (red = live tissue, green = infarct). Data are quantified below, with individual data points to shown N, and means ± SE. p-values (paired t-test) are shown above error bars.

Figure 4 - Supplement 1. Cardiac ischemia-reperfusion (IR) injury and glycative stress response in FEMALE WT vs. *Alkbh7*$^{-/-}$. (A): Experiments were as per Figure 4, except young female mice were used instead of male. Hearts from WT and *Alkbh7*$^{-/-}$ were Langendorff perfused and subjected to 25 min.

ischemia plus 60 min. reperfusion. Cardiac function assessed by left ventricular balloon pressure transducer. Graph shows the product of heart rate multiplied by left ventricular developed pressure, as a percentage of the initial (pre-ischemic) value. **(B):** Post IR staining with TTC for quantitation of myocardial infarct size. Representative TTC-stained heart slices are shown, with pseudo-colored mask images used for quantitation by planimetry (red = live tissue, green = infarct). Data are quantified below, with individual data points to shown N, and means ± SEM. **(C):** Western blot for GLO-1 in female WT and *Alkbh7*$^{-/-}$ heart cytosol. Ponceau stained membrane for normalization is shown below, with quantitation in panel **(D).** (E): GLO-1 activity assay in female WT and *Alkbh7*$^{-/-}$ heart cytosol. **(F/G):** Western blot for anti-MGO protein adducts in female WT and *Alkbh7*$^{-/-}$ heart cytosol (F) and mitochondria (G). Ponceau stained membranes for normalization are shown below, with densitometric quantitation in panel **(H)**. For bar graphs, N for each experiment is shown in parentheses. p-values (paired t-test) are shown above error bars.

Figure 4 – Supplement 2. Response to ex-vivo cardiac ischemia-reperfusion (IR) injury in OLD MALE WT vs. *Alkbh7*$^{-/-}$. Experiments were as per Figure 4, except old male mice (1.5 yrs) were used instead of young males (8-12 wks). Hearts from WT and *Alkbh7*$^{-/-}$ were Langendorff perfused and subjected to 25 min. ischemia plus 60 min. reperfusion. **(A):** Cardiac function assessed by left ventricular balloon pressure transducer. Graph shows the product of heart rate multiplied by left ventricular developed pressure, as a percentage of the initial (pre-ischemic) value. **(B):** Post IR staining with TTC for quantitation of myocardial infarct size. Representative TTC-stained heart slices are shown, with pseudo-colored mask images used for quantitation by planimetry (red = live tissue, green = infarct). Data are quantified below, with individual data points to shown N, and means ± SEM. p-values (paired t-test) are shown above error bars. N for each experiment shown in parentheses.

Figure 5. Mitochondrial PT pore & Ca^{2+} handling in WT vs. *Alkbh7*$^{-/-}$. (A): Opening of the mitochondrial PT pore was assayed spectrophotometrically in isolated cardiac mitochondria from young male WT and *Alkbh7*$^{-/-}$ mice. Average traces are shown, with addition of 100 µM Ca^{2+} to initiate PT pore opening and swelling indicated by the arrow. Dotted lines indicate the presence of the PT pore inhibitor cyclosporin A (CsA). Error bars are omitted for clarity. **(B):** Quantitation of pore opening, as the change in swelling (absorbance at 520 nm) in 5 min. Data are means ± SE, N=7, with significance between groups (unpaired t-test) shown above error bars. **(C):** Mitochondrial Ca^{2+} handling assayed by Ca^{2+} green-5N fluorescence. Isolated cardiac mitochondria from young male WT and *Alkbh7*$^{-/-}$ mice were incubated with Ca^{2+} green-5N to indicate extra-mitochondrial [Ca^{2+}]. Pulses of 10 µM Ca^{2+} were added at ~2 min. intervals as indicated by arrows. Representative traces are shown. **(D):** Quantitation of the number of Ca^{2+} pulses tolerated by mitochondria before PT pore opening occurred (as indicated by a sharp upward deflection in the Ca^{2+} green-5N trace). **(E):** Quantitation of the initial rate of mitochondrial Ca^{2+} uptake, calculated from the downward slope in Ca^{2+} green-5N fluorescence on the first 3 Ca^{2+} pulses. Bar graphs in panels B/D/E show means ± SE, N=5-7, with p-values (unpaired t-test) shown above error bars. In bar graphs, N for each group is shown in parentheses.

Figure 5 - Supplement 1. Cardioprotection against IR injury by dimethyl-L-2-hydroxyglutarate. Hearts from WT mice were Langendorff perfused and subjected to 25 min. ischemia plus 60 min. reperfusion, with optional administration of 10 µM dimethyl-L-2-hydroxyglutarate (DM2HG) for 20 min. prior to the onset of ischemia. **(A):** Cardiac function assessed by left ventricular balloon pressure transducer. Graph shows the product of heart rate multiplied by left ventricular developed pressure, as a percentage of the initial (pre-ischemic) value. **(B):** Post IR staining with TTC for quantitation of myocardial infarct size.

Representative TTC-stained heart slices are shown, with pseudo-colored mask images used for quantitation by planimetry (red = live tissue, green = infarct). Data are quantified below, with individual data points to shown N, and means ± SEM. p-values (paired t-test) are shown above error bars. N for each experiment shown in parentheses.

Figure 5 - Supplement 2. Western blot detection of UPR^{mt} mediators in WT vs. *Alkbh7*$^{-/-}$ hearts. To determine -whether loss of ALKBH7 resulted in activation of the mitochondrial unfolded protein response (UPR^{mt}), the levels of key effectors were determined by western blot. **(A):** Blots show levels of LonP1 and Clpp in cardiac homogenate of WT and *Alkbh7*$^{-/-}$ hearts. Protein loading is shown in the central Ponceau S stained membrane. **(B):** Quantitation of data from blots of LonP1 and Clpp. Graphs show means ± SEM, N=4, with p values (unpaired t-test) above the error bars. **(C):** Blot shows level of Hspd1 (HSP60) in mitochondria from WT and *Alkbh7*$^{-/-}$ hearts. Protein loading is shown in the Ponceau S stained membrane below. **(D):** Quantitation of data from blot of Hspd1. Graphs show means ± SEM, N=4-5, with p values (unpaired t-test) above the error bars. N for each experiment shown in parentheses.

Figure 5 - Supplement 3. Blue-native analysis of mitochondrial respiratory supercomplexes. Heart mitochondria from WT or Alkbh7-/- mice were separated by blue-native PAGE as per the methods. **(A):** Original gel showing positions of respiratory complexes I, V and III, and supercomplexes (SCs) at the top. Note, gel was not stained post-hoc with Coomassie blue, but gel conditions contain the dye, such that gels appear with blue bands immediately upon electrophoresis. **(B):** Complex V in-gel assay. White bands show lead precipitate resulting from ATPase activity of complex V. Monomeric, dimeric, and multimeric forms of complex V are indicated. Gels are representative of at least 3 independent experiments.

Figure 6. Blockade of cardioprotection in *Alkbh7*$^{-/-}$ by GLO-1 inhibition. Hearts from young male WT and *Alkbh7*$^{-/-}$ mice were Langendorff perfused and subjected to IR injury as in Figure 4, with delivery of 1 µM SBB-GSH-CpE for 10 min. prior to ischemia. **(A):** Cardiac function assessed by left ventricular balloon pressure transducer. Graph shows the product of heart rate multiplied by left ventricular developed pressure, as a percentage of the initial value. A significant drop in cardiac function was observed upon drug infusion in *Alkbh7*$^{-/-}$ only (see arrow and p-value). **(B):** Post IR staining with TTC for quantitation of myocardial infarct size. Representative TTC-stained heart slices are shown, with pseudo-colored mask images used for quantitation by planimetry (red = live tissue, green = infarct). Data are quantified below, with individual data points to shown N, and means ± SE. p-values (paired t-test) are shown above error bars. **(C):** Western blot showing abundance of DJ-1 in *Alkbh7*$^{-/-}$ and WT heart mitochondria. Ponceau stained membrane and quantitation are shown below. Bar graph shows means ± SE, N=4, with p-values (paired t-test) shown above error bars. **(D):** Schematic showing proposed events that connect loss of ALKBH7 to cardioprotection. Via mechanisms that may include downregulation of Perilipin 5 and F-1,6-BPase 2, loss of ALKBH7 causes a shift in metabolism away from fatty acid oxidation (FAO) toward elevated glycolysis. GLO-1 is also upregulated, possibly in response to MGO elevation. Both elevated glycolysis and GLO-1 then protect against IR injury. The potential role of GLO-1 as a regulator of the metabolic shift toward glycolysis is also shown.

Figure 6 - Supplement 1. Response to ex-vivo cardiac ischemia-reperfusion (IR) injury in WT vs. *Alkbh7*$^{-/-}$, in the absence of glucose. Experiments were as per Figure 4, except that hearts were perfused with a Krebs-Henseleit buffer lacking glucose (other respiratory substrates including

palmitate conjugated to BSA were still present). Hearts from WT and *Alkbh7*$^{-/-}$ were Langendorff perfused and subjected to 25 min. ischemia plus 60 min. reperfusion. **(A):** Cardiac function assessed by left ventricular balloon pressure transducer. Graph shows the product of heart rate multiplied by left ventricular developed pressure, as a percentage of the initial (pre-ischemic) value. **(B):** Post IR staining with TTC for quantitation of myocardial infarct size. Representative TTC-stained heart slices are shown, with pseudo-colored mask images used for quantitation by planimetry (red = live tissue, green = infarct). Data are quantified below, with individual data points to shown N, and means ± SEM. p-values (paired t-test) are shown above error bars. N for each experiment shown in parentheses.

Supplementary File/Table 1. Proteins identified as interacting with ALKBH7 by immunoprecipitation under control or MMS-treated conditions. Cells transfected with FLAG-tagged ALKBH7 were treated with MMS as per the methods, the anti-FLAG beads used to immunoprecipitate ALKBH7-interacting proteins. Following SDS-PAGE separation (see Fig. 2 - Suppl. 1), excised bands were identified by mass spectrometry of trypsin digests. Proteins are listed by name and accession, with the number of unique peptides identified under each condition indicated in the appropriate columns.

Source data

Source Data 1. Source data for Figure 1 and Supplements

Source Data 2. Source data for Figure 2 and Supplements

Source Data 3. Source data for Figure 3 and Supplements

Source Data 4. Source data for Figure 4 and Supplements

Source Data 5. Source data for Figure 5 and Supplements

Source Data 6. Source data for Figure 6 and Supplements

REFERENCES

1. Islam, M.S., Leissing, T.M., Chowdhury, R., Hopkinson, R.J. & Schofield, C.J. 2-Oxoglutarate-Dependent Oxygenases. *Annu Rev Biochem* **87**, 585-620 (2018).
2. Fedeles, B.I., Singh, V., Delaney, J.C., Li, D. & Essigmann, J.M. The AlkB Family of Fe(II)/alpha-Ketoglutarate-dependent Dioxygenases: Repairing Nucleic Acid Alkylation Damage and Beyond. *J Biol Chem* **290**, 20734-42 (2015).
3. Falnes, P.O., Johansen, R.F. & Seeberg, E. AlkB-mediated oxidative demethylation reverses DNA damage in Escherichia coli. *Nature* **419**, 178-82 (2002).
4. Trewick, S.C., Henshaw, T.F., Hausinger, R.P., Lindahl, T. & Sedgwick, B. Oxidative demethylation by Escherichia coli AlkB directly reverts DNA base damage. *Nature* **419**, 174-8 (2002).
5. Aas, P.A. et al. Human and bacterial oxidative demethylases repair alkylation damage in both RNA and DNA. *Nature* **421**, 859-63 (2003).
6. Duncan, T. et al. Reversal of DNA alkylation damage by two human dioxygenases. *Proc Natl Acad Sci U S A* **99**, 16660-5 (2002).
7. Wu, T.P. et al. DNA methylation on N(6)-adenine in mammalian embryonic stem cells. *Nature* **532**, 329-33 (2016).
8. Xie, Q. et al. N(6)-methyladenine DNA Modification in Glioblastoma. *Cell* **175**, 1228-1243 e20 (2018).
9. Wang, G. et al. The atomic resolution structure of human AlkB homolog 7 (ALKBH7), a key protein for programmed necrosis and fat metabolism. *J Biol Chem* **289**, 27924-36 (2014).
10. Pawar, T., Bjoras, M., Klungland, A. & Eide, L. Metabolism and DNA repair shape a specific modification pattern in mitochondrial DNA. *Mitochondrion* **40**, 16-28 (2018).
11. Bjornstad, L.G. et al. Human ALKBH4 interacts with proteins associated with transcription. *PLoS One* **7**, e49045 (2012).
12. Schweppe, D.K. et al. Mitochondrial protein interactome elucidated by chemical cross-linking mass spectrometry. *Proc Natl Acad Sci U S A* **114**, 1732-1737 (2017).
13. Liu, F., Lossl, P., Rabbitts, B.M., Balaban, R.S. & Heck, A.J.R. The interactome of intact mitochondria by cross-linking mass spectrometry provides evidence for coexisting respiratory supercomplexes. *Mol Cell Proteomics* **17**, 216-232 (2018).
14. Floyd, B.J. et al. Mitochondrial Protein Interaction Mapping Identifies Regulators of Respiratory Chain Function. *Mol Cell* **63**, 621-632 (2016).
15. Fu, D., Jordan, J.J. & Samson, L.D. Human ALKBH7 is required for alkylation and oxidation-induced programmed necrosis. *Genes Dev* **27**, 1089-100 (2013).
16. Jordan, J.J. et al. ALKBH7 drives a tissue and sex-specific necrotic cell death response following alkylation-induced damage. *Cell Death Dis* **8**, e2947 (2017).
17. Solberg, A. et al. Deletion of mouse Alkbh7 leads to obesity. *J Mol Cell Biol* **5**, 194-203 (2013).
18. Walker, A.R. et al. ALKBH7 Variant Related to Prostate Cancer Exhibits Altered Substrate Binding. *PLoS Comput Biol* **13**, e1005345 (2017).
19. Frangogiannis, N.G. Pathophysiology of Myocardial Infarction. *Compr Physiol* **5**, 1841-75 (2015).
20. Meng, S., Zhan, S., Dou, W. & Ge, W. The interactome and proteomic responses of ALKBH7 in cell lines by in-depth proteomics analysis. *Proteome Sci* **17**, 8 (2019).
21. Schweppe, D.K., Huttlin, E.L., Harper, J.W. & Gygi, S.P. BioPlex Display: An Interactive Suite for Large-Scale AP-MS Protein-Protein Interaction Data. *J Proteome Res* **17**, 722-726 (2018).
22. Najt, C.P. et al. Lipid Droplet-Derived Monounsaturated Fatty Acids Traffic via PLIN5 to Allosterically Activate SIRT1. *Mol Cell* **77**, 810-824 e8 (2020).

23. Li, H. et al. Decreased fructose-1,6-bisphosphatase-2 expression promotes glycolysis and growth in gastric cancer cells. *Mol Cancer* **12**, 110 (2013).
24. Gutierrez-Guerrero, Y.T. et al. Genomic consequences of dietary diversification and parallel evolution due to nectarivory in leaf-nosed bats. *Gigascience* **9**(2020).
25. Rabbani, N., Xue, M. & Thornalley, P.J. Dicarbonyls and glyoxalase in disease mechanisms and clinical therapeutics. *Glycoconj J* **33**, 513-25 (2016).
26. Yagensky, O. et al. Increased expression of heme-binding protein 1 early in Alzheimer's disease is linked to neurotoxicity. *Elife* **8**(2019).
27. Ghodsi, R. & Kheirouri, S. Carnosine and advanced glycation end products: a systematic review. *Amino Acids* **50**, 1177-1186 (2018).
28. Nadtochiy, S.M. et al. Metabolomic profiling of the heart during acute ischemic preconditioning reveals a role for SIRT1 in rapid cardioprotective metabolic adaptation. *J Mol Cell Cardiol* **88**, 64-72 (2015).
29. Almeida, F. et al. Pyridoxamine reverts methylglyoxal-induced impairment of survival pathways during heart ischemia. *Cardiovasc Ther* **31**, e79-85 (2013).
30. Wang, X.L. et al. Methylglyoxal increases cardiomyocyte ischemia-reperfusion injury via glycative inhibition of thioredoxin activity. *Am J Physiol Endocrinol Metab* **299**, E207-14 (2010).
31. Del Re, D.P., Amgalan, D., Linkermann, A., Liu, Q. & Kitsis, R.N. Fundamental Mechanisms of Regulated Cell Death and Implications for Heart Disease. *Physiol Rev* **99**, 1765-1817 (2019).
32. Tate, M. et al. The Mitochondria-Targeted Methylglyoxal Sequestering Compound, MitoGamide, Is Cardioprotective in the Diabetic Heart. *Cardiovasc Drugs Ther* **33**, 669-674 (2019).
33. Rahman, M.M., Sykiotis, G.P., Nishimura, M., Bodmer, R. & Bohmann, D. Declining signal dependence of Nrf2-MafS-regulated gene expression correlates with aging phenotypes. *Aging Cell* **12**, 554-62 (2013).
34. Boengler, K., Schulz, R. & Heusch, G. Loss of cardioprotection with ageing. *Cardiovasc Res* **83**, 247-61 (2009).
35. Nguyen, L.T. et al. Attenuation of isoflurane-induced preconditioning and reactive oxygen species production in the senescent rat heart. *Anesth Analg* **107**, 776-82 (2008).
36. Calabrese, E.J., Dhawan, G., Kapoor, R., Iavicoli, I. & Calabrese, V. What is hormesis and its relevance to healthy aging and longevity? *Biogerontology* **16**, 693-707 (2015).
37. Evans, B., Griner, E. & Reproducibility Project: Cancer, B. Registered report: Oncometabolite 2-hydroxyglutarate is a competitive inhibitor of alpha-ketoglutarate-dependent dioxygenases. *Elife* **4**, e07420 (2015).
38. Wang, P. et al. Oncometabolite D-2-Hydroxyglutarate Inhibits ALKBH DNA Repair Enzymes and Sensitizes IDH Mutant Cells to Alkylating Agents. *Cell Rep* **13**, 2353-2361 (2015).
39. Chen, F. et al. Oncometabolites d- and l-2-Hydroxyglutarate Inhibit the AlkB Family DNA Repair Enzymes under Physiological Conditions. *Chem Res Toxicol* **30**, 1102-1110 (2017).
40. Sridharan, V. et al. O(2)-sensing signal cascade: clamping of O(2) respiration, reduced ATP utilization, and inducible fumarate respiration. *Am J Physiol Cell Physiol* **295**, C29-37 (2008).
41. Wang, Y.T. et al. Cardioprotection by the mitochondrial unfolded protein response requires ATF5. *Am J Physiol Heart Circ Physiol* **317**, H472-H478 (2019).
42. Melber, A. & Haynes, C.M. UPR(mt) regulation and output: a stress response mediated by mitochondrial-nuclear communication. *Cell Res* **28**, 281-295 (2018).
43. Wagner, A. et al. Mitochondrial Alkbh1 localizes to mtRNA granules and its knockdown induces the mitochondrial UPR in humans and C. elegans. *J Cell Sci* **132**(2019).

44. Baines, C.P. et al. Loss of cyclophilin D reveals a critical role for mitochondrial permeability transition in cell death. *Nature* **434**, 658-62 (2005).
45. Speer, O. et al. Rapid suppression of mitochondrial permeability transition by methylglyoxal. Role of reversible arginine modification. *J Biol Chem* **278**, 34757-63 (2003).
46. Giorgio, V. et al. Dimers of mitochondrial ATP synthase form the permeability transition pore. *Proc Natl Acad Sci U S A* **110**, 5887-92 (2013).
47. Lee, J.Y. et al. Human DJ-1 and its homologs are novel glyoxalases. *Hum Mol Genet* **21**, 3215-25 (2012).
48. Shimizu, Y. et al. DJ-1 protects the heart against ischemia-reperfusion injury by regulating mitochondrial fission. *J Mol Cell Cardiol* **97**, 56-66 (2016).
49. Shimizu, Y. et al. Role of DJ-1 in Modulating Glycative Stress in Heart Failure. *J Am Heart Assoc* **9**, e014691 (2020).
50. Parker, B.L. et al. An integrative systems genetic analysis of mammalian lipid metabolism. *Nature* **567**, 187-193 (2019).
51. Gaffney, D.O. et al. Non-enzymatic Lysine Lactoylation of Glycolytic Enzymes. *Cell Chem Biol* **27**, 206-213 e6 (2020).
52. Zhang, D. et al. Metabolic regulation of gene expression by histone lactylation. *Nature* **574**, 575-580 (2019).
53. Casin, K.M. et al. S-Nitrosoglutathione Reductase Is Essential for Protecting the Female Heart From Ischemia-Reperfusion Injury. *Circ Res* **123**, 1232-1243 (2018).
54. Ma, H. et al. Advanced glycation endproduct (AGE) accumulation and AGE receptor (RAGE) up-regulation contribute to the onset of diabetic cardiomyopathy. *J Cell Mol Med* **13**, 1751-64 (2009).
55. Kenny, H.C. & Abel, E.D. Heart Failure in Type 2 Diabetes Mellitus. *Circ Res* **124**, 121-141 (2019).
56. Ravingerova, T. et al. Acute diabetes modulates response to ischemia in isolated rat heart. *Mol Cell Biochem* **210**, 143-51 (2000).
57. Nawata, T. et al. Cardioprotection by streptozotocin-induced diabetes and insulin against ischemia/reperfusion injury in rats. *J Cardiovasc Pharmacol* **40**, 491-500 (2002).
58. Chen, H. et al. Paradoxically enhanced heart tolerance to ischaemia in type 1 diabetes and role of increased osmolarity. *Clin Exp Pharmacol Physiol* **33**, 910-6 (2006).
59. Rabbani, N., Xue, M., Weickert, M.O. & Thornalley, P.J. Multiple roles of glyoxalase 1-mediated suppression of methylglyoxal glycation in cancer biology-Involvement in tumour suppression, tumour growth, multidrug resistance and target for chemotherapy. *Semin Cancer Biol* **49**, 83-93 (2018).
60. Winkler, J.W., Uddin, J., Serhan, C.N. & Petasis, N.A. Stereocontrolled total synthesis of the potent anti-inflammatory and pro-resolving lipid mediator resolvin D3 and its aspirin-triggered 17R-epimer. *Org Lett* **15**, 1424-7 (2013).
61. Smith, C.O. et al. Cardiac metabolic effects of KNa1.2 channel deletion and evidence for its mitochondrial localization. *FASEB J*, fj201800139R (2018).
62. Hoffman, D.L., Salter, J.D. & Brookes, P.S. Response of mitochondrial reactive oxygen species generation to steady-state oxygen tension: implications for hypoxic cell signaling. *Am J Physiol Heart Circ Physiol* **292**, H101-8 (2007).
63. Lowry, O.H., Rosebrough, N.J., Farr, A.L. & Randall, R.J. Protein measurement with the Folin phenol reagent. *J Biol Chem* **193**, 265-75 (1951).
64. Brookes, P.S. et al. Concentration-dependent effects of nitric oxide on mitochondrial permeability transition and cytochrome c release. *J Biol Chem* **275**, 20474-9 (2000).

65. Brookes, P.S. et al. UCPs--unlikely calcium porters. *Nat Cell Biol* **10**, 1235-7; author reply 1237-40 (2008).
66. Stoehr, A. et al. Prolyl hydroxylation regulates protein degradation, synthesis, and splicing in human induced pluripotent stem cell-derived cardiomyocytes. *Cardiovasc Res* **110**, 346-58 (2016).
67. Fu, D. et al. Human AlkB homolog ABH8 Is a tRNA methyltransferase required for wobble uridine modification and DNA damage survival. *Mol Cell Biol* **30**, 2449-59 (2010).
68. Zhang, J. et al. Accumulation of Succinate in Cardiac Ischemia Primarily Occurs via Canonical Krebs Cycle Activity. *Cell Rep* **23**, 2617-2628 (2018).
69. Aittokallio, T. Dealing with missing values in large-scale studies: microarray data imputation and beyond. *Brief Bioinform* **11**, 253-64 (2010).
70. Nadtochiy, S.M., Wang, Y.T., Nehrke, K., Munger, J. & Brookes, P.S. Cardioprotection by nicotinamide mononucleotide (NMN): Involvement of glycolysis and acidic pH. *J Mol Cell Cardiol* **121**, 155-162 (2018).
71. Beutner, G., Alanzalon, R.E. & Porter, G.A., Jr. Cyclophilin D regulates the dynamic assembly of mitochondrial ATP synthase into synthasomes. *Sci Rep* **7**, 14488 (2017).
72. Porter, G.A., Urciuoli, W.R., Brookes, P.S. & Nadtochiy, S.M. SIRT3 deficiency exacerbates ischemia-reperfusion injury: implication for aged hearts. *Am J Physiol Heart Circ Physiol* **306**, H1602-9 (2014).
73. Wang, H. et al. Synthesis and Antineoplastic Evaluation of Mitochondrial Complex II (Succinate Dehydrogenase) Inhibitors Derived from Atpenin A5. *ChemMedChem* **12**, 1033-1044 (2017).
74. Chouchani, E.T. et al. Identification of S-nitrosated mitochondrial proteins by S-nitrosothiol difference in gel electrophoresis (SNO-DIGE): implications for the regulation of mitochondrial function by reversible S-nitrosation. *Biochem J* **430**, 49-59 (2010).
75. Trounce, I.A., Kim, Y.L., Jun, A.S. & Wallace, D.C. Assessment of mitochondrial oxidative phosphorylation in patient muscle biopsies, lymphoblasts, and transmitochondrial cell lines. *Methods Enzymol* **264**, 484-509 (1996).
76. Wanders, R.J. et al. Long-chain 3-hydroxyacyl-CoA dehydrogenase deficiency: identification of a new inborn error of mitochondrial fatty acid beta-oxidation. *J Inherit Metab Dis* **13**, 311-4 (1990).
77. Weinberger, M.J., Rinaldo, P., Strauss, A.W. & Bennett, M.J. Intact alpha-subunit is required for membrane-binding of human mitochondrial trifunctional beta-oxidation protein, but is not necessary for conferring 3-ketoacyl-CoA thiolase activity to the beta-subunit. *Biochem Biophys Res Commun* **209**, 47-52 (1995).
78. Arai, M., Nihonmatsu-Kikuchi, N., Itokawa, M., Rabbani, N. & Thornalley, P.J. Measurement of glyoxalase activities. *Biochem Soc Trans* **42**, 491-4 (2014).

A

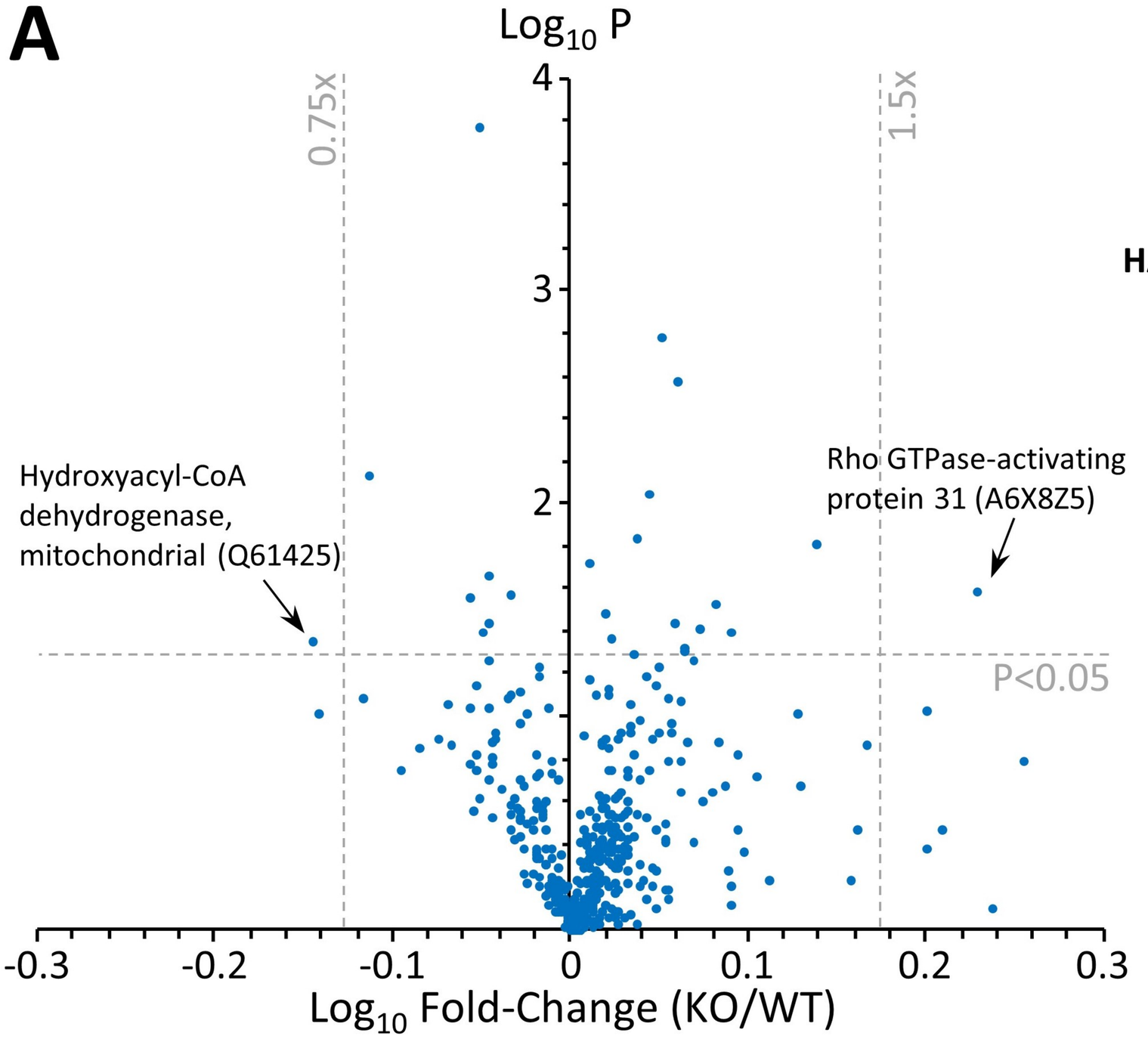

C

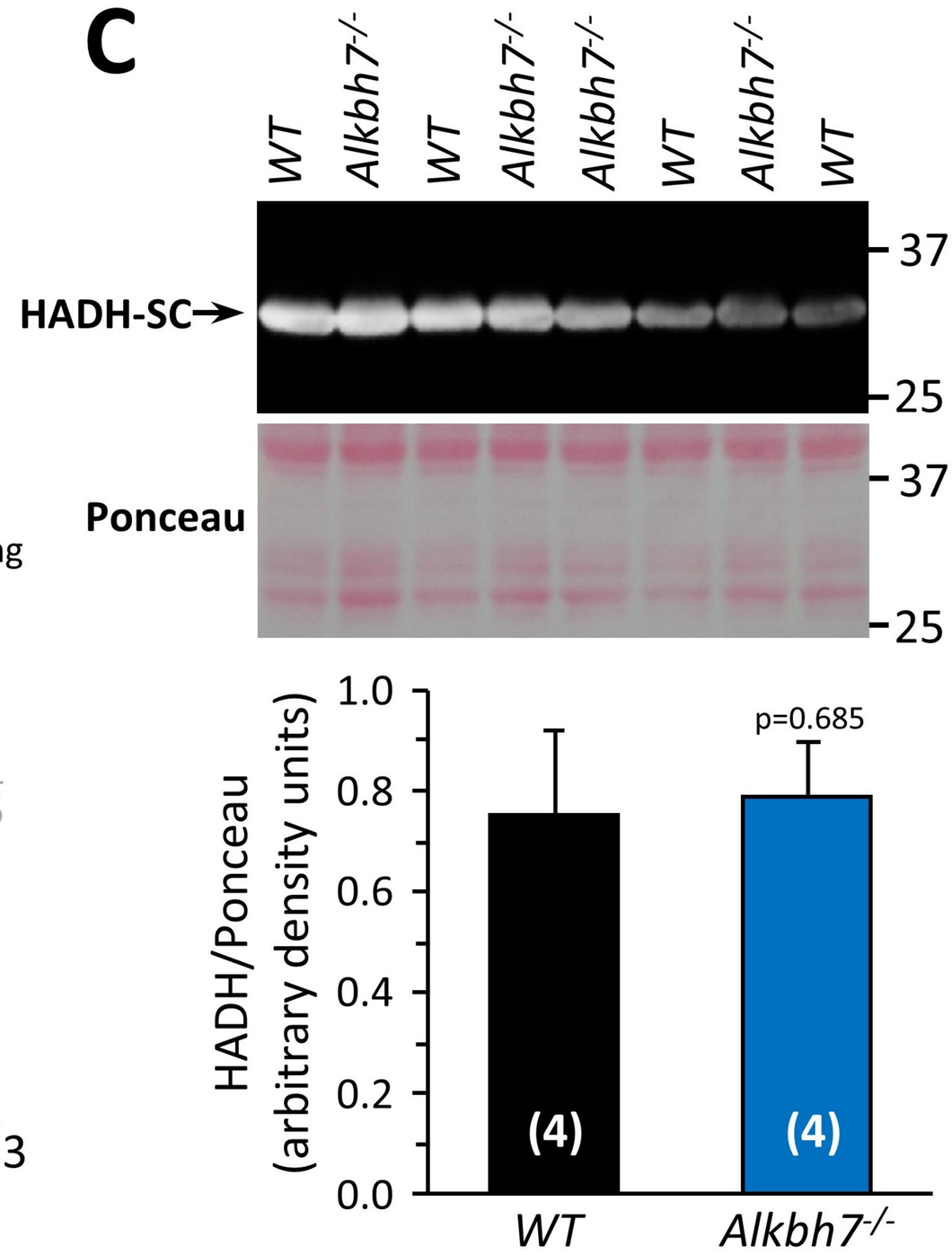

B Top 5 proteins with prolyl hydroxylation up/down in *Alkbh7*$^{-/-}$ vs. *WT*

Protein ID (Accession #)	*KO/WT Raw P-OH*	*KO/WT Abundance*	*KO/WT Net P-OH*	*p*	*Sequence (**P-OH** sites)*
LESS P-OH					
Hydroxyacyl-CoA dehydrogenase (Q61425)	0.68±0.13	0.93±0.06	0.72±0.09	0.04	$_{250}$LGAGY**P**MG**P**FELLDYVGLDTTK$_{271}$
L-lactate dehydrogenase B chain (P16125)	0.72±0.12	1.00±0.01	0.72±0.12	0.10	$_{128}$YSPDCTIIVVSN**P**VDILTYVTWK$_{150}$
Cytochrome c_1 heme protein (Q9D0M3)	0.79±0.14	1.00±0.02	0.80±0.14	0.17	$_{229}$EGLYFN**P**YFPGQAIGMAPPIYTEV LEYDDGTPATMSQVAK$_{268}$
CCH domain-containing protein 2 (Q9D1L0)	0.87±0.07	1.08±0.05	0.82±0.10	0.14	$_{29}$A**P**AAQ**P**PAAAAPSAVGSPAAAPR$_{51}$
Collagen α1(III) chain (P08121)	0.90±0.07	1.09±0.10	0.84±0.08	0.12	$_{526}$DGT**P**GG**P**GIR$_{535}$
MORE P-OH					
Involucrin (P48997)	1.20±0.25	0.85±0.09	1.59±0.50	0.42	$_{435}$ELSDQ**P**LDQALVK$_{447}$
Ras GAP binding protein 2 (P97379)	1.73±0.32	1.08±0.03	1.62±0.31	0.33	$_{225}$SATPPPAE**P**ASL**P**QEPPK$_{242}$
Rho GTPase activating protein 31 (A6X8Z5)	1.31±0.37	0.96±0.06	1.69±0.27	0.03	$_{666}$TS**P**I**P**ESS**P**A**P**F**P**FPEAPGSLPSSSAPR$_{693}$
Major vault protein (Q9EQK5)	1.76±0.75	1.08±0.06	1.73±0.82	0.79	$_{92}$LAQDPF**P**LY**P**GELLEK$_{107}$
Malate dehydrogenase, mito (P08249)	1.83±0.47	1.02±0.02	1.80±0.47	0.16	$_{92}$GCDVVVI**P**AGVPR$_{104}$

D

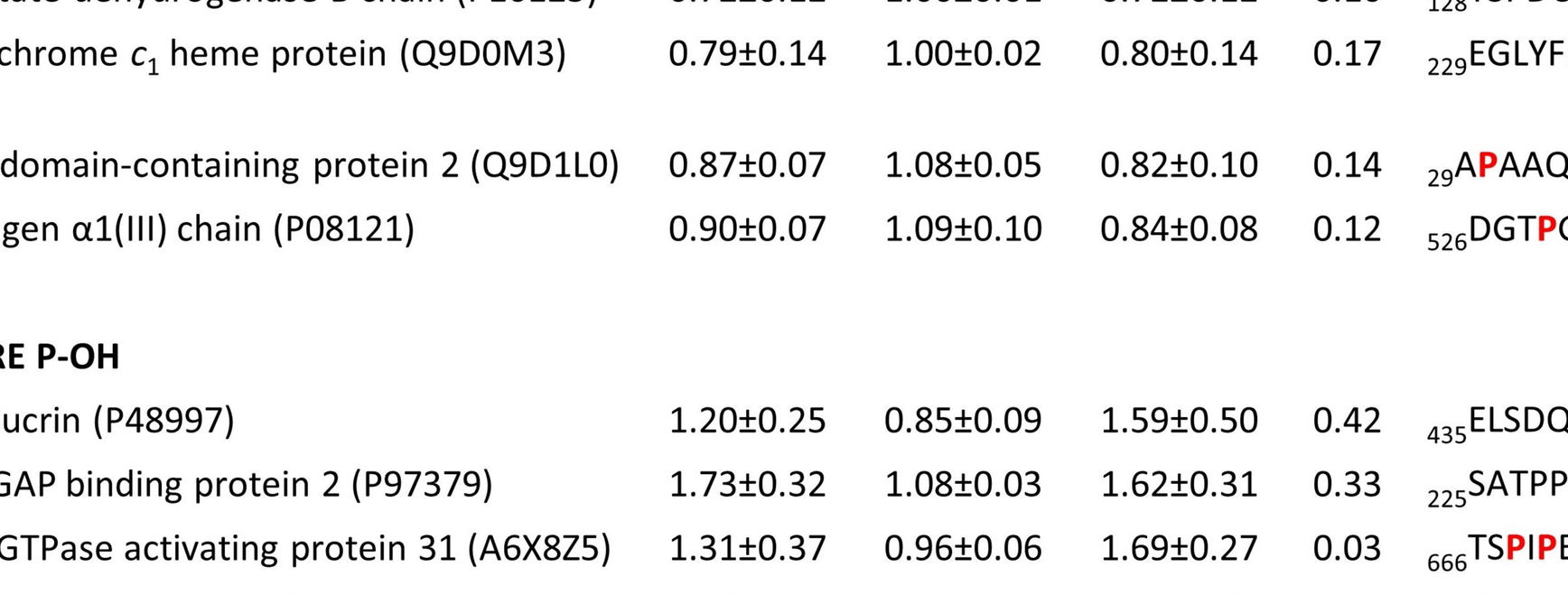

A

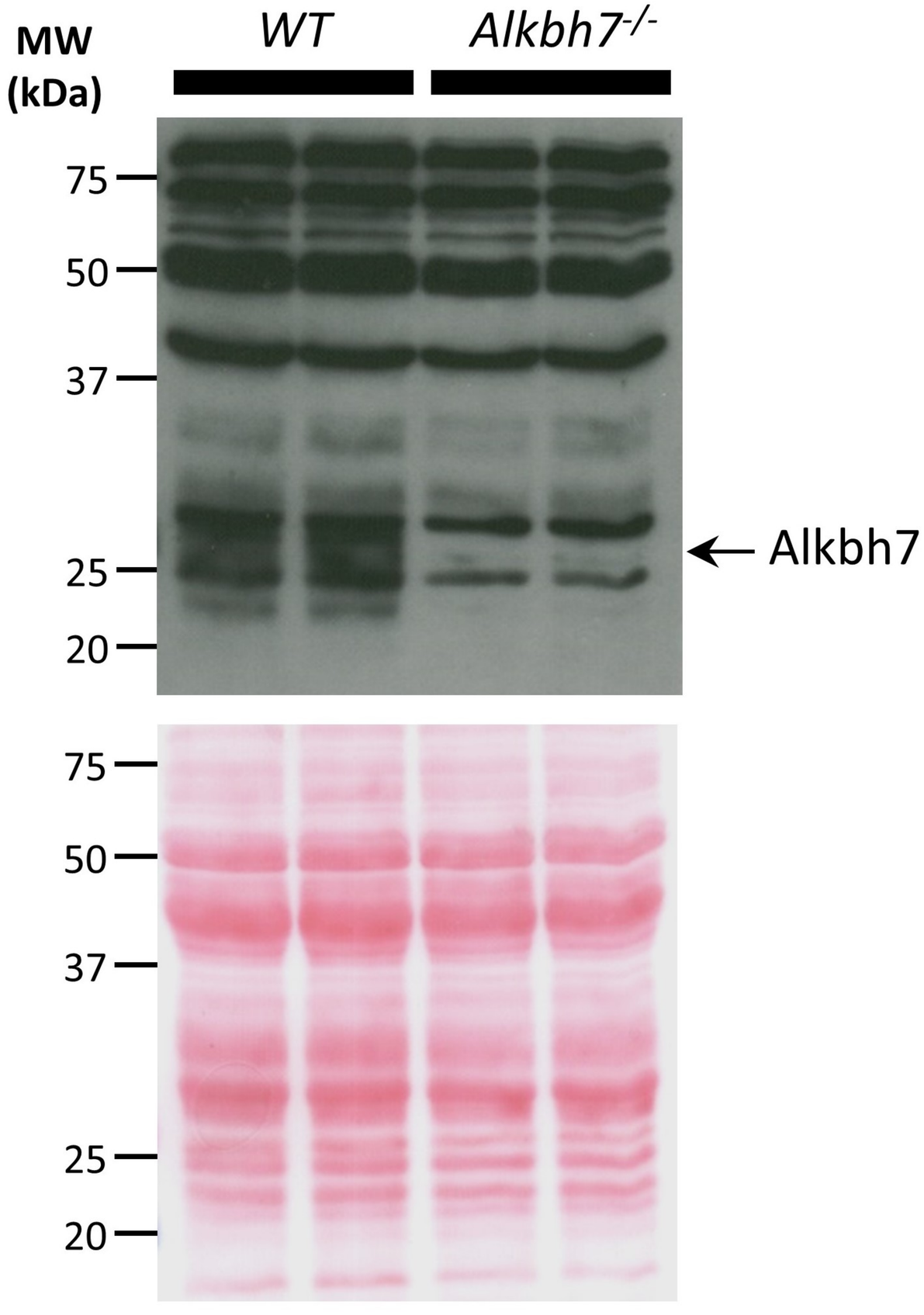
MW
(kDa)
WT
Alkbh7-/-
75
50
37
25
20
Alkbh7
75
50
37
25
20

B

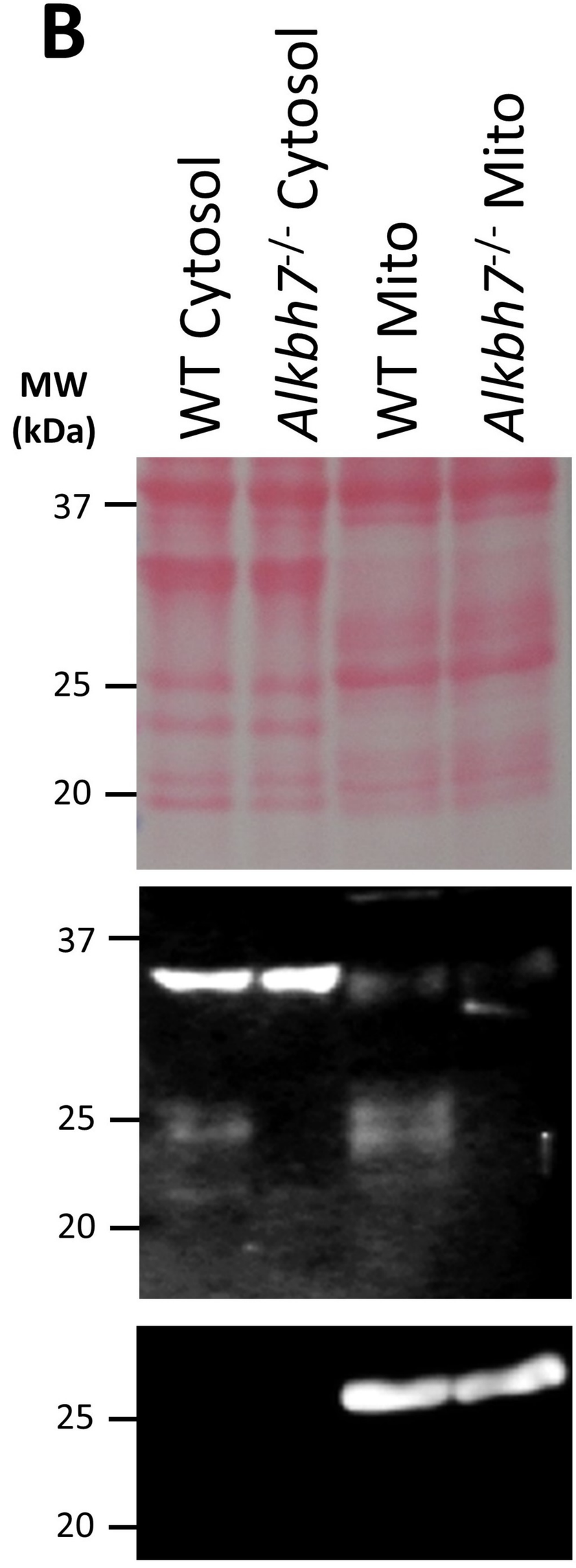
MW
(kDa)
WT Cytosol
Alkbh7-/- Cytosol
WT Mito
Alkbh7-/- Mito
37
25
20
37
25
20
Alkbh7
25
20
ANT1

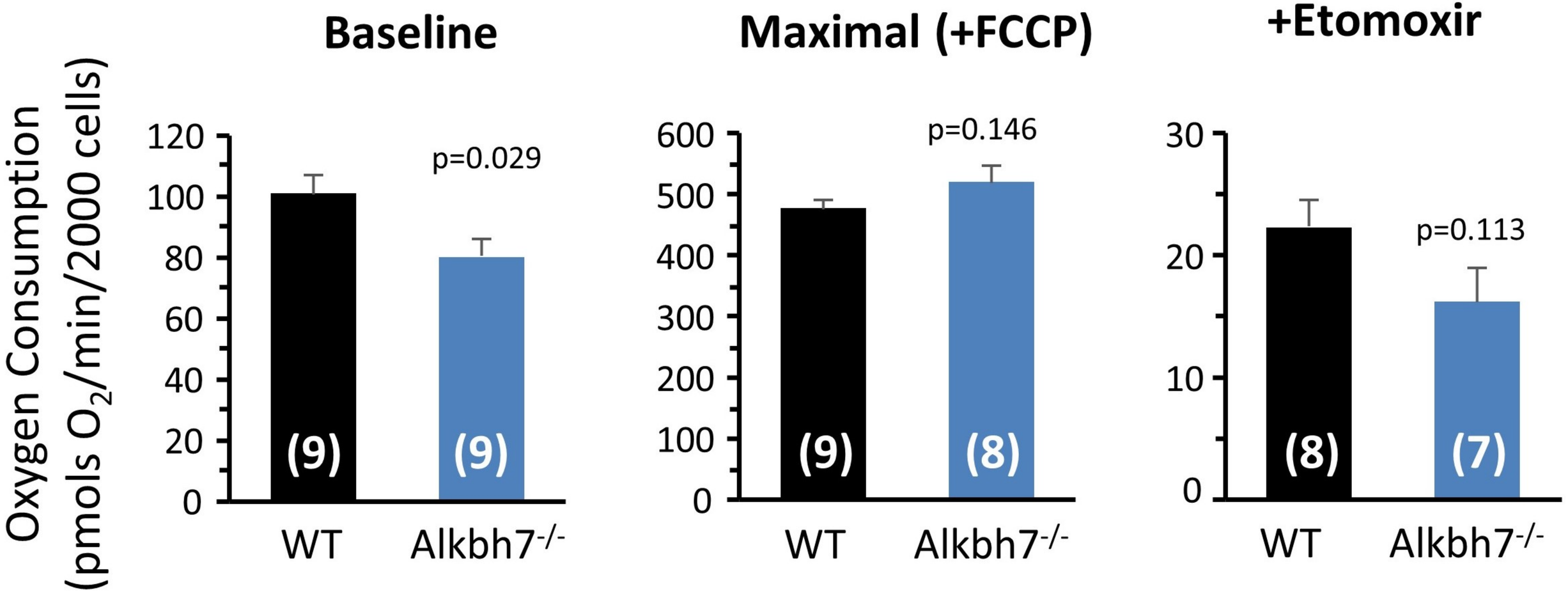
Baseline
Maximal (+FCCP)
+Etomoxir
Oxygen Consumption
(pmols O_2/min/2000 cells)
120
100
80
60
40
20
0
p=0.029
(9)
(9)
WT
Alkbh7-/-
600
500
400
300
200
100
0
p=0.146
(9)
(8)
WT
Alkbh7-/-
30
20
10
0
p=0.113
(8)
(7)
WT
Alkbh7-/-

A

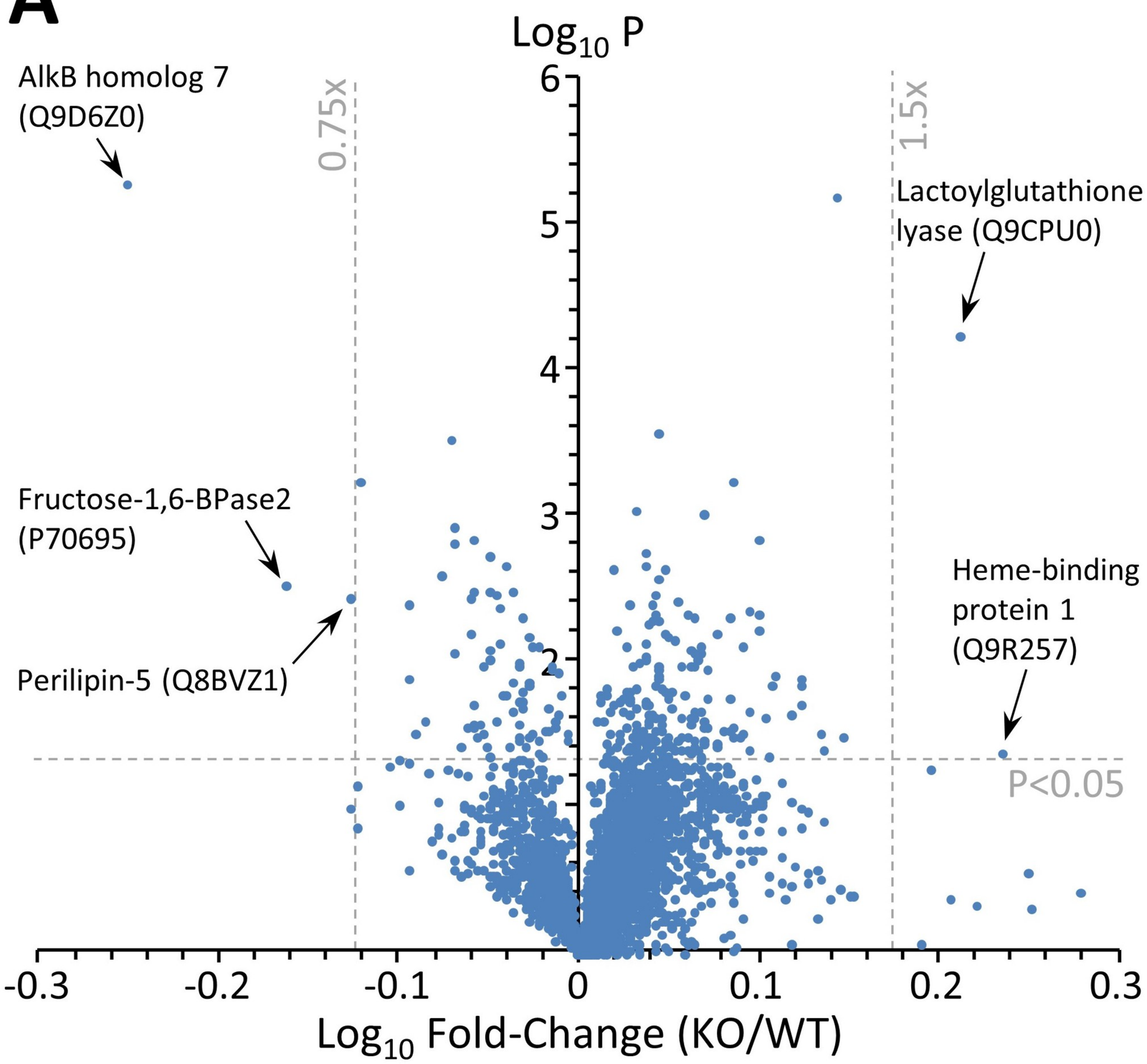
Log10 P
AlkB homolog 7 (Q9D6Z0)
0.75x
1.5x
Lactoylglutathione lyase (Q9CPU0)
Fructose-1,6-BPase2 (P70695)
Heme-binding protein 1 (Q9R257)
Perilipin-5 (Q8BVZ1)
P<0.05
6
5
4
3
2
-0.3
-0.2
-0.1
0
0.1
0.2
0.3
Log10 Fold-Change (KO/WT)

B

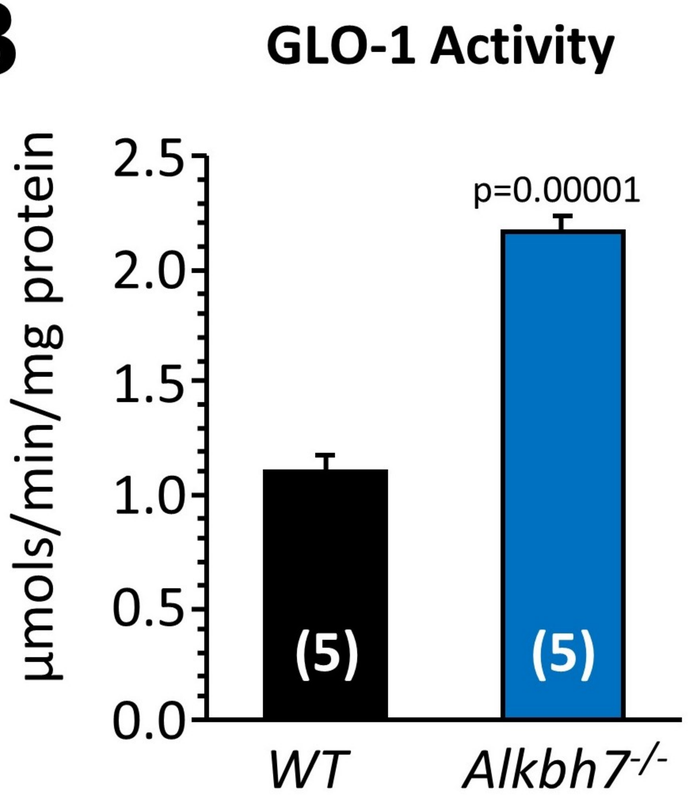
GLO-1 Activity
µmols/min/mg protein
2.5
2.0
1.5
1.0
0.5
0.0
p=0.00001
(5)
(5)
WT
Alkbh7-/-

C

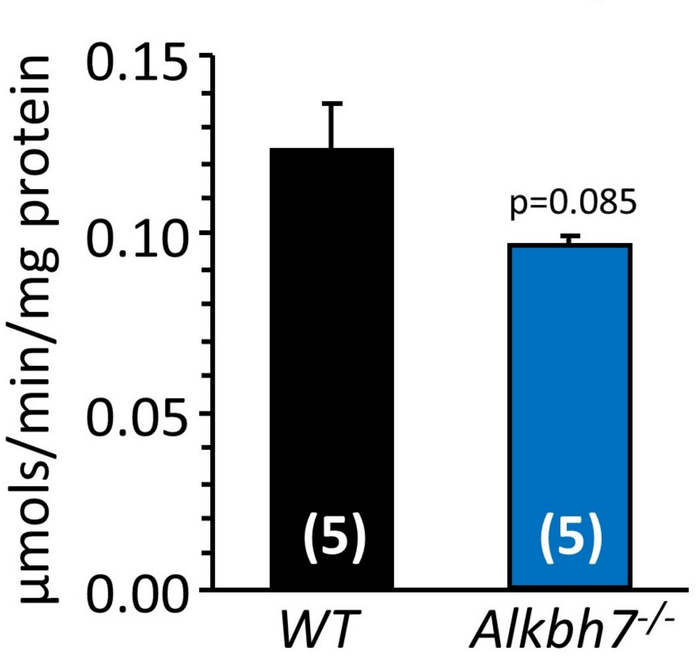
GLO-2 Activity
µmols/min/mg protein
0.15
0.10
0.05
0.00
p=0.085
(5)
(5)
WT
Alkbh7-/-

D

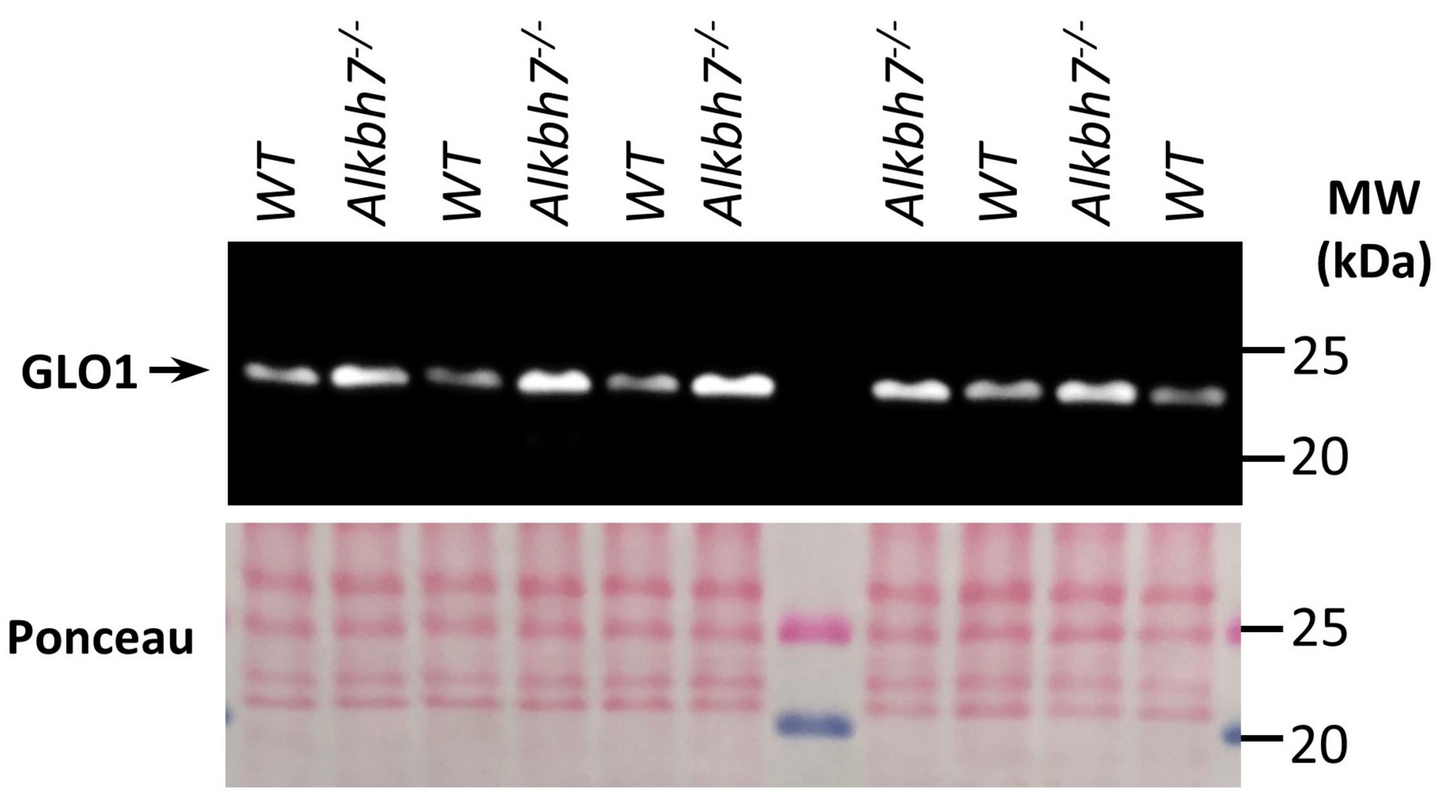
WT
Alkbh7-/-
MW (kDa)
GLO1
25
20
Ponceau
25
20

E

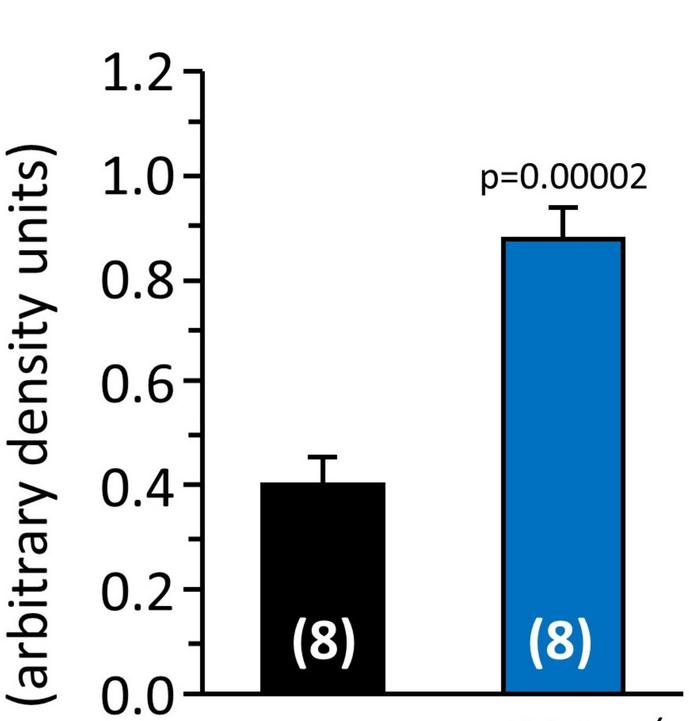
GLO-1/Ponceau (arbitrary density units)
1.2
1.0
0.8
0.6
0.4
0.2
0.0
p=0.00002
(8)
(8)
WT
Alkbh7-/-

F

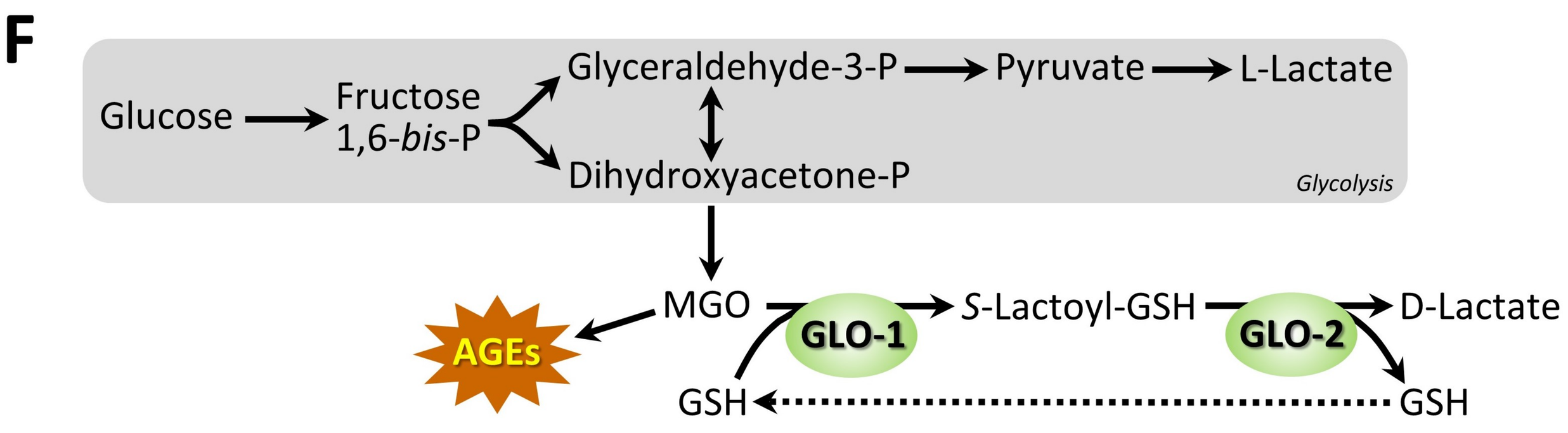
Glucose
Fructose 1,6-bis-P
Glyceraldehyde-3-P
Pyruvate
L-Lactate
Dihydroxyacetone-P
Glycolysis
MGO
AGEs
GLO-1
S-Lactoyl-GSH
GLO-2
D-Lactate
GSH
GSH

Cell Line:	Ctrl. (vector only)	ALKBH7-FLAG		
Hrs. post-MMS:	-	-	1.0	1.5	2.0

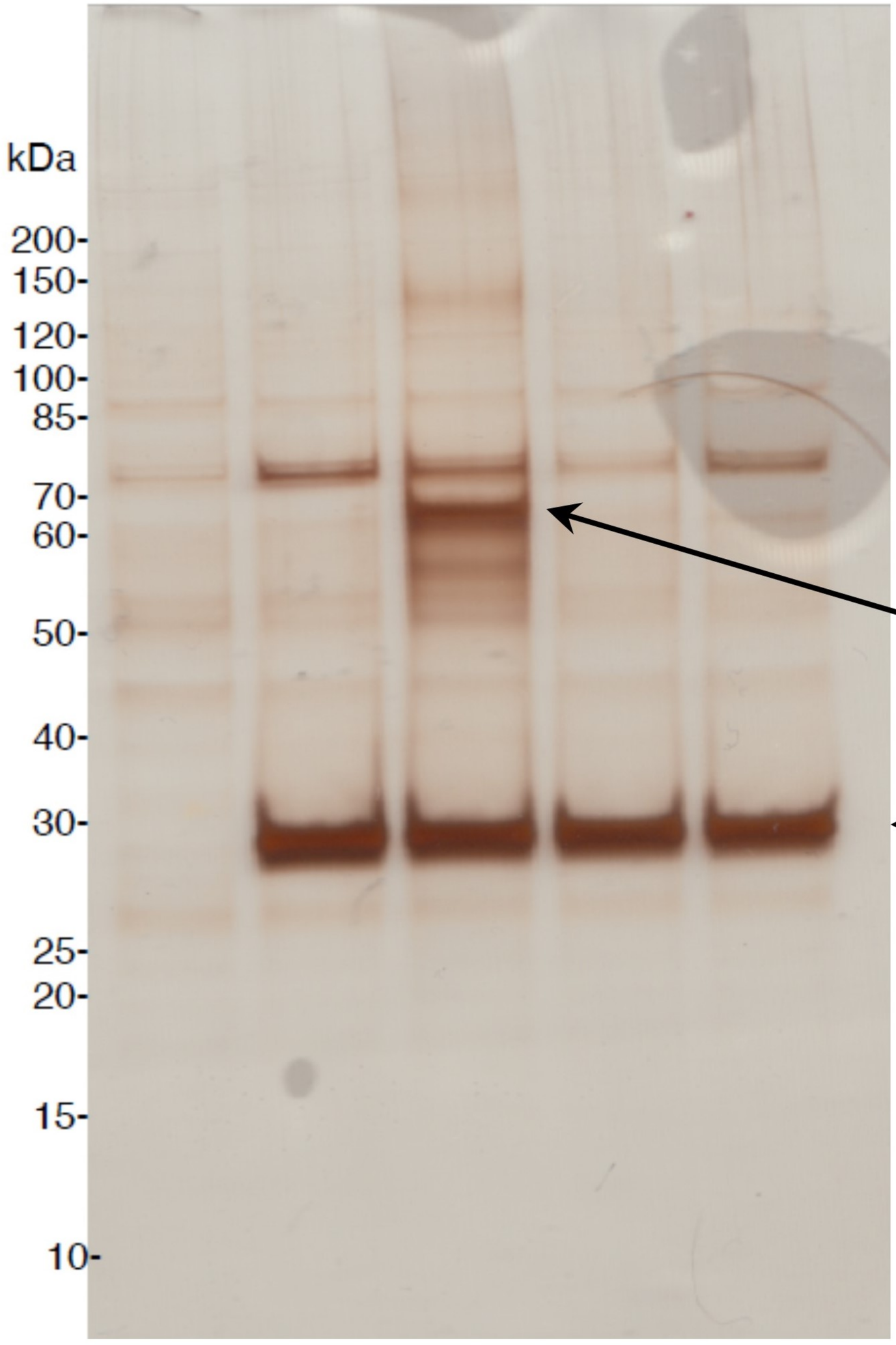

A

HEART MITOCHONDRIA

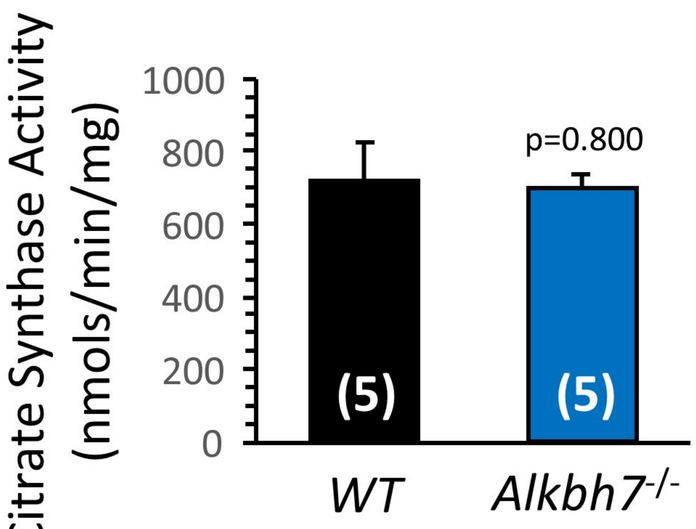

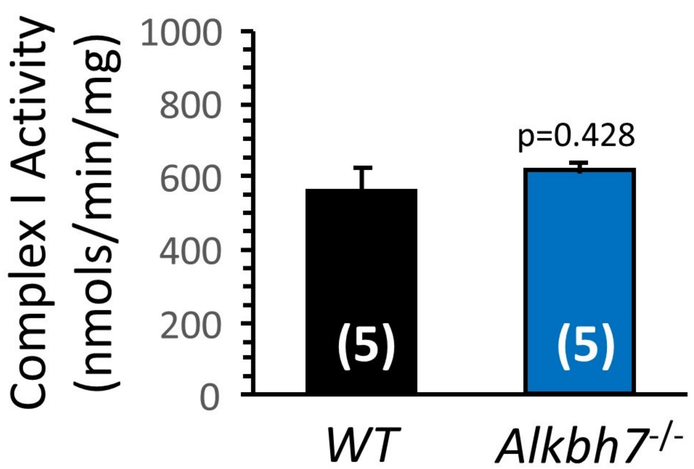

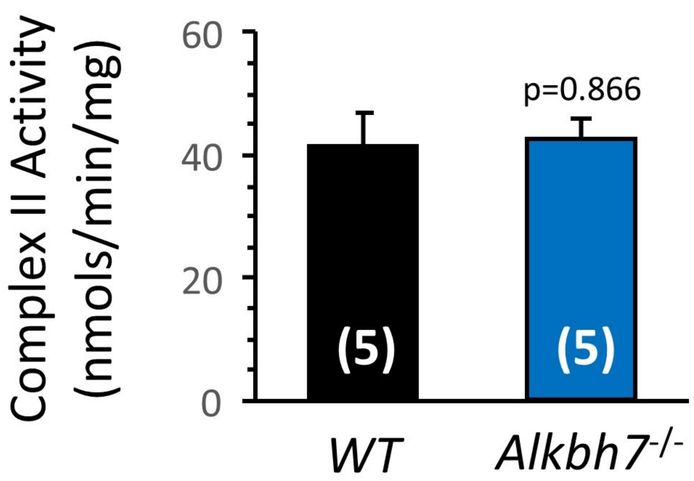

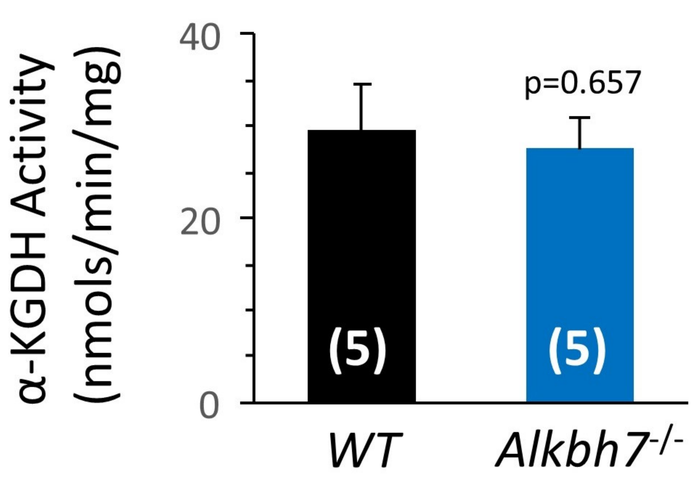

B

LIVER MITOCHONDRIA

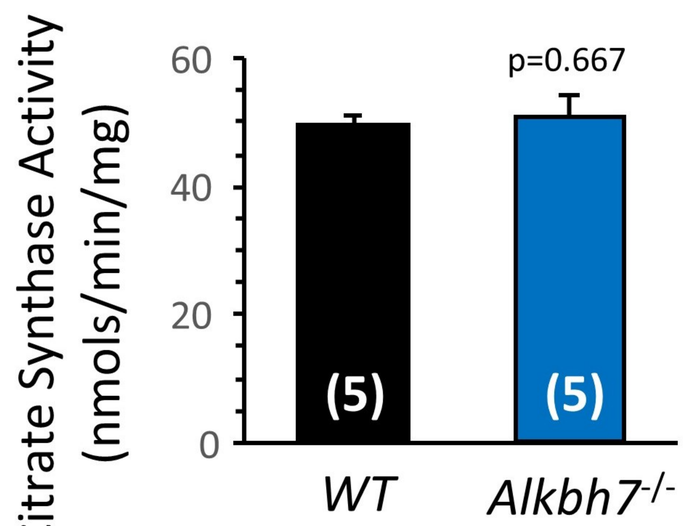

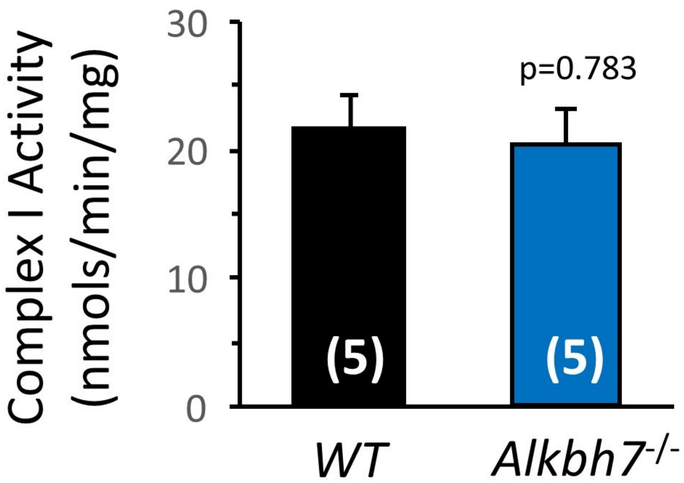

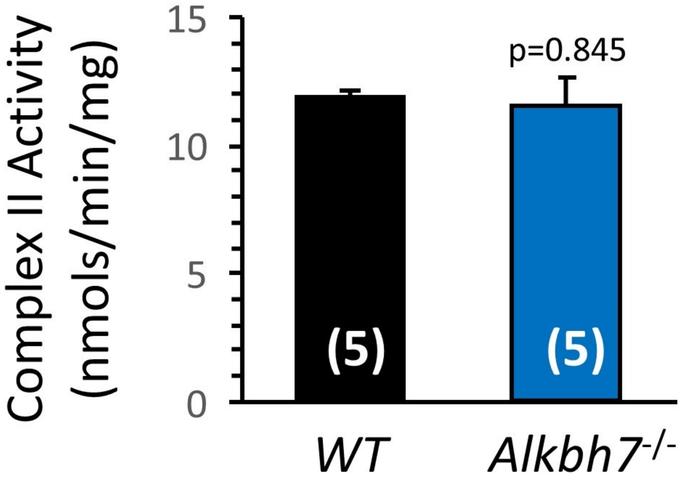

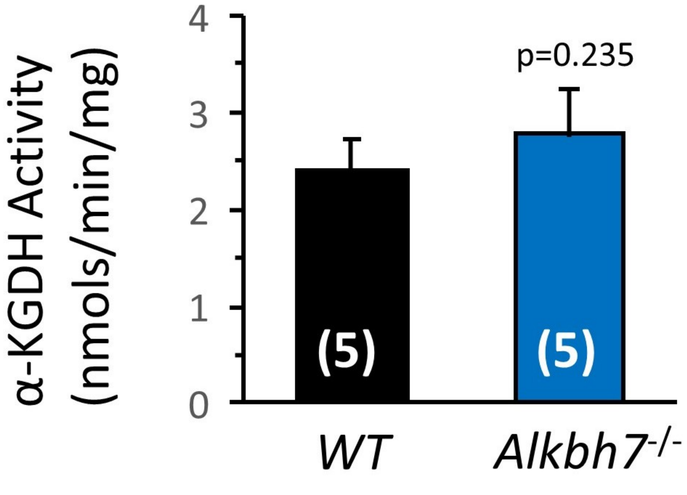

C

LIVER CYTOSOL

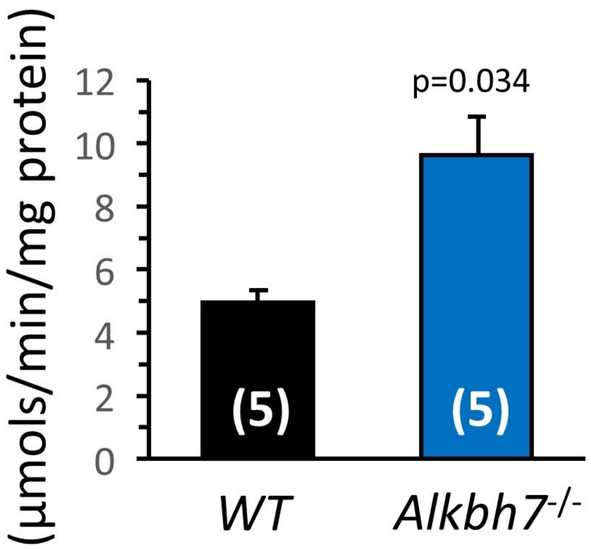

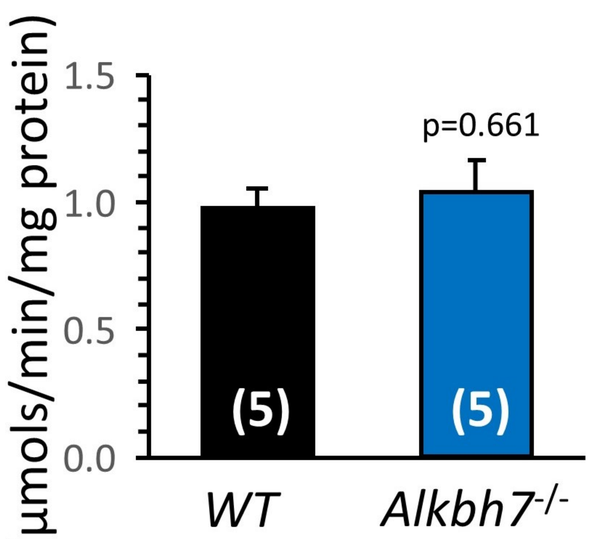

A

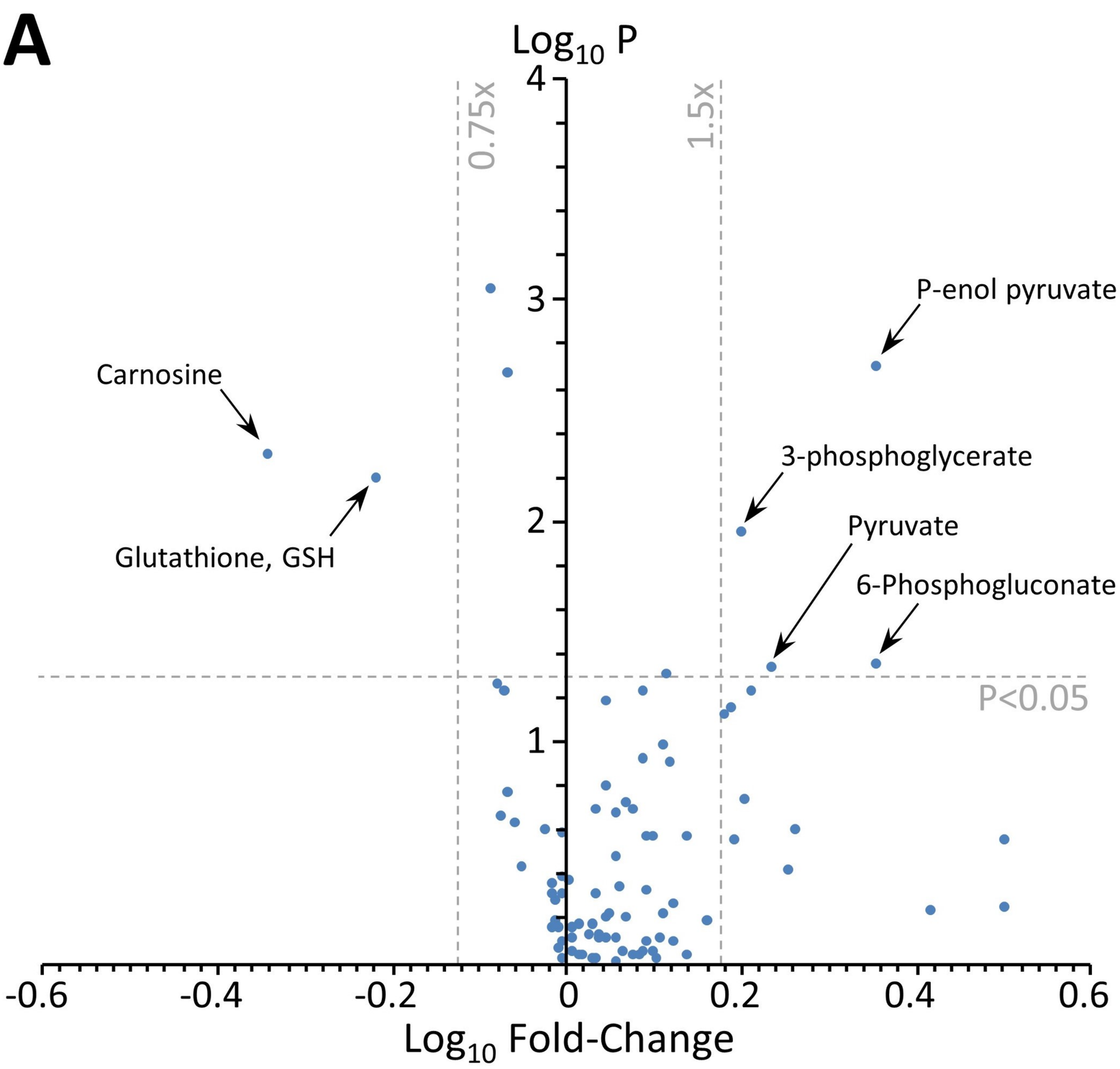
Log10 P
4
3
2
1
0.75x
1.5x
P<0.05
Carnosine
Glutathione, GSH
P-enol pyruvate
3-phosphoglycerate
Pyruvate
6-Phosphogluconate
-0.6
-0.4
-0.2
0
0.2
0.4
0.6
Log10 Fold-Change

B

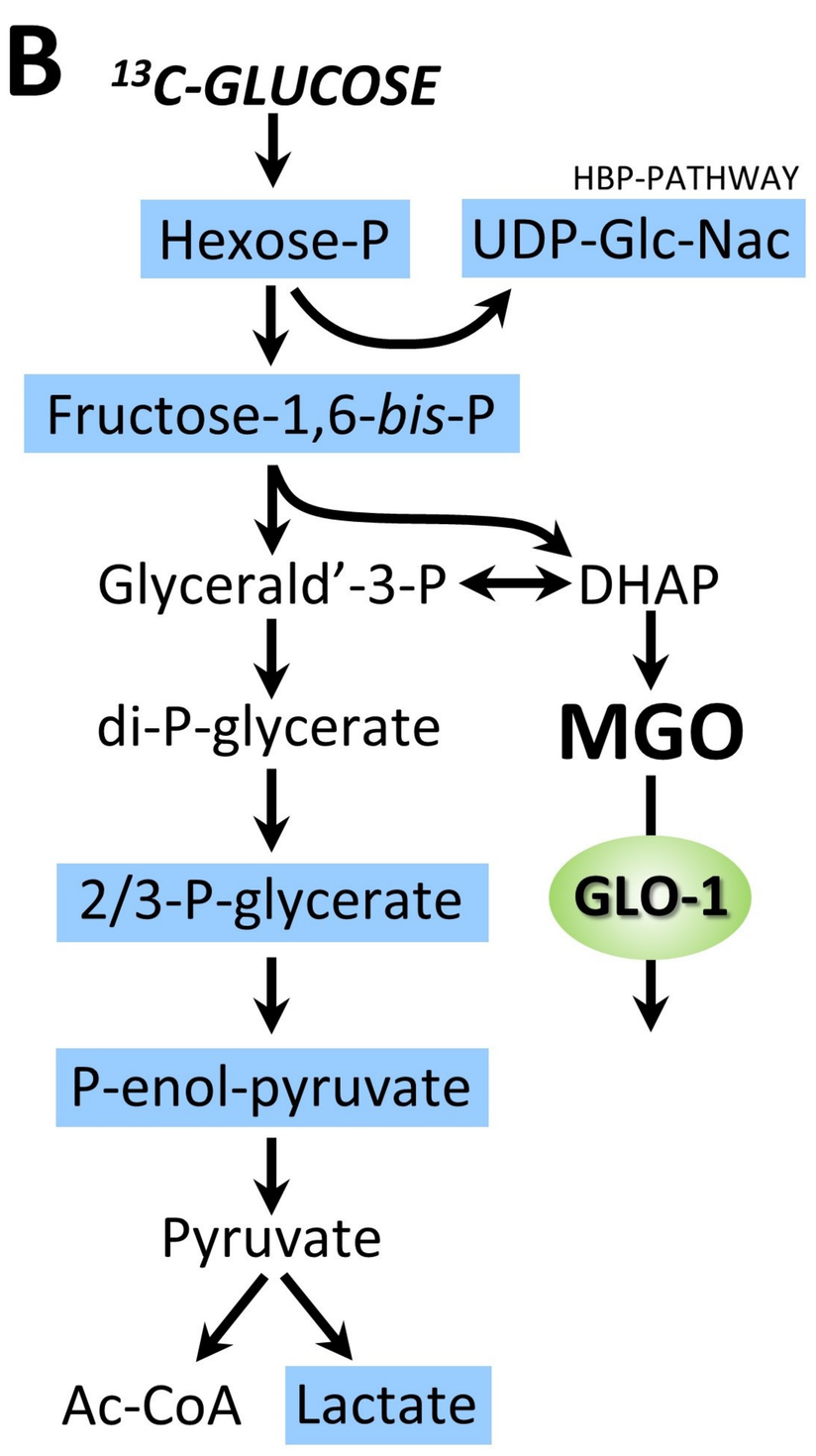
13C-GLUCOSE
HBP-PATHWAY
Hexose-P
UDP-Glc-Nac
Fructose-1,6-bis-P
Glycerald'-3-P
DHAP
di-P-glycerate
MGO
GLO-1
2/3-P-glycerate
P-enol-pyruvate
Pyruvate
Ac-CoA
Lactate

C

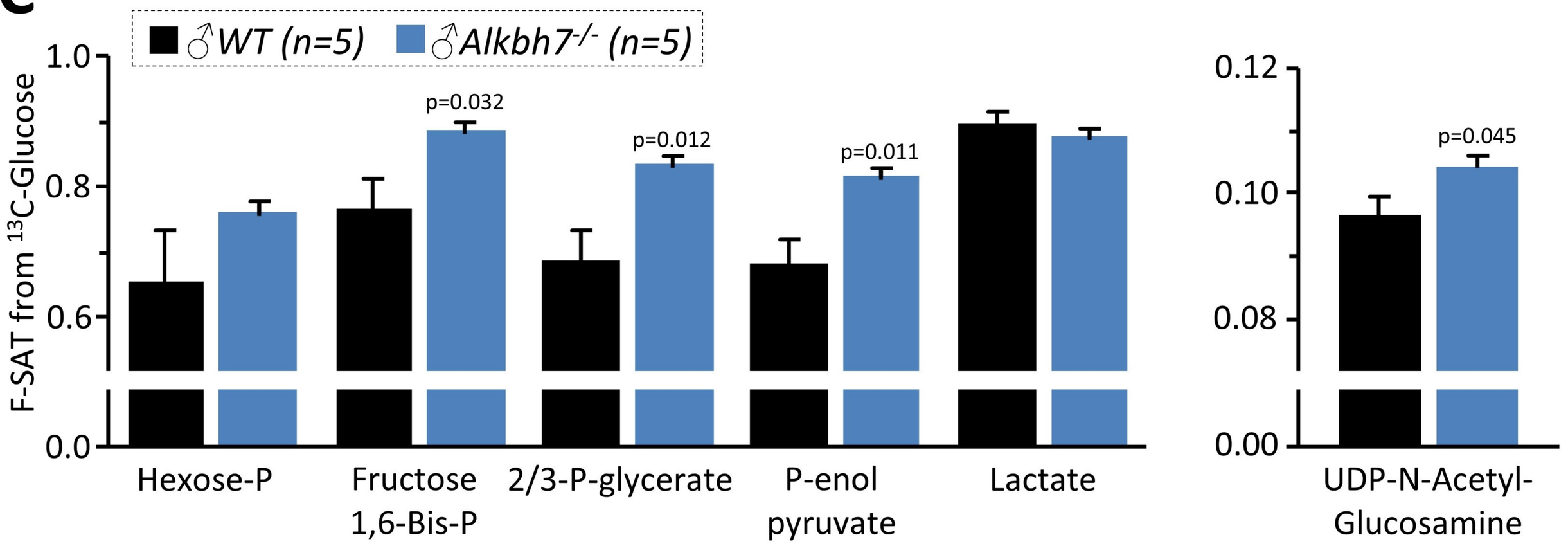
♂WT (n=5)
♂Alkbh7-/- (n=5)
F-SAT from 13C-Glucose
1.0
0.8
0.6
0.0
p=0.032
p=0.012
p=0.011
Hexose-P
Fructose 1,6-Bis-P
2/3-P-glycerate
P-enol pyruvate
Lactate
0.12
0.10
0.08
0.00
p=0.045
UDP-N-Acetyl-Glucosamine

D

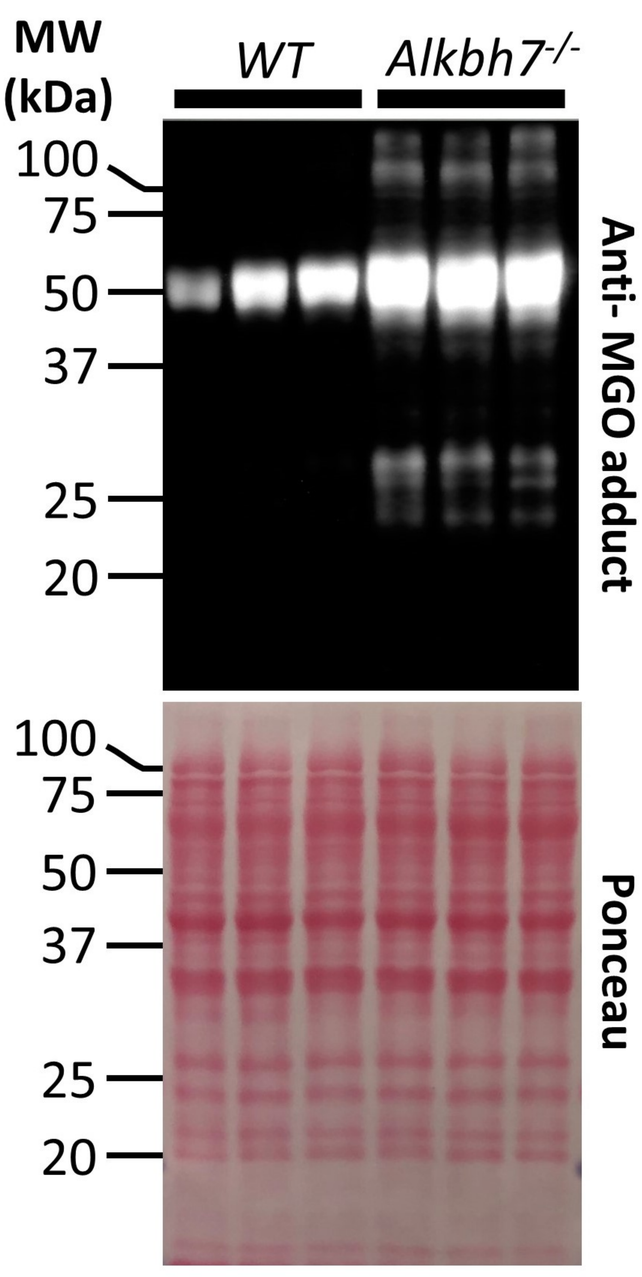
MW (kDa)
WT
Alkbh7-/-
100
75
50
37
25
20
Anti- MGO adduct
Ponceau

E

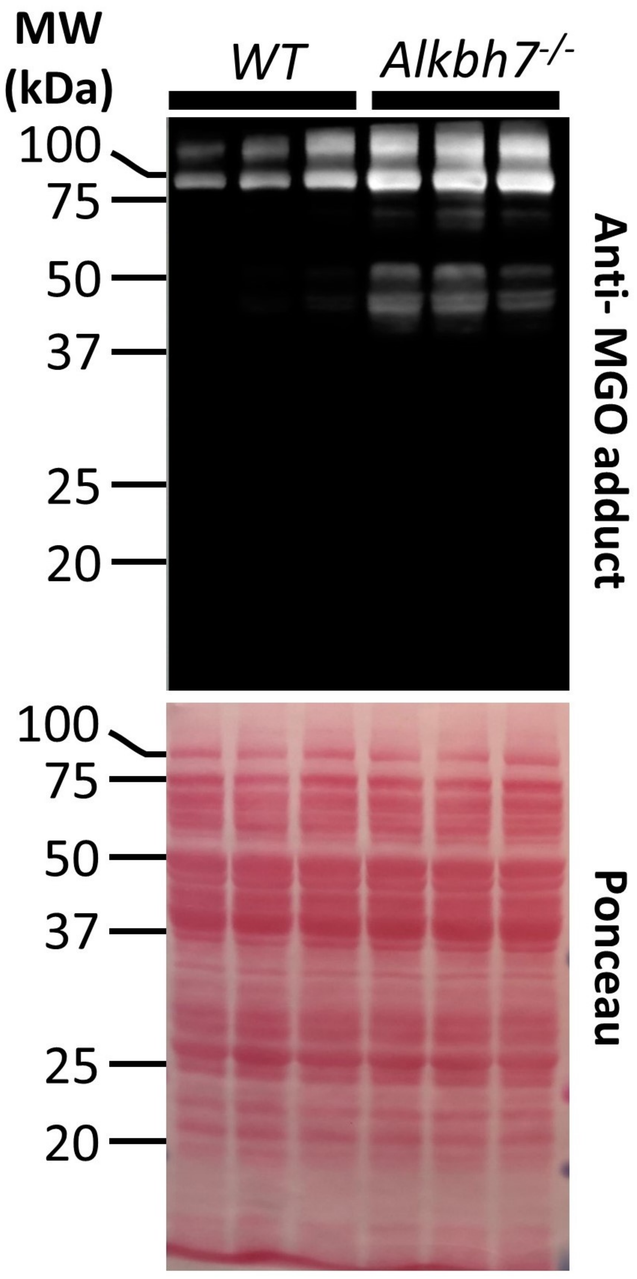
MW (kDa)
WT
Alkbh7-/-
100
75
50
37
25
20
Anti- MGO adduct
Ponceau

F

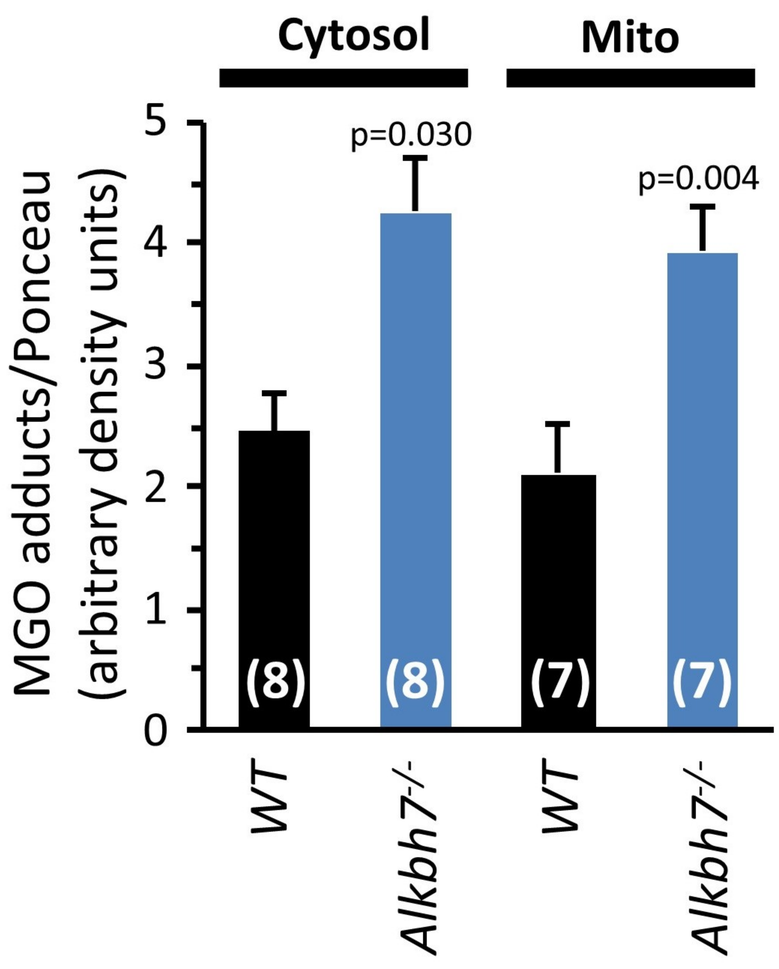
Cytosol
Mito
MGO adducts/Ponceau (arbitrary density units)
5
4
3
2
1
0
p=0.030
p=0.004
(8)
(8)
(7)
(7)
WT
Alkbh7-/-
WT
Alkbh7-/-

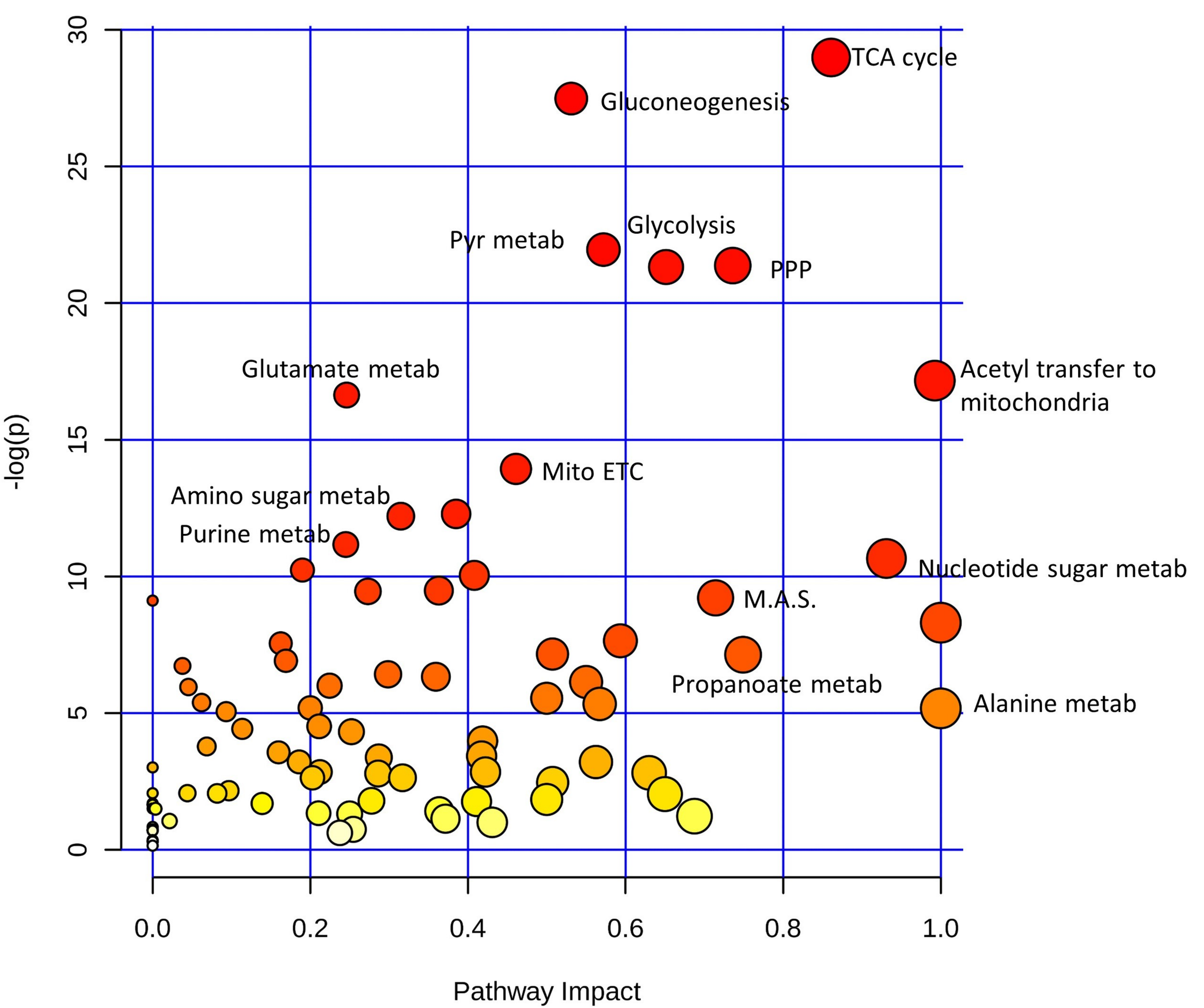
TCA cycle
Gluconeogenesis
Pyr metab
Glycolysis
PPP
Glutamate metab
Acetyl transfer to mitochondria
Mito ETC
Amino sugar metab
Purine metab
Nucleotide sugar metab
M.A.S.
Propanoate metab
Alanine metab
30
25
20
15
10
5
0
0.0
0.2
0.4
0.6
0.8
1.0
-log(p)
Pathway Impact

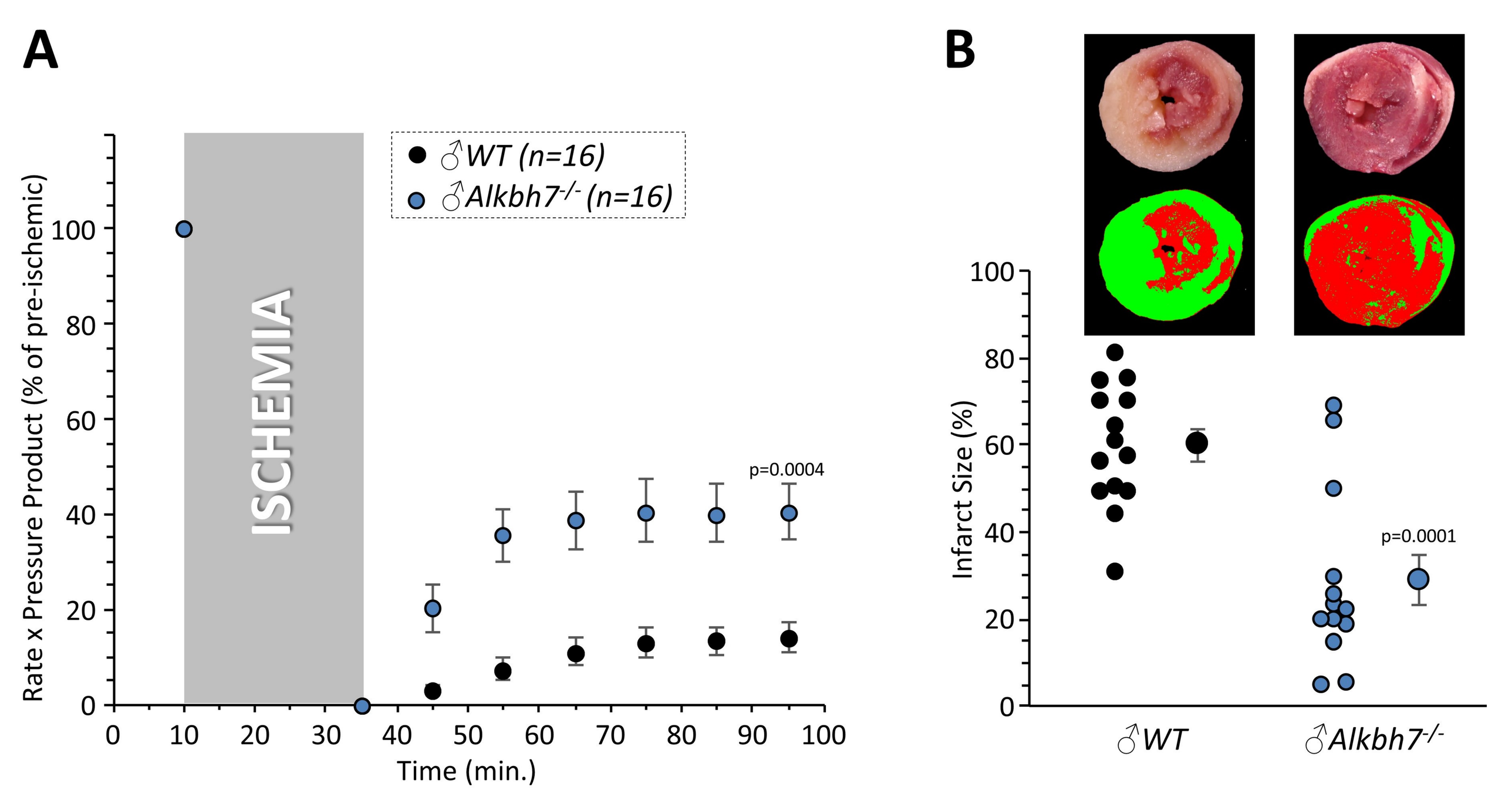
A
♂WT (n=16)
♂Alkbh7-/- (n=16)
ISCHEMIA
Rate x Pressure Product (% of pre-ischemic)
Time (min.)
p=0.0004
B
Infarct Size (%)
p=0.0001
♂WT
♂Alkbh7-/-

A

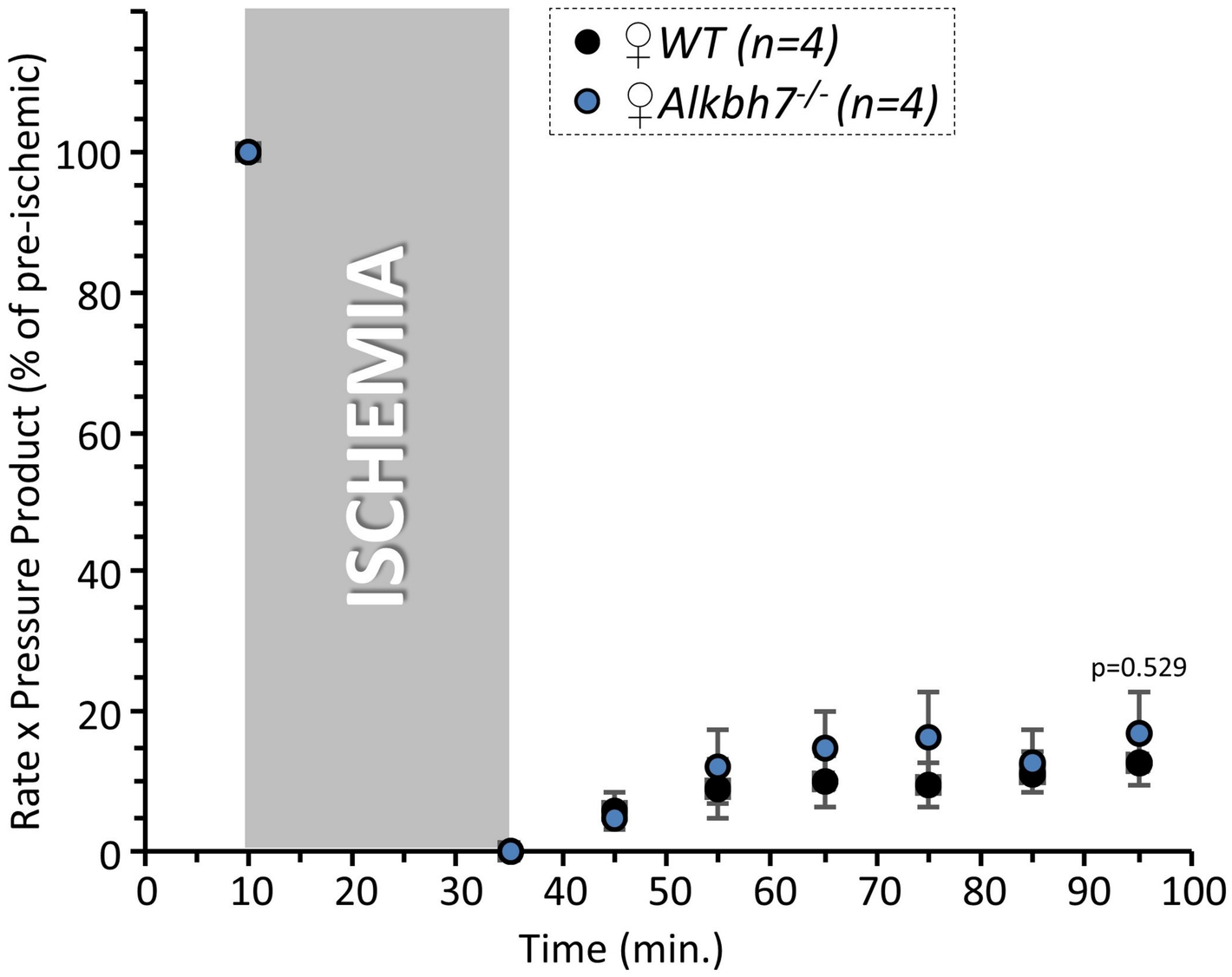
♀WT (n=4)
♀Alkbh7-/- (n=4)
ISCHEMIA
Rate x Pressure Product (% of pre-ischemic)
0
20
40
60
80
100
0
10
20
30
40
50
60
70
80
90
100
Time (min.)
p=0.529

B

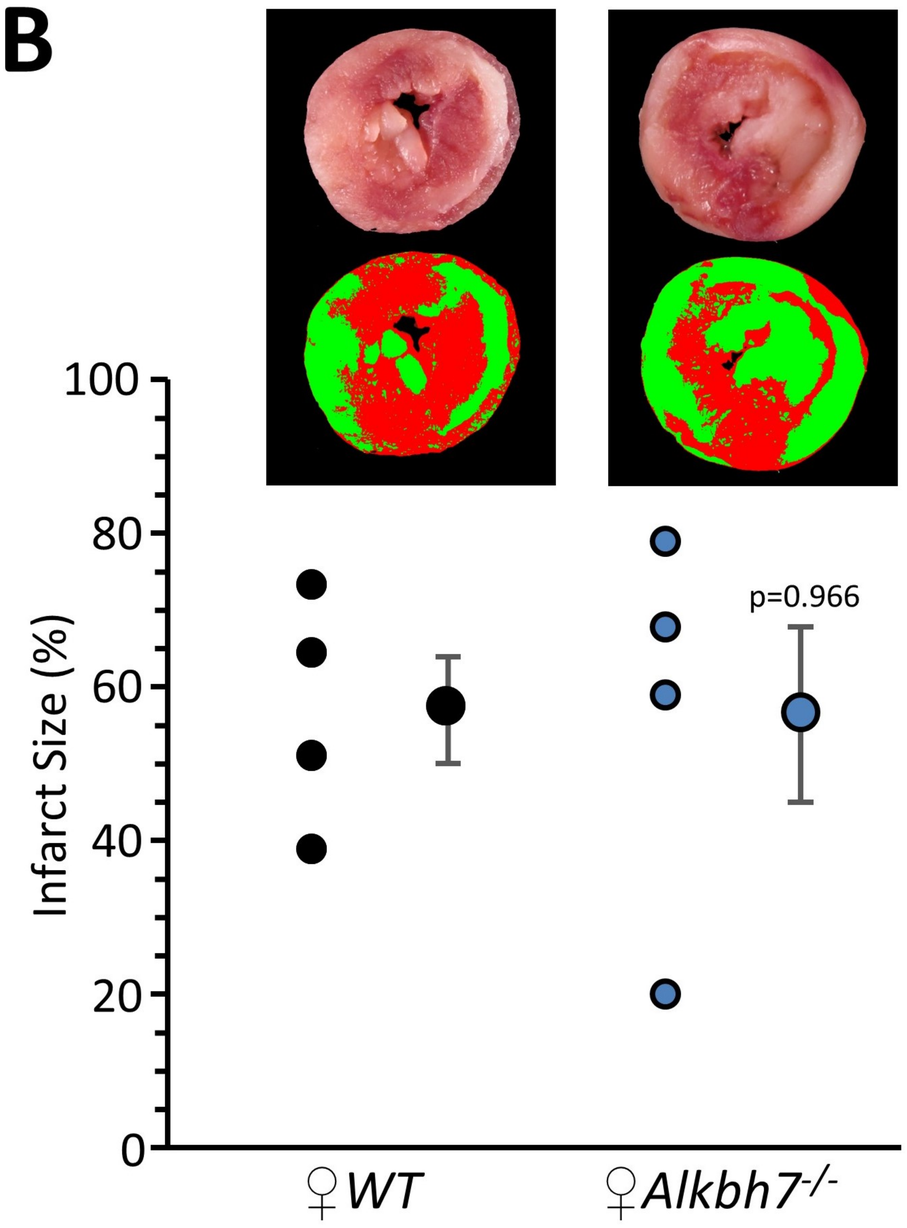
Infarct Size (%)
0
20
40
60
80
100
p=0.966
♀WT
♀Alkbh7-/-

C

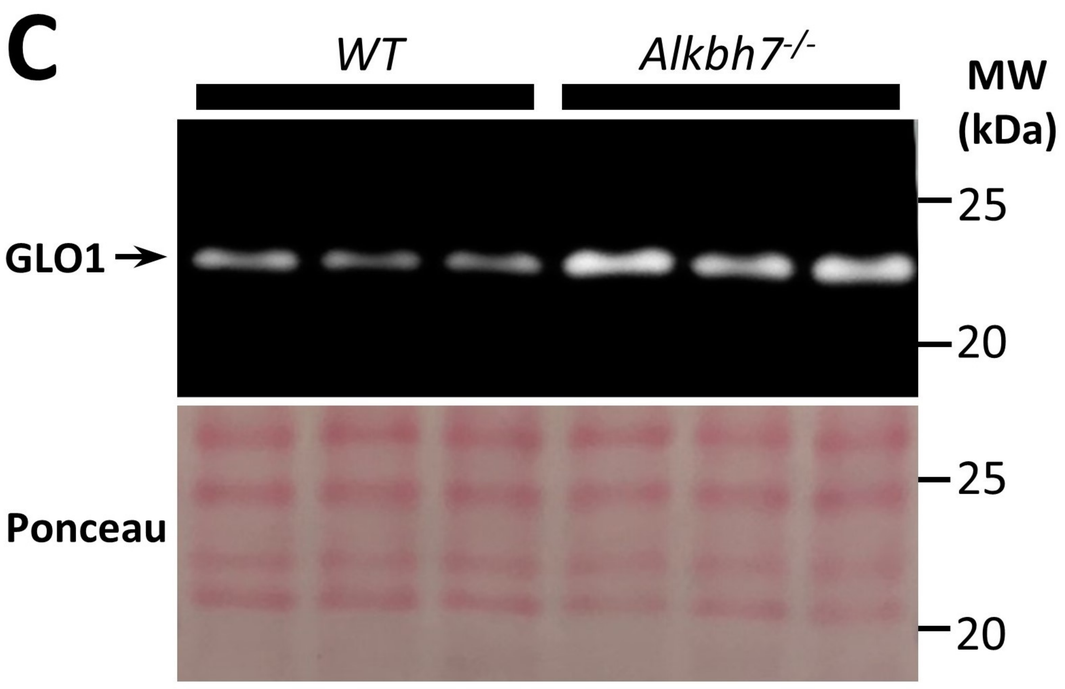
WT
Alkbh7-/-
MW (kDa)
GLO1
Ponceau
25
20
25
20

D

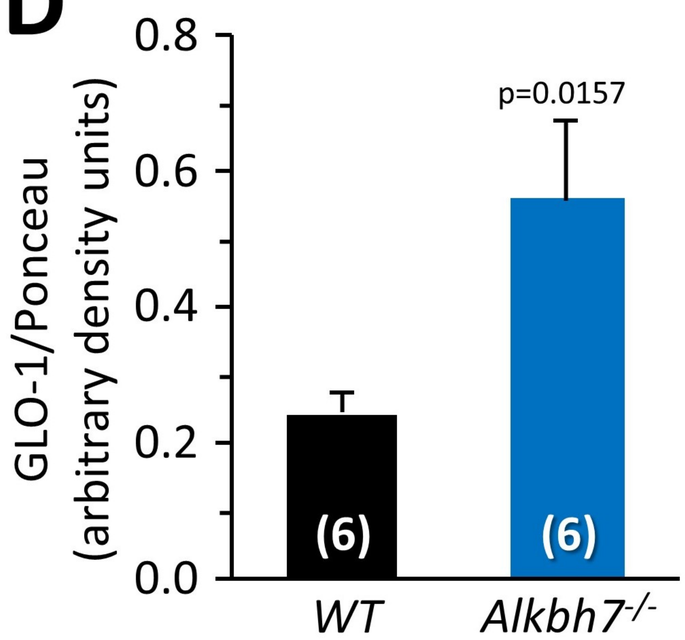
GLO-1/Ponceau (arbitrary density units)
0.0
0.2
0.4
0.6
0.8
p=0.0157
(6)
(6)
WT
Alkbh7-/-

E

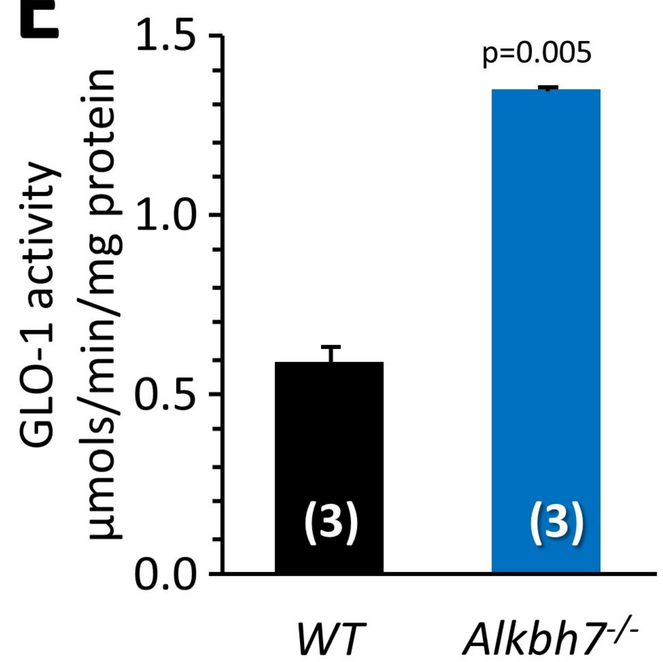
GLO-1 activity µmols/min/mg protein
0.0
0.5
1.0
1.5
p=0.005
(3)
(3)
WT
Alkbh7-/-

F

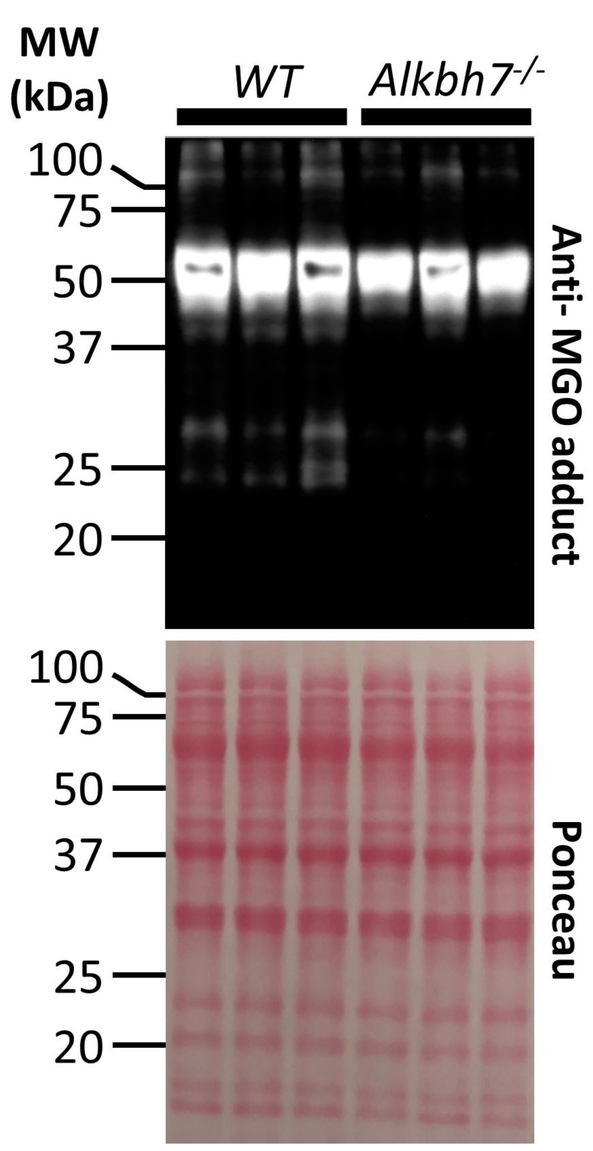
MW (kDa)
WT
Alkbh7-/-
100
75
50
37
25
20
Anti- MGO adduct
Ponceau

G

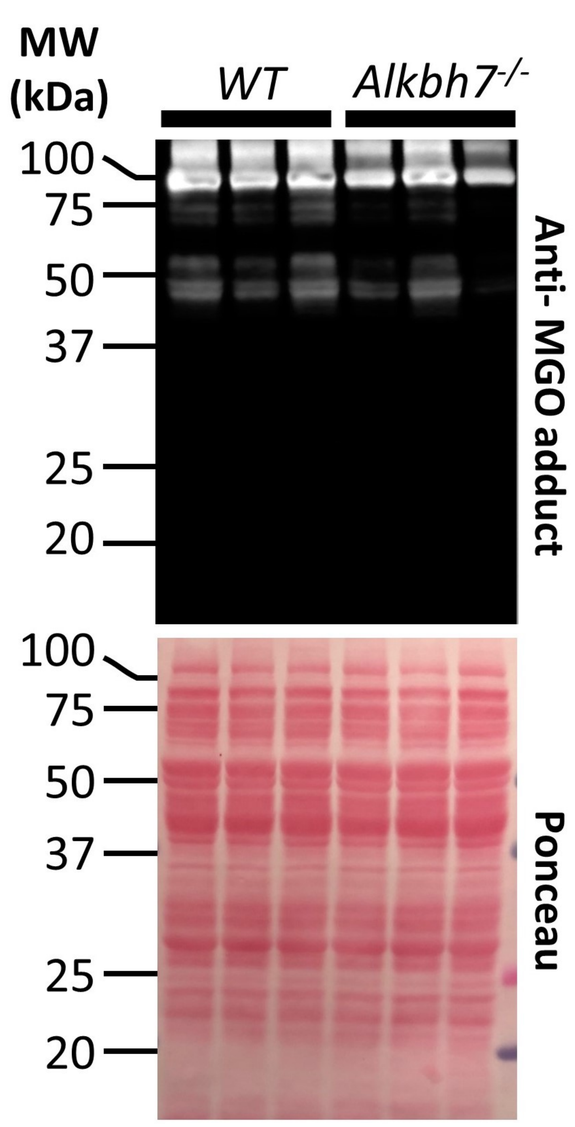
MW (kDa)
WT
Alkbh7-/-
100
75
50
37
25
20
Anti- MGO adduct
Ponceau

H

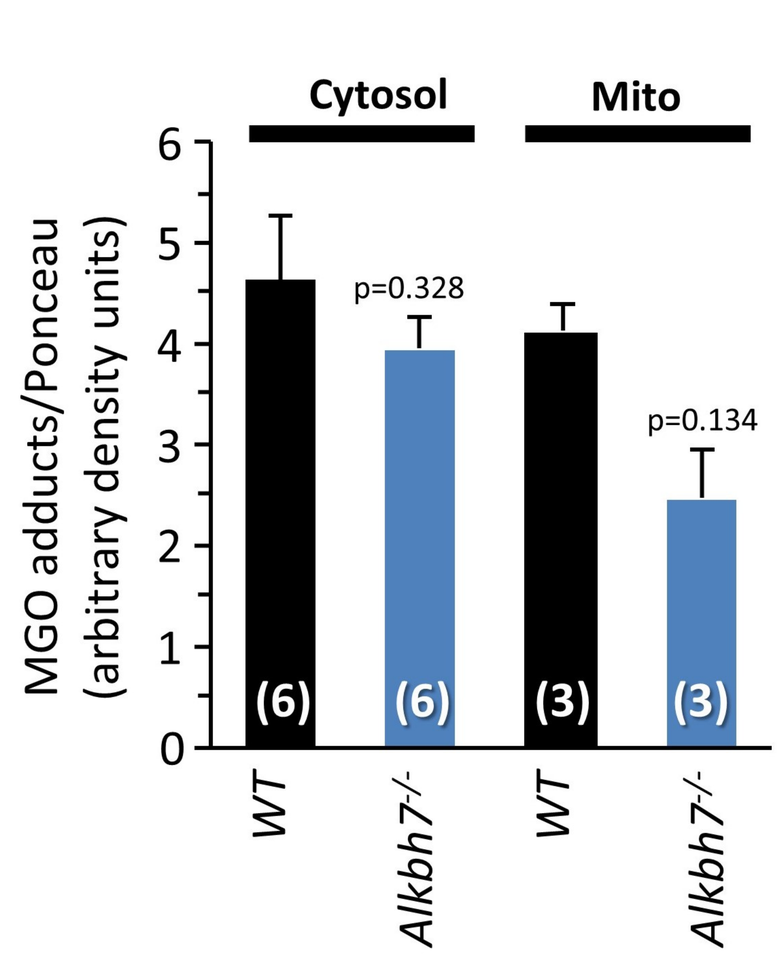
Cytosol
Mito
MGO adducts/Ponceau (arbitrary density units)
0
1
2
3
4
5
6
p=0.328
p=0.134
(6)
(6)
(3)
(3)
WT
Alkbh7-/-
WT
Alkbh7-/-

A

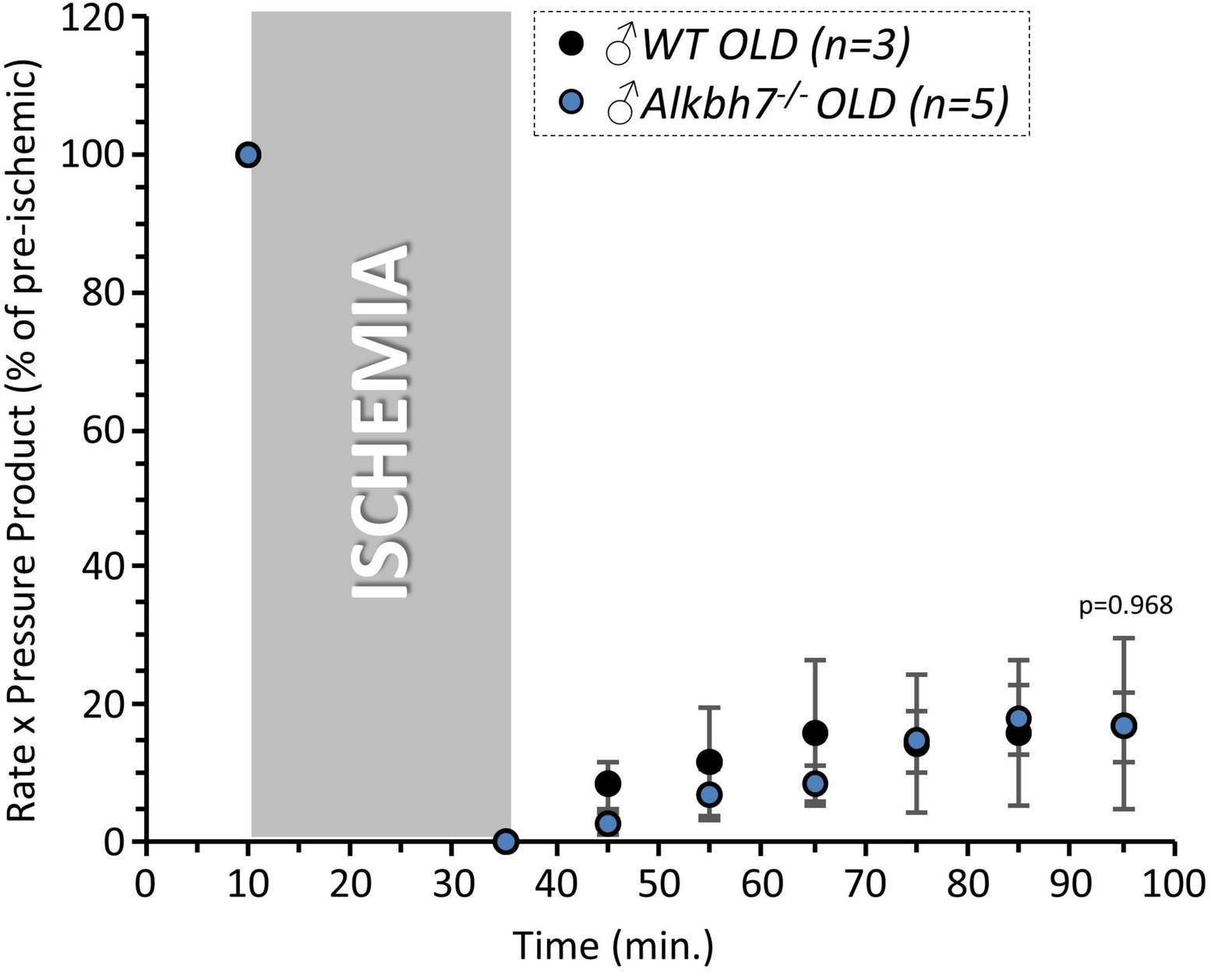
♂WT OLD (n=3)
♂Alkbh7-/- OLD (n=5)
ISCHEMIA
Rate x Pressure Product (% of pre-ischemic)
Time (min.)
p=0.968
0
20
40
60
80
100
120
0
10
20
30
40
50
60
70
80
90
100

B

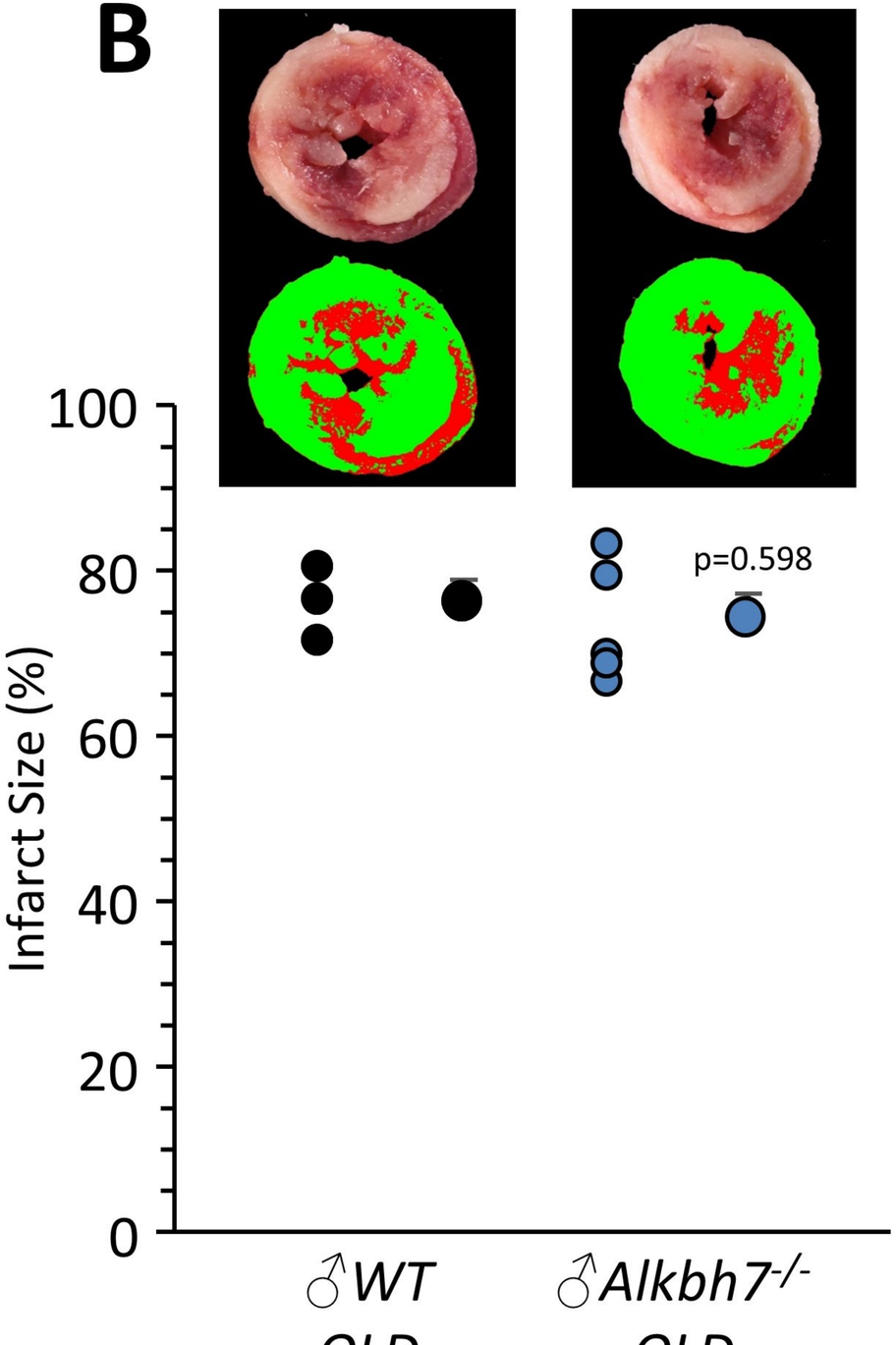
Infarct Size (%)
p=0.598
0
20
40
60
80
100
♂WT OLD
♂Alkbh7-/- OLD

A

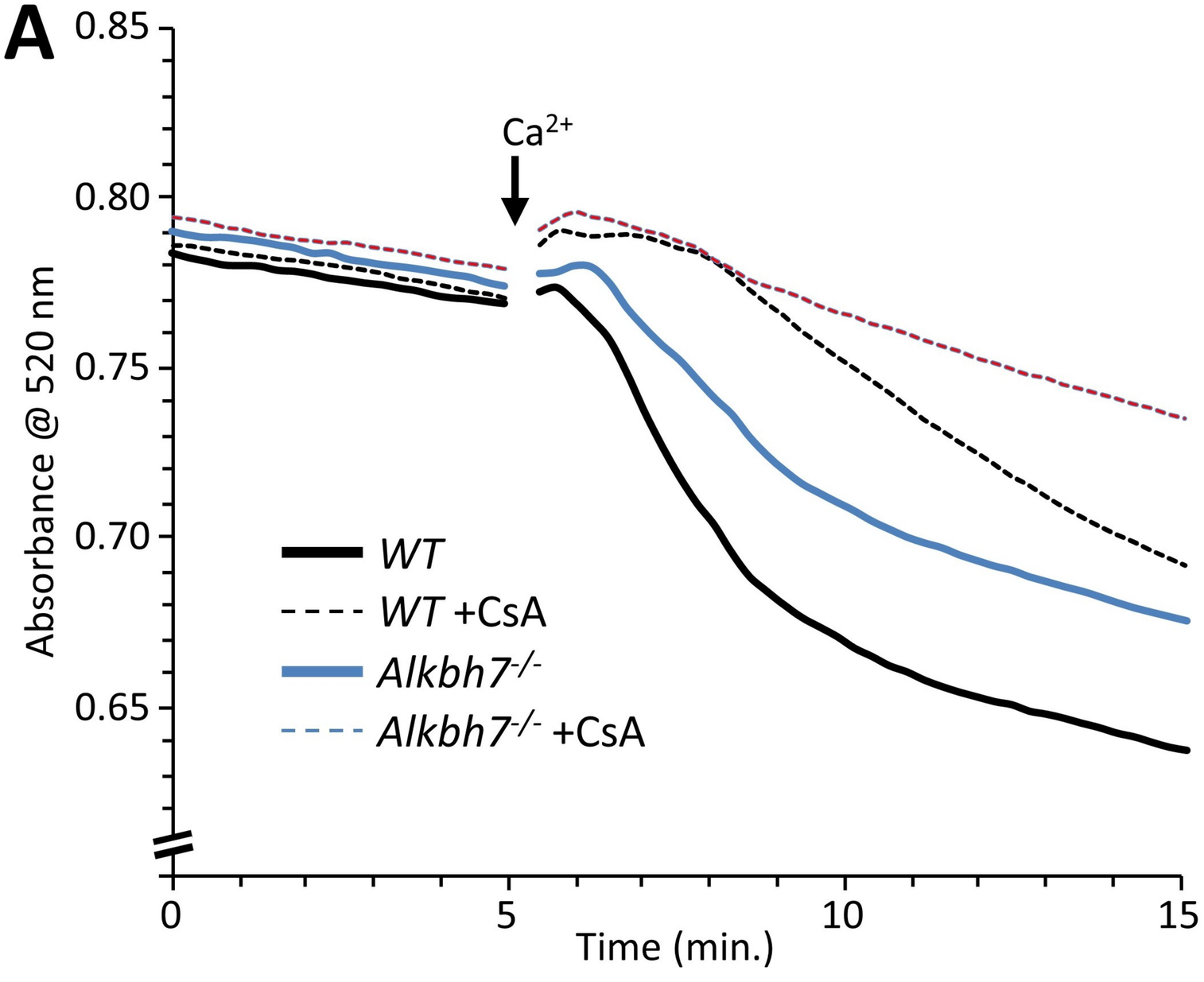
0.85
0.80
0.75
0.70
0.65
Absorbance @ 520 nm
Ca2+
WT
WT +CsA
Alkbh7-/-
Alkbh7-/- +CsA
0
5
10
15
Time (min.)

B

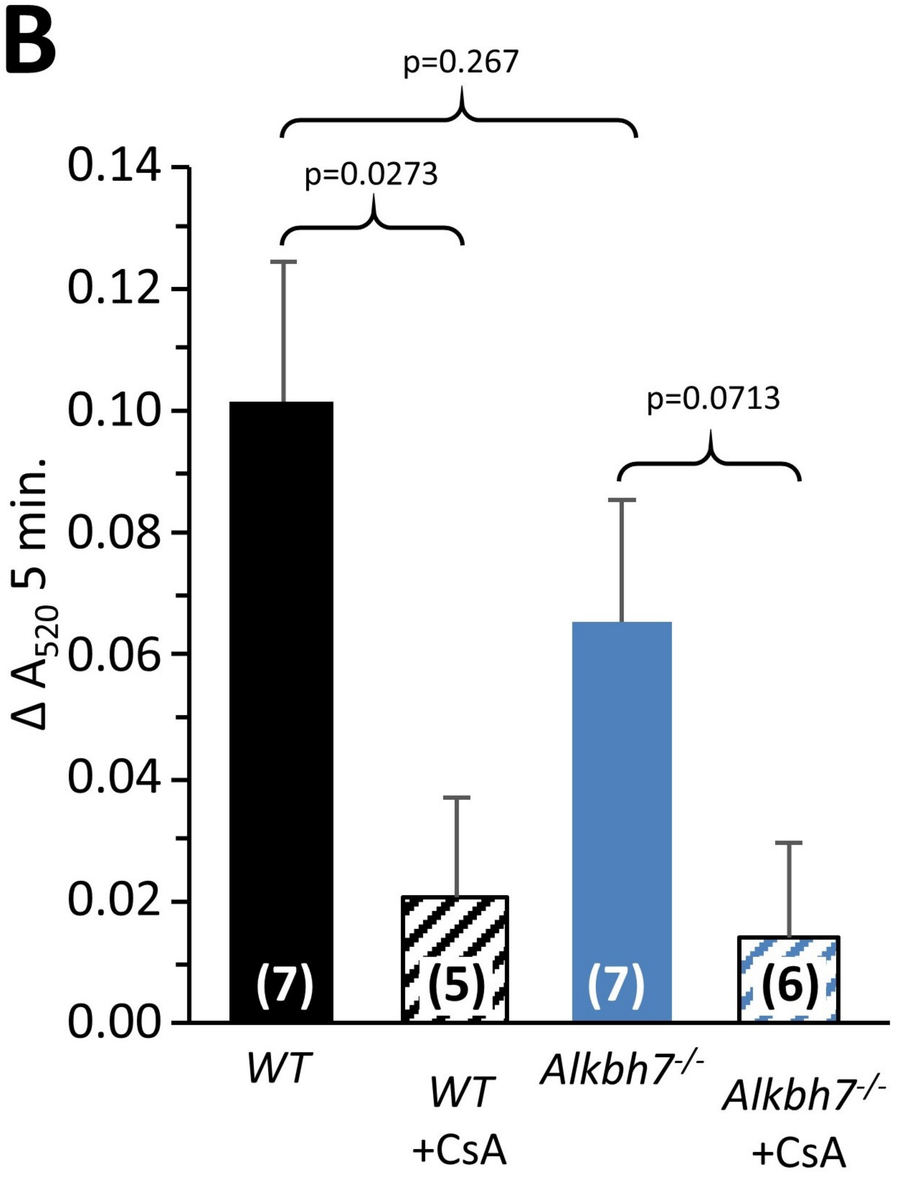
p=0.267
p=0.0273
p=0.0713
0.14
0.12
0.10
0.08
0.06
0.04
0.02
0.00
Δ A520 5 min.
(7)
(5)
(7)
(6)
WT
WT +CsA
Alkbh7-/-
Alkbh7-/- +CsA

C

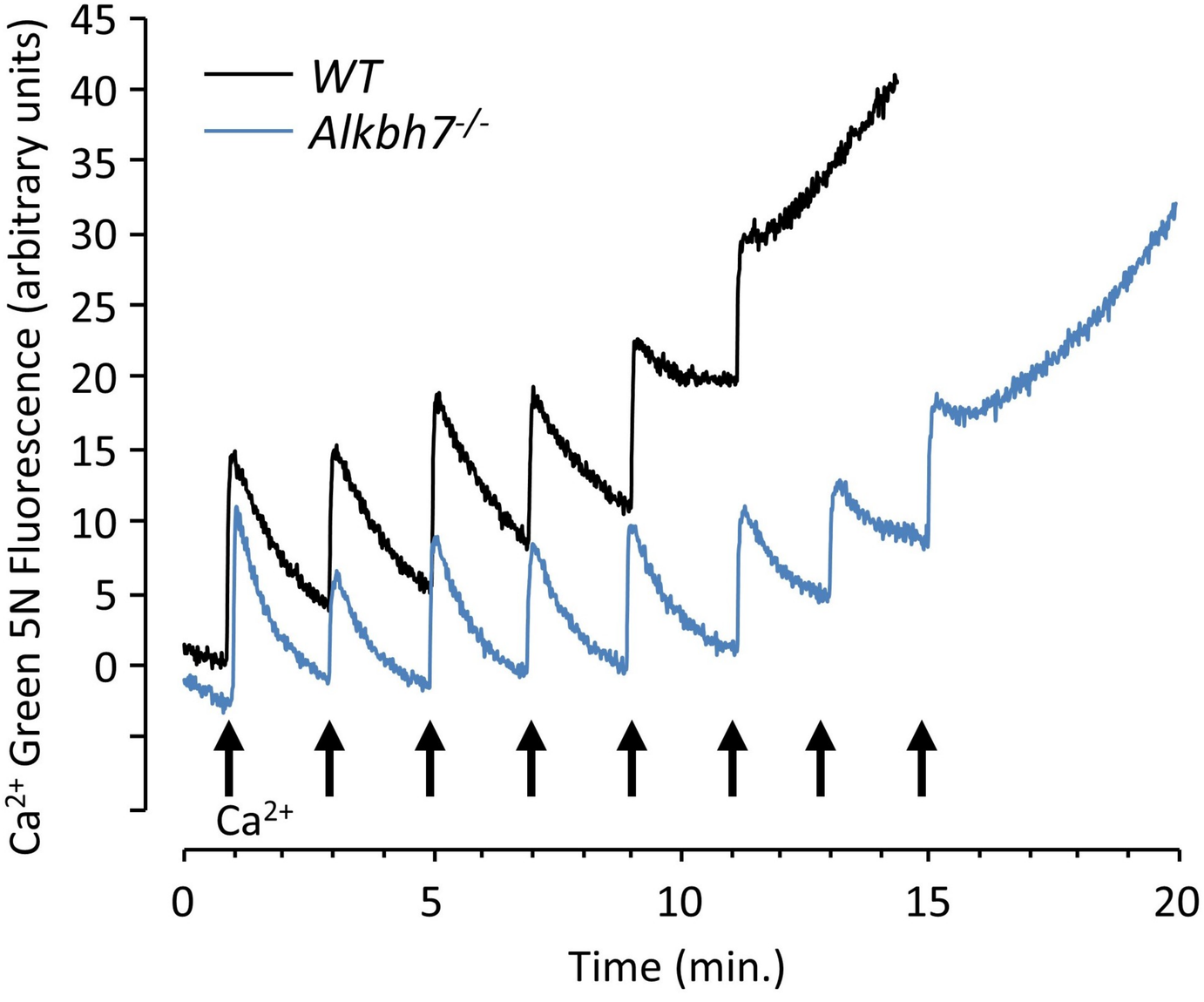
45
40
35
30
25
20
15
10
5
0
Ca2+ Green 5N Fluorescence (arbitrary units)
WT
Alkbh7-/-
Ca2+
0
5
10
15
20
Time (min.)

D

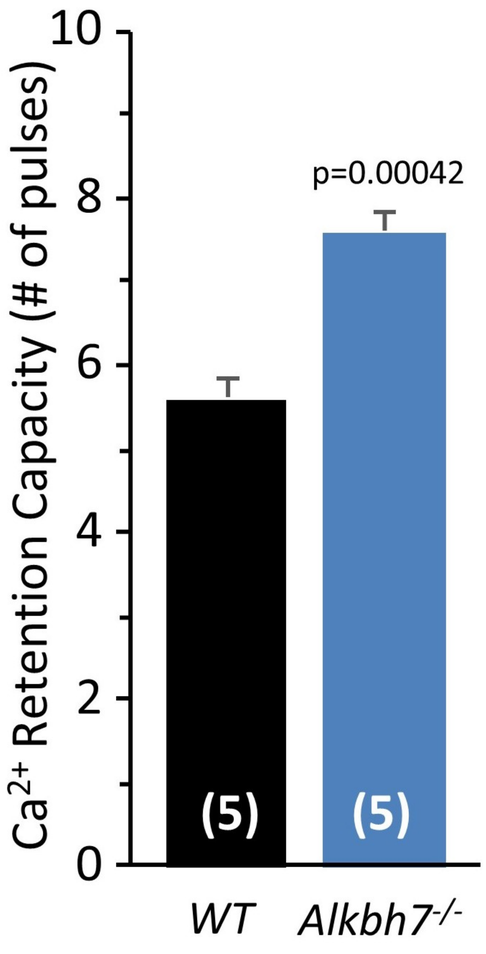
10
8
6
4
2
0
Ca2+ Retention Capacity (# of pulses)
p=0.00042
(5)
(5)
WT
Alkbh7-/-

E

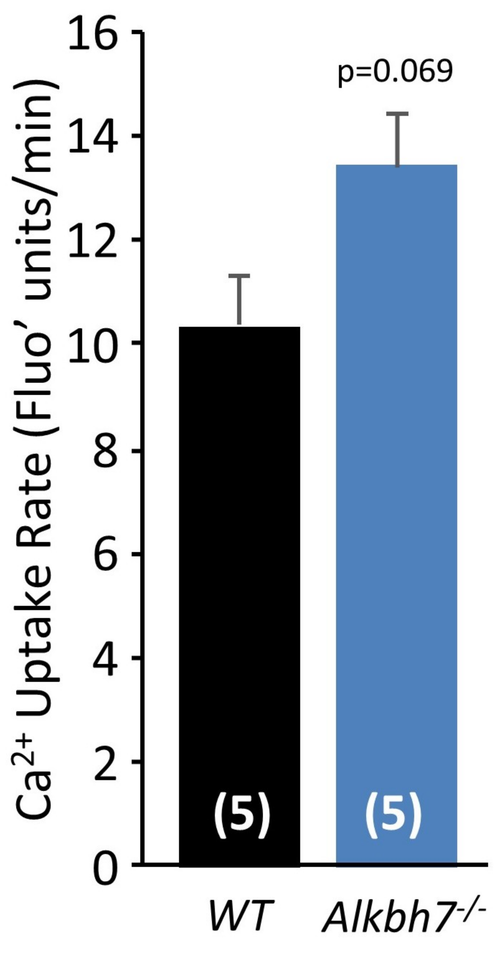
16
14
12
10
8
6
4
2
0
Ca2+ Uptake Rate (Fluo' units/min)
p=0.069
(5)
(5)
WT
Alkbh7-/-

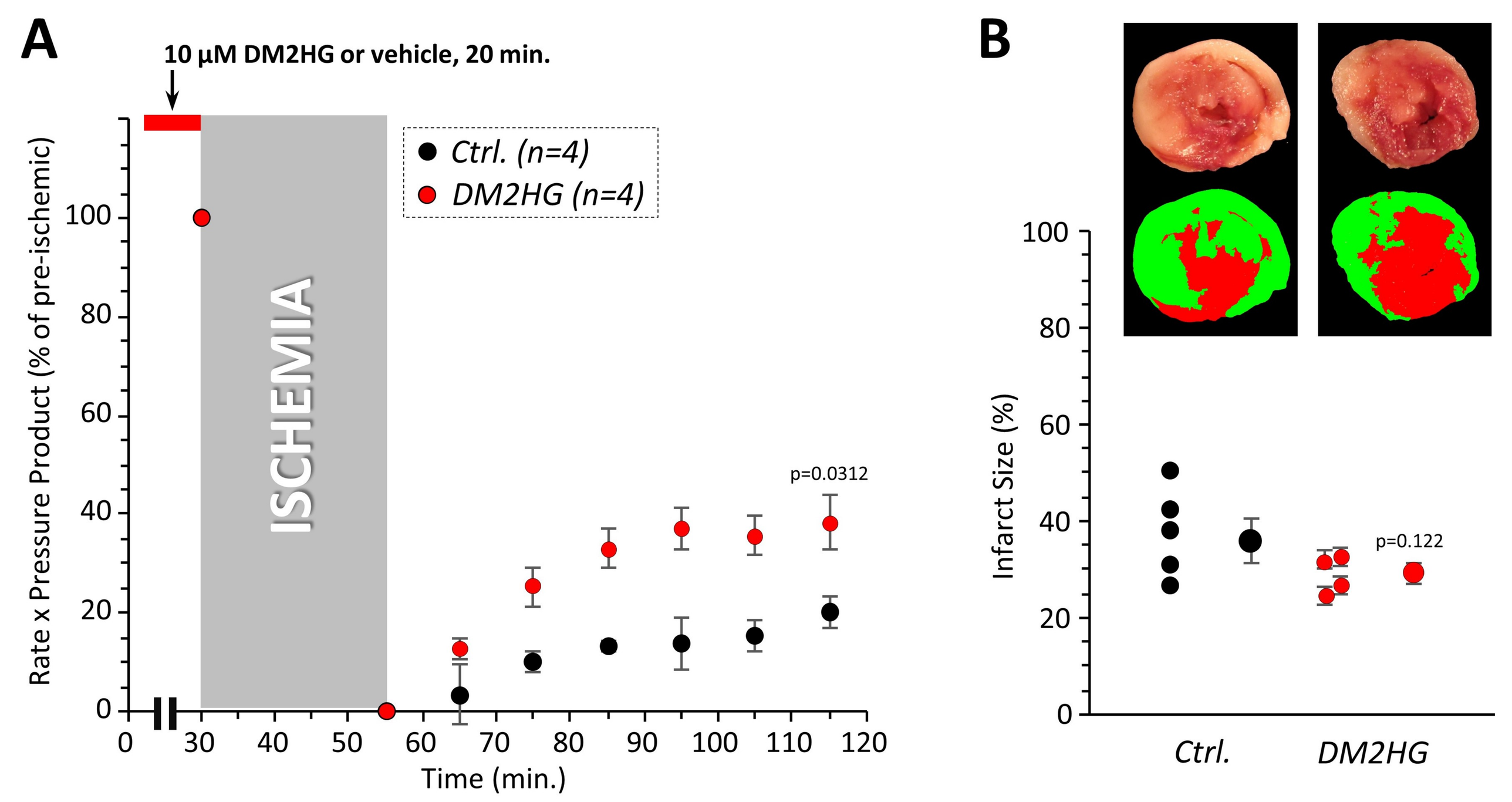
A
10 µM DM2HG or vehicle, 20 min.
Ctrl. (n=4)
DM2HG (n=4)
ISCHEMIA
Rate x Pressure Product (% of pre-ischemic)
Time (min.)
p=0.0312
B
Infarct Size (%)
p=0.122
Ctrl.
DM2HG

A

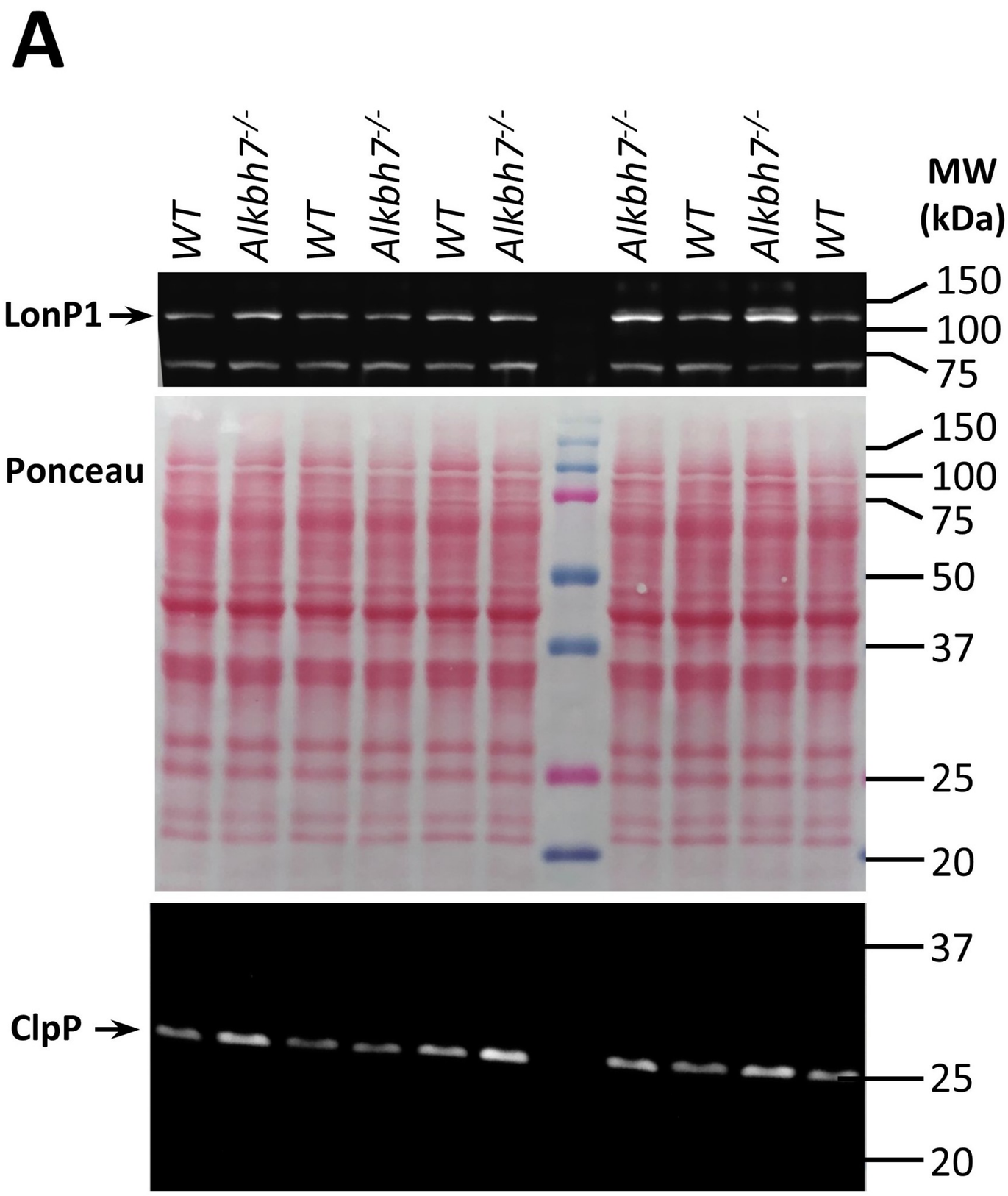
WT
Alkbh7-/-
WT
Alkbh7-/-
WT
Alkbh7-/-
Alkbh7-/-
WT
Alkbh7-/-
WT
MW (kDa)
LonP1
150
100
75
Ponceau
150
100
75
50
37
25
20
ClpP
37
25
20

B

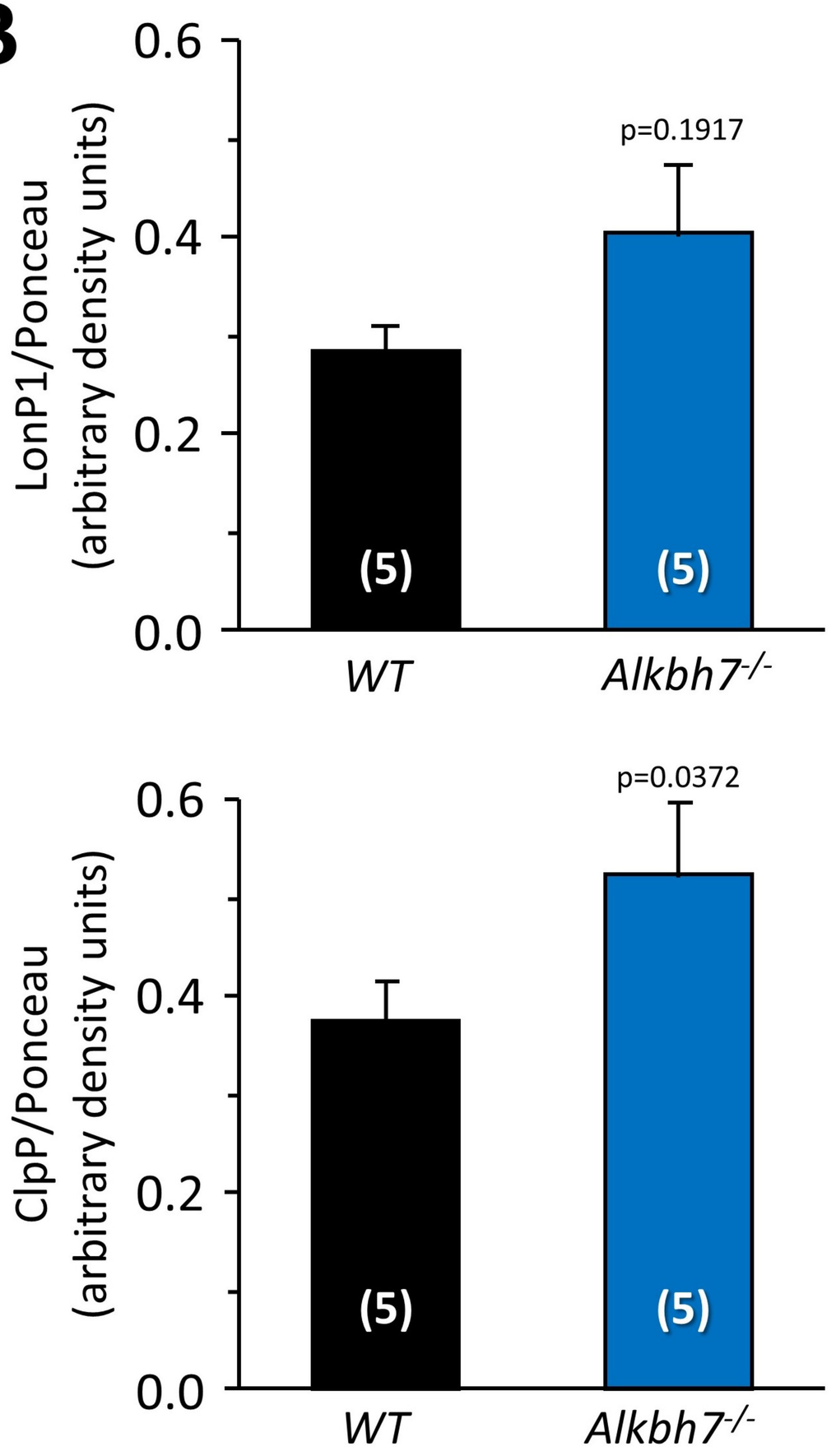
LonP1/Ponceau (arbitrary density units)
0.6
0.4
0.2
0.0
p=0.1917
(5)
(5)
WT
Alkbh7-/-
ClpP/Ponceau (arbitrary density units)
0.6
0.4
0.2
0.0
p=0.0372
(5)
(5)
WT
Alkbh7-/-

C

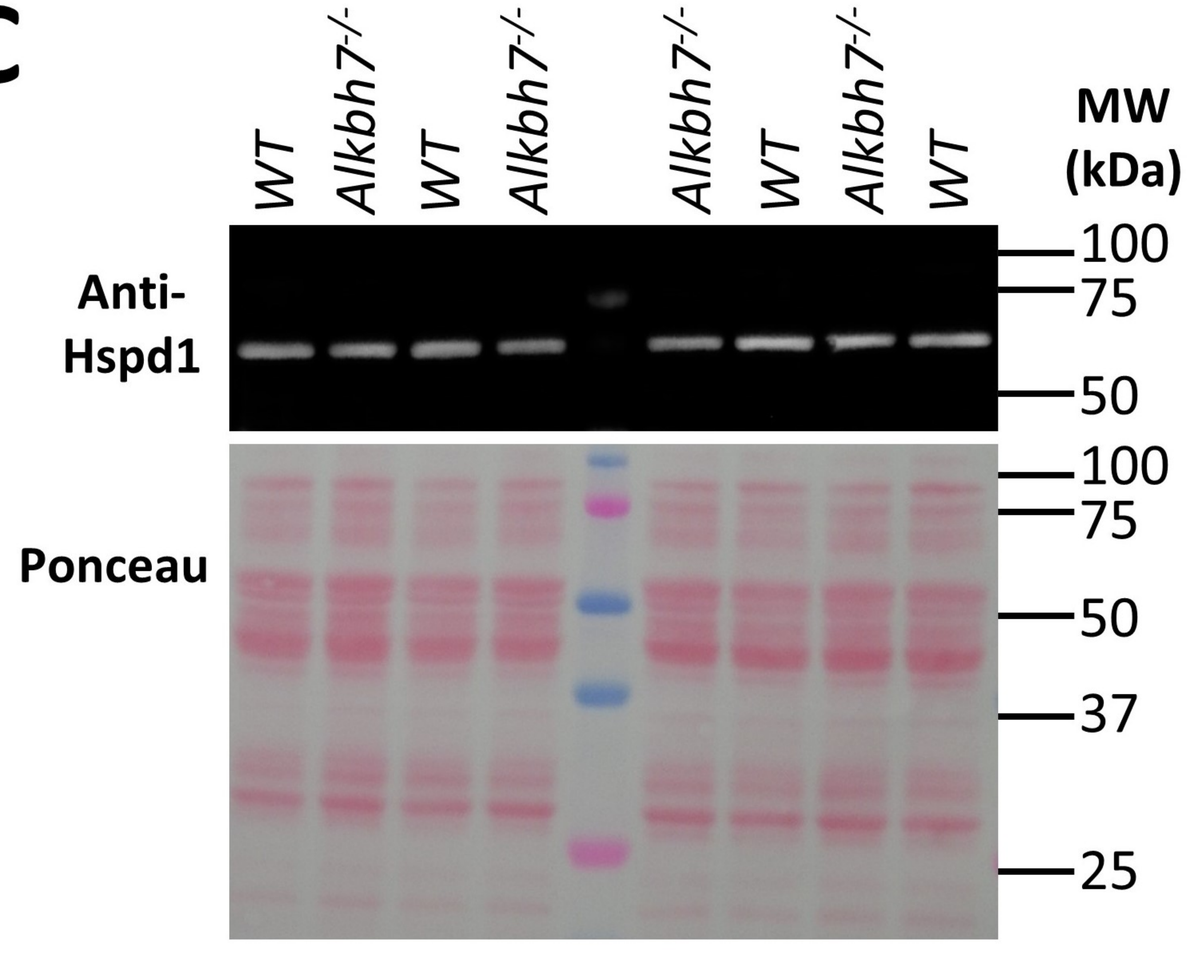
WT
Alkbh7-/-
WT
Alkbh7-/-
Alkbh7-/-
WT
Alkbh7-/-
WT
MW (kDa)
Anti-Hspd1
100
75
50
Ponceau
100
75
50
37
25

D

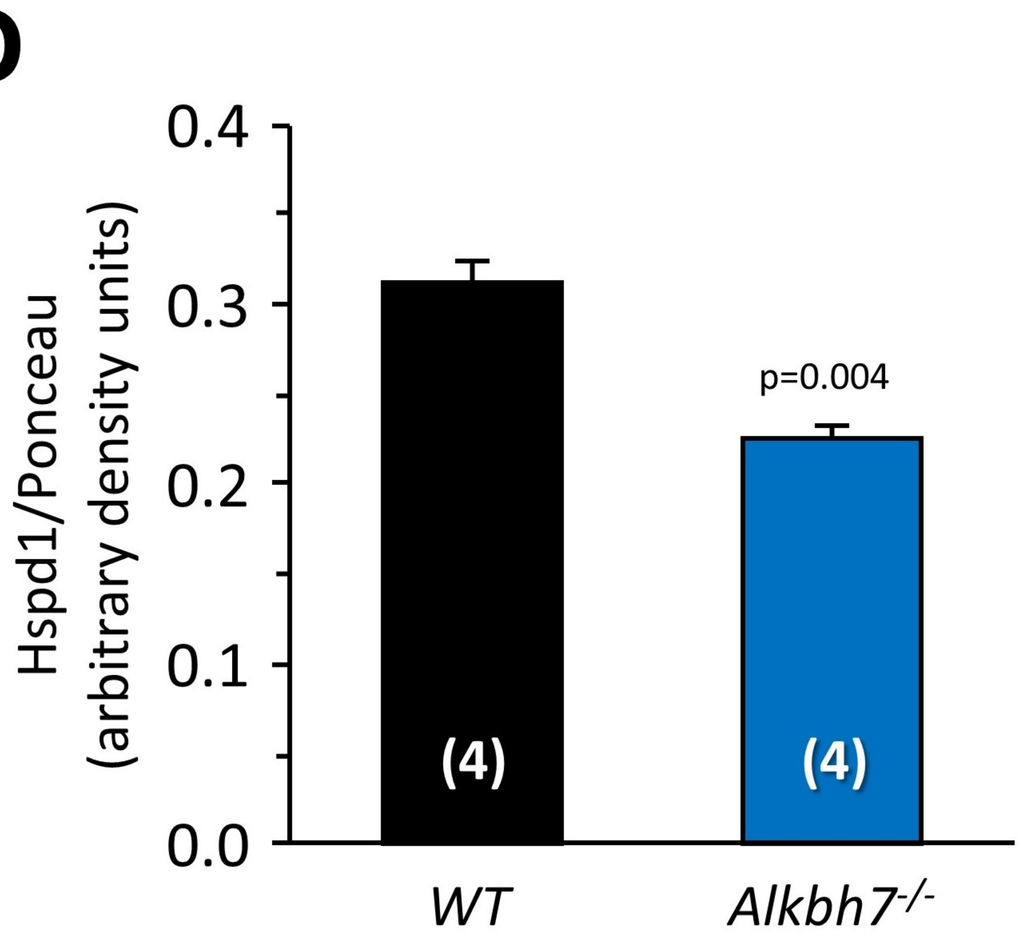
Hspd1/Ponceau (arbitrary density units)
0.4
0.3
0.2
0.1
0.0
p=0.004
(4)
(4)
WT
Alkbh7-/-

WT

Alkbh7

SCs

CxI

CxV

CxIII

Coomassie

WT

Alkbh7

multimers

dimer

monomer

CxV In-gel Assay

A

1 µM SBB-GSH-CpE, 10 min.

WT (n=5)

Alkbh7$^{-/-}$ (n=5)

ISCHEMIA

p=0.016

p=0.0064

Rate x Pressure Product (% of original)

Time (min.)

B

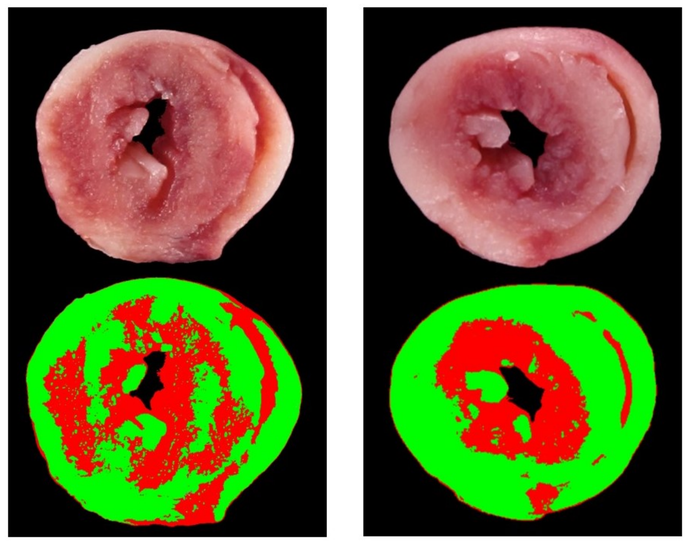

p=0.0005

Infarct Size (%)

WT

Alkbh7$^{-/-}$

C

MW (kDa)

WT | Alkbh7$^{-/-}$ | WT | Alkbh7$^{-/-}$ | WT | Alkbh7$^{-/-}$

25

20

DJ-1

25

20

p=0.669

DJ-1/Ponceau (arbitrary density units)

(3)

(3)

WT

Alkbh7$^{-/-}$

D

ALKBH7

↓F-1,6-BPase2

↓PLIN5

?

ΔMETABOLISM

(FAO → Glycolysis)

↑MGO

?

↑GLO-1

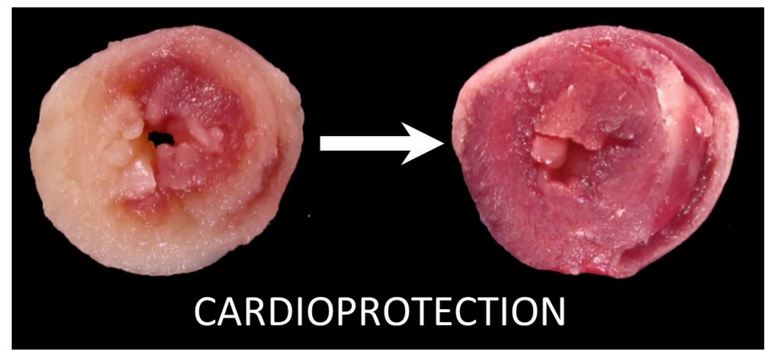

CARDIOPROTECTION

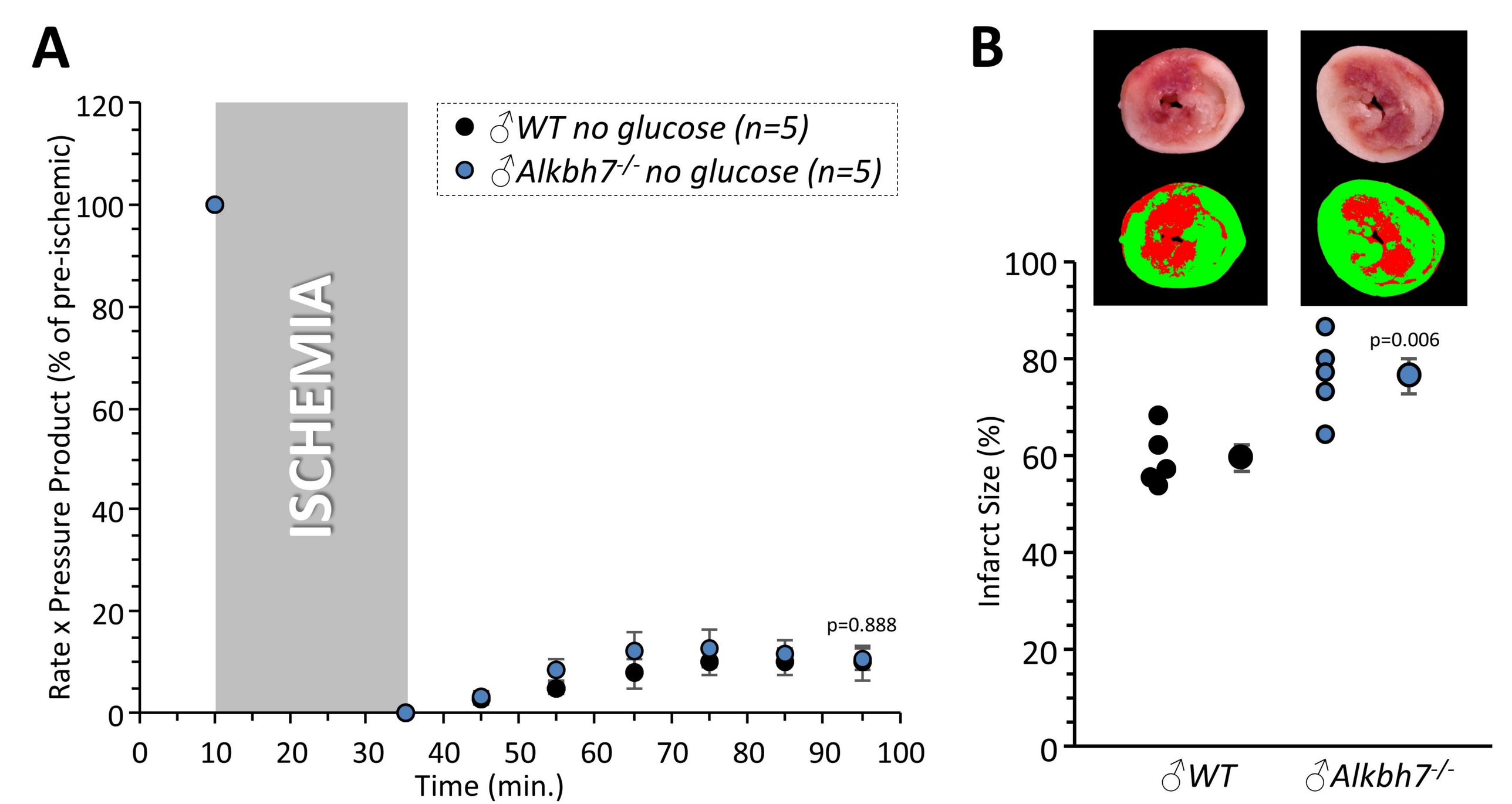
A
Rate x Pressure Product (% of pre-ischemic)
120
100
80
60
40
20
0
ISCHEMIA
♂WT no glucose (n=5)
♂Alkbh7-/- no glucose (n=5)
p=0.888
0
10
20
30
40
50
60
70
80
90
100
Time (min.)
B
Infarct Size (%)
100
80
60
40
20
0
p=0.006
♂WT
♂Alkbh7-/-